5-8-2004

Simulation of Combustion and Thermal Flow inside an Industrial Boiler

Raja Saripalli
University of New Orleans

SIMULATION OF COMBUSTION AND THERMAL FLOW INSIDE AN INDUSTRIAL BOILER

A Thesis

Submitted to the Graduate Faculty of the
University of New Orleans
in partial fulfillment of the
requirements for the degree of

Master of Science
in
The Department of Mechanical Engineering

by

Raja Saripalli

B.Tech, J.N.T.U, India, 2001

August,2004

…. Dedicated to my parents

ACKNOWLEDGEMENTS

I would like to express my sincere appreciation and gratitude to my advisor Dr.Ting Wang for his support, guidance and assistance that made me accomplish this thesis. The coordination, valuable suggestions, instructions via classes and productive discussions with Dr.Wang has helped me and inspired me towards the successful completion of this task.

I would also like to take this opportunity to thank Dr.Carsie A Hall and Dr.Kazim M Akyuzlu for serving on my defense committee.

I extend my special thanks to my family members, ECCC staff, and friends for their encouragement and moral support in this regard.

TABLE OF CONTENTS

LIST OF FIGURES

List of Figures (Continued)

LIST OF TABLES

NOMENCLATURE

a	Local speed of sound (m/s, ft/s)
c	Concentration (mass/volume, moles/volume)
c_p, c_v	Specific heat at constant pressure, volume (J/kg-K, Btu/lbm-°F)
d	Diameter (m, ft)
D_H	Hydraulic diameter (m, ft)
D_{ij}	Mass diffusion coefficient (m^2 /s, ft^2 /s)
E	Total energy, activation energy (J, kJ, cal, Btu)
f	Mixture fraction (dimensionless)
g	Gravitational acceleration (m/s^2 , ft/s^2)
Gr	Grashof number = $\frac{g\beta(T_s - T_\infty)L^3}{\nu^2}$ (dimensionless)
H	Total enthalpy (energy/mass, energy/mole)
h	Heat transfer coefficient (W/m^2 -K, Btu/ft^2 -h-°F)
h	Species enthalpy
h_0	Standard state enthalpy of formation (energy/mass, energy/mole)
I	Radiation intensity (energy per area of emitting surface per unit solid angle)
J	Mass flux; diffusion flux (kg/m^2-s, lbm/ft^2 -s)
K	Equilibrium constant = forward rate constant/backward rate constant (units vary)
k	Kinetic energy per unit mass (J/kg, Btu/lbm)
k	Reaction rate constant, e.g., k_1, k_{-1},$k_{f;r}$, $k_{b;r}$ (units vary)
k	Thermal conductivity (W/m-K, Btu/ft-h-°F)
k_B	Boltzmann constant (1.38 x10^{-23} J/mole-K)
k,kc	Mass transfer coefficient (units vary)
l, L	Length scale (m, cm, ft, in)
m	Mass (g, kg, lbm)
$\dot{m}$	Mass flow rate (kg/s, lbm/s)
M_w	Molecular weight (kg/kgmol)
M	Mach number = ratio of fluid velocity magnitude to local speed of sound
Nu	Nusselt number ≡ $\frac{hL}{k}$ (dimensionless)
p	Pressure (Pa, atm, mm Hg, lbf /ft^2)
Pr	Prandtl number = $\frac{\nu}{\alpha}$ (dimensionless)
Q	Flow rate of enthalpy (W, Btu/h)
q	Heat flux (W/m^2 , Btu/ft^2-h)
R	Gas-law constant (8.31447 =10^3 J/kgmol-K, 1.98588 Btu/lbmol-°F)

r	Radius (m, ft)
R	Reaction rate (units vary)
Re	Reynolds number $\equiv \frac{VL}{\nu}$ (dimensionless)
S	Total entropy (J/K, J/kgmol-K, Btu/lbmol-°F)
s	Species entropy
s_0	standard state entropy (J/kgmol-K, Btu/lbmol-°F)
Sc	Schmidt number = $\frac{\nu}{D}$ (dimensionless)
S_{ij}	Mean rate-of-strain tensor (s^{-1})
T	Temperature (K, °C, °R, °F)
t	Time (s)
U	Free-stream velocity (m/s, ft/s)
u; v; w	Velocity magnitude (m/s, ft/s); also written with directional sub-scripts (e.g., vx, vy, vz, vr)
V	Volume (m^3, ft^3)
$\vec{v}$	Overall velocity vector (m/s, ft/s)
X	Mole fraction (dimensionless)
Y	Mass fraction (dimensionless)
α	Permeability, or flux per unit pressure difference (L/m^2-h-atm, ft^3/ft^2-h-(lb_f/ft^2))
α	Thermal diffusivity (m^2/s, ft^2/s)
α	Volume fraction (dimensionless)
β	Coefficient of thermal expansion (K^{-1})
γ	Porosity (dimensionless)
γ	Specific heat ratio, c_p/c_v (dimensionless)
Δ	Change in variable, final - initial (e.g., Δp, Δt, ΔH, ΔS, ΔT)
δ	Delta function (units vary)
ε	Emissivity (dimensionless)
ε	Turbulent dissipation rate (m^2/s^3, ft^2/s^3)
$\eta'\eta''$	Rate exponents for reactants, products (dimensionless)
θ_r	Radiation temperature (K)
ν	Dynamic viscosity (cP, Pa-s, lbm/ft-s)
μ	Kinematic viscosity (m^2/s, ft^2/s)
ν', ν''	Stoichiometric coefficients for reactants, products (dimensionless)
ρ	Density (kg/m^3, lbm/ft^3)
σ	Stefan-Boltzmann constant (5.67×10^{-8} W/m^2-K^4)
σ_s	Scattering coefficient (m^{-1})
$\tilde{\tau}$	Stress tensor (Pa, lbf/ft^2)
τ	Shear stress (Pa, lbf/ft^2)
τ	Time scale, e.g., τ_c, τ_p, τ_c (s)
Φ	Equivalence ratio (dimensionless)

ABSTRACT

Industrial boilers that produce steam or electric power represent a large capital investment as well as a crucial facility for overall plant operations. In real applications, the operation of the superheater for producing high-pressure, high-temperature steam may result in problems frequently caused by ruptured superheater tubes. To make the boiler more efficient, less emission and less prone to tube rupture problems, it is important to understand the combustion and thermal flow behaviors inside the boiler. This study performs a detailed simulation of combustion and thermal flow behaviors inside an industrial boiler.

The simulations are conducted using the commercial CFD package FLUENT. The 3-D Navier-Stokes equations and five species transport equations are solved with the eddy-breakup combustion model. Calculation of NOx is performed after obtaining a converged flow, thermal and combustion solution. The results provide insight into the detailed thermal-flow and combustion in the boiler and showing possible reasons for superheater rupture.

CHAPTER ONE

INTRODUCTION

1.1 Background

During the past three decades, due to economic and environmental demands, engineers had to focus on improving the efficiency of energy producing power generation systems and in the meantime reduce their pollution emissions. Computer simulation is one of the best tools that can be applied in search for optimal solutions.

Boilers are commonly used in industries to burn fuel to generate process steam and electric power. A situation may arise in which a considerable amount of unburned fuel is being picked up by the gas and carried out of the boiler; this is known in the industry as carryover. As a result, unburned fuel may be blown out of the boiler, causing efficiency and emissions problems. Poor emissions could be caused by unburned hydrocarbon (UHC) and non-uniform heating induced by cold and hot spots, which produce CO and NOx respectively. Also a situation may arise where the superheater tubes break due to excessive heating, which may lead to boiler shutdown and thus increase the expenses incurred.

Steam that has been heated above the temperature corresponding to its pressure is said to be "superheated". This steam contains more energy than does saturated steam at the same pressure and the heat added provides more energy for the turbine for conversion to electric power. Overheating of the super-heater tubes is prevented by using the appropriate materials and

designing the unit to accommodate the heat transfer required for a given steam velocity through the super-heater tubes, based on the desired exit temperature. In real applications, however, the operation of the superheater for producing high-pressure, high-temperature steam may result in problems frequently caused by ruptured superheater tubes. The damage or rupture of the superheater tubes may be caused by many possible reasons including, galvanic corrosion, thermal contraction and expansion, composition of the combustion gases, accumulations of soot outside the pipes, accumulation of slag inside the pipe or high temperature distribution above material yield temperature and high thermal stress. The damage caused by high temperature can be minimized by providing uniform combustion and temperature distribution and keep fouling resistance low, Installation of soot-blowers to remove accumulated soot and other particulates, and optimizing the combustion conditions.

To help industry improve boiler's efficiency, reduce emissions, avoid rupture of superheater tubes, and understand the thermal flow transport in the boiler, this study employs the Computational Fluid Dynamics (CFD) scheme. CFD simulations could provide a clear picture of what is happening at any point within the boiler, making it easy in most cases to identify the problem and develop a solution. A CFD analysis provides fluid velocity, pressure, and temperature values throughout the solution domain for problems with complex geometries and boundary conditions. During the analysis, the geometry of the system or boundary conditions such as inlet velocity and flow rate can be easily changed to view their effects on thermal-flow patterns or species concentration distributions. CFD can also provide detailed parametric studies that can significantly reduce the amount of experimentation necessary to identify problems and to optimize the operating conditions.

1.2 Objectives

The objective of the study is to model and simulate the thermal flow behavior of an industrial natural gas fired boiler. The boiler information is provided by Dynegy Gas Plant at Venice, Louisiana. The gas flow and temperature distribution is simulated with the commercial CFD package FLUENT (6.1.22). FLUENT is a finite volume CFD code for solving transport equations of mass, momentum and energy conservation. The specific goals are

1. To develop an appropriate numerical model to simulate the combustion features in the boiler.
2. To investigate the flow pattern and temperature distribution inside the boiler.
3. To study the flow behavior and heat transfer near the superheater tubes.
4. To study the flow and aerodynamic behavior through the chimney.
5. To calculate emissions NOx.
6. To identify means that can help improve boiler efficiency, reduce emissions and avoid superheater tube rupture.

CHAPTER TWO

LITERATURE SEARCH

The literature search focuses on introducing fundamental functions, requirements and classification of the boilers, combustion, and NOx formation mechanisms and reduction technologies.

2.1 Boiler

A boiler is a closed vessel in which water, under pressure, is transformed into steam by the application of heat. In the furnace, the chemical energy in the fuel is converted into heat and this heat is transferred to water to convert to steam.

2.1.1 Requirements of an efficient boiler

The ideal, reliable, economic and efficient boilers will embodies the following features:

- Simplicity in construction, excellent workmanship, and materials conducive to low maintenance cost.
- Design and construction to accommodate expansion and contraction properties of materials.
- Adequate steam and water space, delivery of clean steam, and good water circulation.
- A furnace setting conducive to efficient combustion and maximum rate of heat transfer.
- Responsiveness to sudden demands and overloads.

- Should have low initial cost, installation cost and maintenance cost.
- Should be compact.
- Easy accessibility for cleaning and repair.

A boiler is designed to absorb the maximum amount of heat released in the process of combustion. The heat is transmitted to the boiler by radiation, conduction and convection, the percentage of each depending upon the boiler design.

2.1.2 Steam Utilization

Steam is generated for the following plant uses:

1. Driving turbine for electric generating equipment, blowers and pumps.
2. Process for direct contact with products, direct contact sterilization and non-contact for processing temperatures for drying and sterilization.
3. Heating and air conditioning via absorption chillers for comfort and equipment.
4. Providing processing steam for water-shift reaction and other chemical process.

The efficiency achievable with steam generation relies heavily on the system's ability to return condensed steam to the operating cycle. Many of the systems described above return a significant portion of the condensed steam to the generation cycle.

2.1.3 Classification of boilers

Boilers are manufactured in many different sizes and configurations depending on the characteristics of the fuel, the specified heating output, and the required emissions controls.

Some boilers are only capable of producing hot water, while others are designed to produce steam. Boilers can be classified by various ways.

a) **Method of transporting hot gases:**

On this basis, boilers can be classified as: Fire tube boiler and water tube boiler.

Fire tube boiler

In a fire tube boiler, hot gases pass through the tubes and water surrounds them. Heat from the gases (produced by combustion) is transferred to water, which is then converted to steam. Examples: Cochran, Lancashire, Cornish, Locomotive boilers

Water tube boilers

In water tube boiler, water flows inside the tubes and the hot gases flow outside the tubes. Examples: Babcock and Wilcox boiler (which has straight but inclined water tubes); Stirling boiler (which has bent water tube).

Fire tube boilers need stronger outer shell to contain steam pressure, water tube boilers does not need that.

b) **Method of firing:**

Internally fired: Furnace region is provided inside the boiler shell and is completely surrounded by water-cooled surfaces. e.g., Lancashire, Locomotive boilers.

Externally fired: Furnace region is provided outside. e.g., Babcock and Wilcox boiler

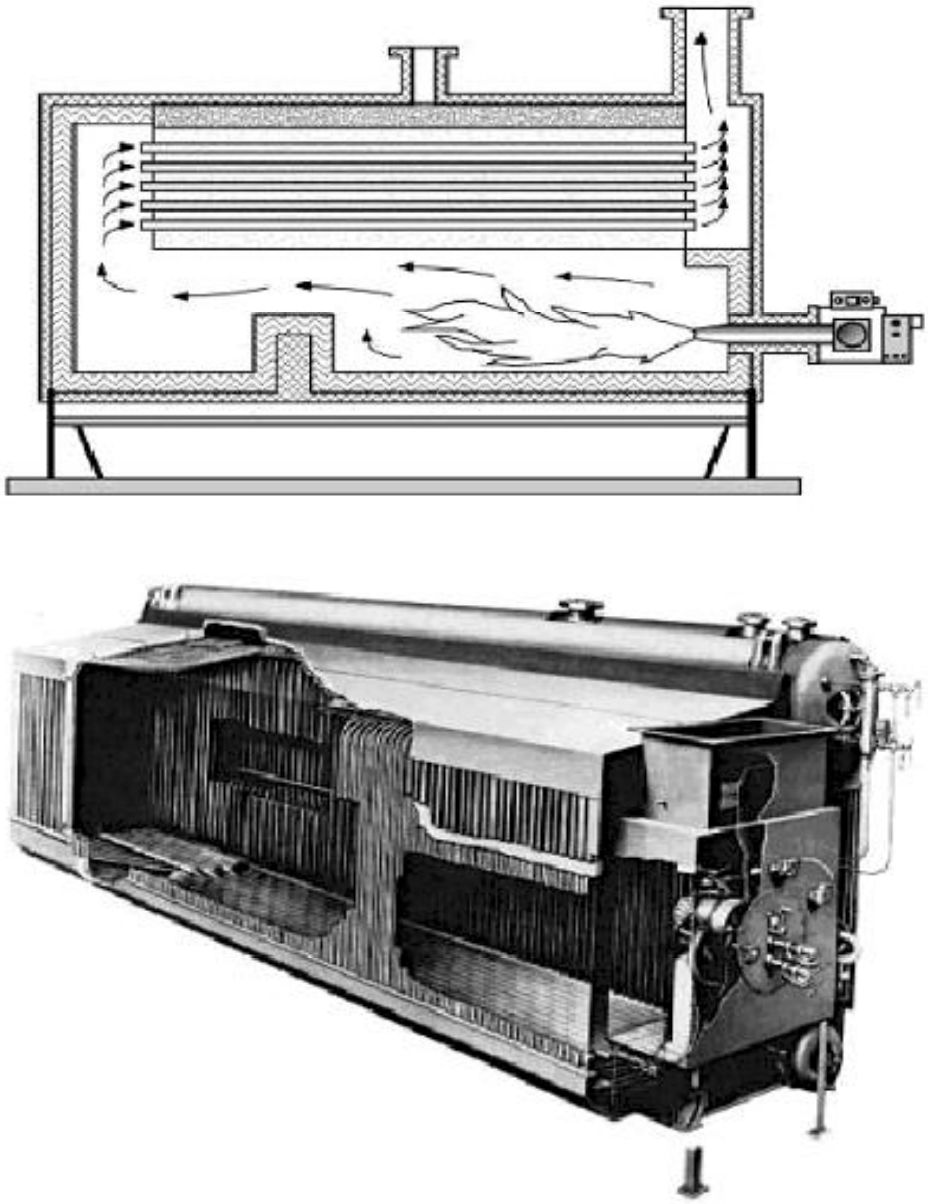

Figure 2.1 a) Fire tube boiler (above) b) Water tube boiler (below)

c) **Pressure of steam:**

Low pressure boiler: Steam pressure below 80 bars.

Examples: Cochran, Cornish, Lancashire, locomotive boilers

High pressure boiler: Pressure above 80 bars.

Examples: Babcock & Wilcox, Lamont

d) **Circulation of water:**

Natural circulation: Circulation of water in the boiler takes place by natural convection current produced by the application of heat.

Examples: Lancashire, Locomotive, and Babcock & Wilcox boilers.

Forced circulation: Circulation of water takes by forced convection.

2.2 Combustion

Combustion occurs in boilers, refineries, drying kilns, incinerators, industrial ovens and is also used to generate energy from biomass (e.g. from wood, straw, organic waste). Combustion is the process whereby oxygen reacts with fuel, resulting in the release of heat and light. The effectiveness of combustion can be measured by analyzing the flue gas and the amount of soot. Perfect combustion is obtained when the flue gas analysis shows no carbon monoxide, hydrogen or oxygen and when the percentage of carbon dioxide is at a maximum.

There are several factors or parameters that will affect combustion of heavy fuels in a boiler:

1. Design of the combustion chamber
2. Design of the burner(s)
3. Condition of the burner(s)
4. Air and fuel ratio. Excess air of a few percent is normal
5. How well the air and fuel are mixed
6. Temperature and air speed in the combustion chamber
7. Air and fuel preheating
8. Physical properties of the oil (viscosity, density, surface tension)

9. Chemical properties of the oil (asphaltenes, waxes, metal content)
10. Fuel droplet size if liquid fuels are used.

The combustion process provides tremendous amount of energy from a fuel and this energy is converted or transformed to heat for cooking, making hot water, generating steam for manufacturing or turning a turbine to produce shaft power and electricity, producing mechanical motion as in an auto engine, or thrust as in an aero-engine.

The combustion of fuels requires the consumption of a large quantity of air. For example, 150 Lbs of a fuel (oil) requires about 2000 Lbs of air and resulting to 250 Lbs of CO_2. Small quantities of pollutants such as NO, CO and hydrocarbons are also formed, these quantities being negligible from engineering calculations standpoint but very significant from the environmental standpoint.

The combustion process involves some 1000 reactions to complete the oxidation process forming CO_2 and H_2O, the ultimate products of combustion. However, pollutants such as CO, unburned hydrocarbons (UHC), soot, NOx, SO_2 are also formed during the combustion process as a result of the various reactions.

2.3 Pollutants

Control of pollutant emissions is a major factor in the design of modern combustion system. Pollutants of concern include (i) particulate matter such as soot, fly ash, metal fumes, various aerosols etc, (ii) the sulfur oxides SO_2 and SO_3, (iii) unburned and partially burned hydrocarbons such as aldehydes, and (iv) oxides of Nitrogen, NOx which consists of NO and NO_2, CO & greenhouse gases such as N_2O.

Effects of Pollutants

Primary and secondary air pollutants affect our environment and human health in many ways. Primary pollutants are those emitted directly from the sources, while secondary pollutants are those formed via reactions involving primary pollutants in the atmosphere.

Four major negative effects of pollutants are

1. Altered properties of the atmosphere and precipitants
2. Harm to vegetation
3. Foiling and deterioration of materials
4. Potential increase of morbidity and mortality in humans
5. Depleting ozone layer
6. Affecting Global warming
7. Producing Acid rains

2.4 NO_x

NO_x emission consists of mostly nitric oxide (NO). It also contains nitrogen oxide (NO_2) and nitrous oxide (N_2O). NO_x is a precursor for photochemical energy and contributes to acid rain and causes ozone depletion. The quantity of NOx formed depends on three T's : Temperature, Time, and Turbulence.

Oxides of Nitrogen Formation:

In every circumstance where combustion occurs, the formations of nitrogen oxides (NOx) are inevitable. From a home open fire to a coal fired power plant, NOx is formed as an undesired product and a contributor to air pollution.

NOx is used to refer to NO and NO_2. NO is the primary form in combustion products (typically 95 percent of total NOx). NO is subsequently oxidized to NO_2 in the atmosphere.

Nitrogen Oxide Formation occurs through three reaction paths, each having unique characteristics which is responsible for the formation of NOx during combustion processes:

(1) Thermal NOx, which is formed by the combination of atmospheric nitrogen and oxygen at high temperatures;

(2) Fuel NOx, which is formed from the oxidation of fuel-bound nitrogen; and

(3) Prompt NOx, which is formed by the reaction of fuel-derived hydrocarbon fragments with atmospheric nitrogen in an early phase of the flame front.

NOx emissions do not form in significant amounts until flame temperatures reach 2800 F. Once that threshold is passed, any further rise in temperature causes a rapid increase in the rate of NOx formation. Lower excess air levels (fuel rich) starve the reaction for oxygen, and higher excess air levels (lean burn) drive down the flame temperature, slowing the rate of reaction.

In the combustion of fuels that contains no nitrogen, nitric oxide is formed by three chemical mechanisms:

1. The Thermal or Zeldovich Mechanism
2. The Prompt or Fenimore Mechanism
3. The N_2O Intermediate Mechanism

2.4.1 Thermal NOx Formation

Thermally produced NOx is the largest contributor to these types of emissions. Thermal NOx is produced during the combustion process when nitrogen and oxygen are present at elevated temperatures. The two elements combine to form NO or NO_2. NOx is generated by many combustion processes. It combines with other pollutants in the atmosphere and creates O_3, a substance known as ground level ozone.

The formation of thermal mechanism dominates in high-temperature combustion over a fairly wide range of equivalence ratios. Equivalence ratio is defined as the ratio of actual fuel/air ratio over the theoretical fuel/air ratio. The formation of thermal NOx is determined by a set of highly temperature-dependent chemical reactions known as the extended Zeldovich mechanism. The principal reactions governing the formation of thermal NOx from molecular nitrogen are as follows:

$$O + N_2 \Leftrightarrow NO + N \quad (2.4.1)$$

$$N + O2 \Leftrightarrow NO + O \quad (2.4.2)$$

A third reaction, particularly at near-stoichiometric conditions and in fuel-rich mixtures which contributes to the mechanism is

$$N + OH \Leftrightarrow NO + H \quad (2.4.3)$$

The activation energy for first reaction (2.4.1) is relatively large, 319,050 kJ/kmol. Therefore this reaction has very strong temperature dependence. The thermal mechanism is unimportant at temperatures below 1800 K. Compared with the time scales of fuel oxidation

processes, NO is formed rather slowly by thermal mechanism; thus, thermal NO is generally considered to be formed in post flame gases.

2.4.2 Fuel NOx Formation

Fuel NO_X formation is a more complex process involving local concentration of oxygen and nitrogen and is reduced by minimizing the availability of oxygen during various stages of the combustion process. Fuel-bound NOx is generated from nitrogen compounds present in the fuel itself. Gaseous fuels, such as natural gas or propane, are free of nitrogen compounds. However, fuel oils and coal can contain significant amounts of fuel-bound nitrogen. During combustion, the conversion rate of fuel-bound nitrogen to NOx varies widely over a range of 20 to 70%.

During combustion process, nitrogen-containing organic compounds present in liquid or solid fossil fuel contributes to the total NOx formed. The fuel nitrogen is a particularly important source of nitrogen oxide emissions for residual duel oil, coke, and coal, which typically contain 0.3-2% nitrogen by weight. The fuel-bound NOx contribution depends on the amount of nitrogen that is chemically bound in the fuel. The fuel NOx formation is generally important in non-premixed combustion. The fuel NOx formation is not important in premixed combustion applications since most fuels used in premixed combustion contain little or no bound nitrogen.

Under the reducing conditions surrounding the burning droplets or particles, the fuel-bound nitrogen is converted to fixed nitrogen species such as HCN and NH_3. These, in turn, are readily oxidized to form NO if they reach the lean zone of the flame. Between 20 and 80 percent of the bound nitrogen is typically converted to NOx, depending on the design of the combustion

equipment. With prolonged exposure (order of 100 ms) to high temperature and reducing conditions, however, these fixed nitrogen species can be converted to molecular nitrogen, thus avoiding the NO formation path. The fuel NOx mechanism is shown in the Figure 2.2.

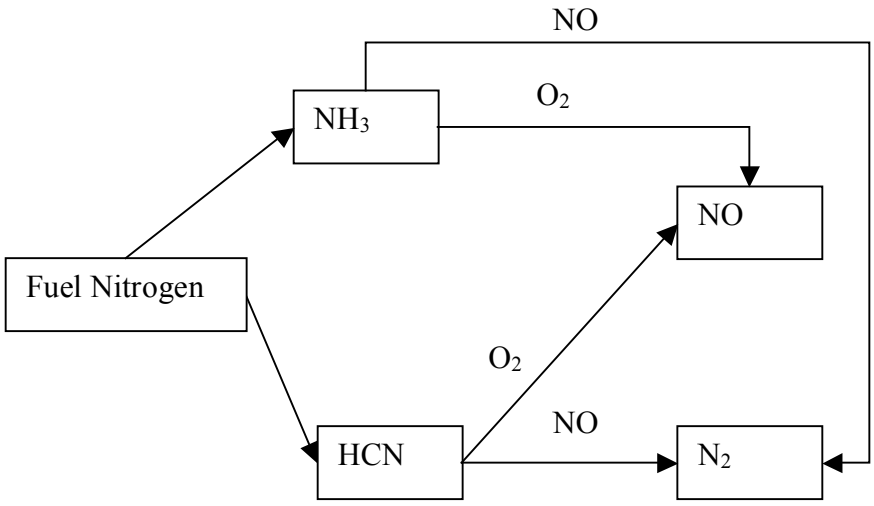

Figure 2.2 Fuel NOx mechanism

2.4.3 PROMPT NOx Formation

Prompt NOx is the third and least significant NOx formation mechanism. In this mechanism, nitrogen from combustion air reacts with hydrocarbon radicals from the fuel to form a hydrogen cyanide intermediate. The hydrogen cyanide then reacts with oxygen and nitrogen in combustion air to form nitrogen oxide.

Hydrocarbon fragments (such as C, CH, CH_2) may react with atmospheric nitrogen under fuel-rich conditions to yield fixed nitrogen species such as NH, HCN, H_2CN, and CN. These, in turn, can be oxidized to NO in the lean zone of the flame. In most flames, especially those from

nitrogen-containing fuels, the prompt mechanism is responsible for only a small fraction of the total NOx. Its control is important only when attempting to reach the lowest possible emissions.

The formation of prompt NOx is governed by a set of equations known as Fenimore mechanism. The scheme of Fenimore mechanism is that hydrocarbon radicals react with molecular nitrogen to form amines or cyano compounds. The amines and cyano compounds are then converted to inverted compounds that ultimately form NO. The Fenimore mechanism is given as:

$$CH + N_2 \Leftrightarrow HCN + N \quad (2.4.4)$$

$$C + N_2 \Leftrightarrow CN + N \quad (2.4.5)$$

$$N + O_2 \Leftrightarrow NO + O \quad (2.4.6)$$

$$HCN + OH \Leftrightarrow CN + H_2O \quad (2.4.7)$$

$$N + OH \Leftrightarrow NO + H \quad (2.4.8)$$

In the atmosphere, nitric oxide ultimately oxidizes to form nitrogen oxide, which contribute to production of acid rain and photochemical smog. Production of NO associated with the Fenimore prompt mechanism is shown in Figure. 2.3.

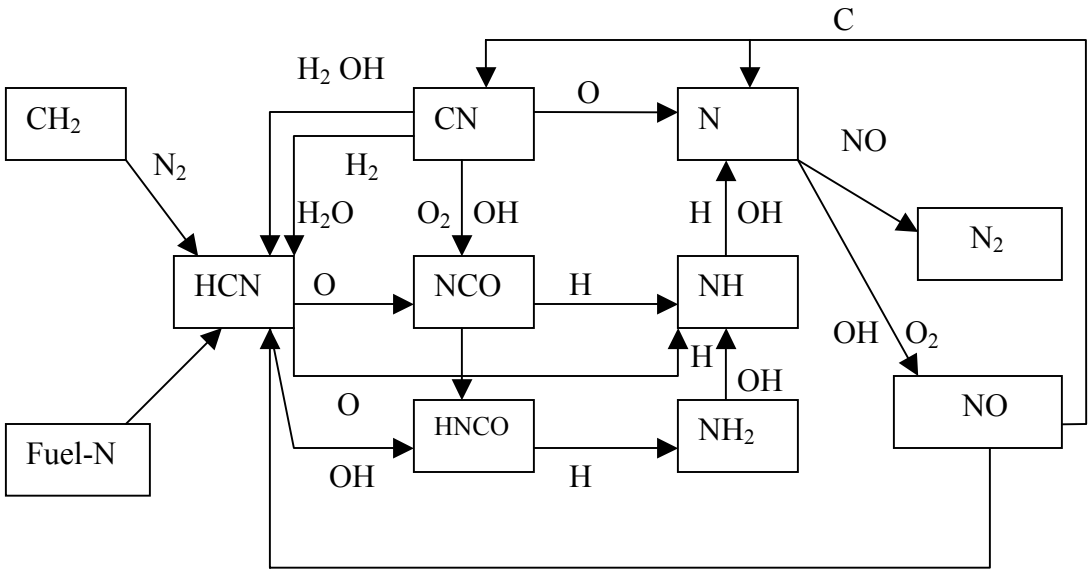

F

igure 2.3 NO production associated with Fenimore prompt mechanism

Prompt NOx formation is proportional to the number of carbon atoms present per unit volume and is independent of the parent hydrocarbon identity. The quantity of HCN formed increases with the concentration of hydrocarbon radicals, which in turn increases with equivalence ratio. As the equivalence ratio increases, prompt NOx production increases, then passes a peak, and finally decreases due to deficiency in oxygen.

2.4.4 NOx Formation From Reburning

In Reburning NO mechanism, NO reacts with hydrocarbons and is subsequently reduced. In general the mechanism is given as

$$CH_i + NO \longrightarrow HCN + \text{products} \qquad (2.4.9)$$

Three reburn reactions for temperature range $1600 \leq T \leq 2100$ are

$$CH + NO \xrightarrow{K1} HCN + O \quad (2.4.10)$$

$$CH_2 + NO \xrightarrow{K2} HCN + OH \quad (2.4.11)$$

$$CH_3 + NO \xrightarrow{K3} HCN + H_2O \quad (2.4.12)$$

Where K1, K2 and K3 are rate constants for the above reactions

$K_1 = 1 * 10^8$ $[m^3 / gmol\text{-}s]$

$K_2 = 1.4 * 10^6 * e^{-550/T}$ $[m^3 / gmol\text{-}s]$

$K_3 = 2 * 10^5$ $[m^3 / gmol\text{-}s]$

2.4.5 NOx Control

NOx control technologies currently used within the industry can be grouped into two categories i.e combustion modifications and post-combustion NOx control technologies. The first addresses reducing the production of NOx by making changes in the combustion process or the fuel stream. The second involves mitigating the NOx that has been produced by the application of post-combustion technology through the use of chemical reagents. For coal-fired applications, combustion system modifications are generally less costly and may independently result in emissions levels that satisfy regulatory requirements. Several methods are available to effectively limit NOx formation during combustion. The optimum combustion system redesign may blend several of these, selected on the basis of unit capacity and fuels to be fired and of applicable NOx reduction requirements.

For processes dominated by thermal NOx formation, time, temperature, and oxygen availability are the primary variables affecting NOx yields. Production of thermal NOx can be

controlled by reducing the thermal loading to the combustion zone. NOx mechanisms include (1) increasing the size of the combustion zone for a given thermal input, (2) reducing the rate of combustion and peak flame temperatures with specially designed burners, and (3) addition of recirculated flue gas to the combustion air to depress flame temperature.

Fuel NOx formation can be reduced by switching to, or co-firing with, fuel with lower nitrogen content and/or by limiting oxygen availability during the early stages of combustion. Oxygen reduction mechanisms include reducing excess air, reducing burner stoichiometry by removing a portion of the combustion air from the burner zone and introducing this air later through NOx or overfire air (OFA) ports (air staging), and limiting the rate that air is introduced to the fuel during the early stages of combustion with specially designed burners.

Combustion Modifications for NOx control

Low Excess Air ---- Reducing the air supplied in the furnace lowers NOx production. Thermal NOx emissions peak at leaner than stoichiometric equivalence ratios. The NOx creation rate typically peaks at excess oxygen levels of 5-7% where the combination of high combustion temperatures and the higher oxygen concentration act together. At both lower and higher air/fuel ratios, NOx production falls off due to lower flame temperature at high excess air levels and lower oxygen at low air levels. Low air is achieved by changes in operating procedures, system controls or both. The NOx reduction technique involves reducing the air supplied. Only limited NOx reductions are possible when low air level is supplied because excessive reduction in air can be accompanied by significant increases in CO.

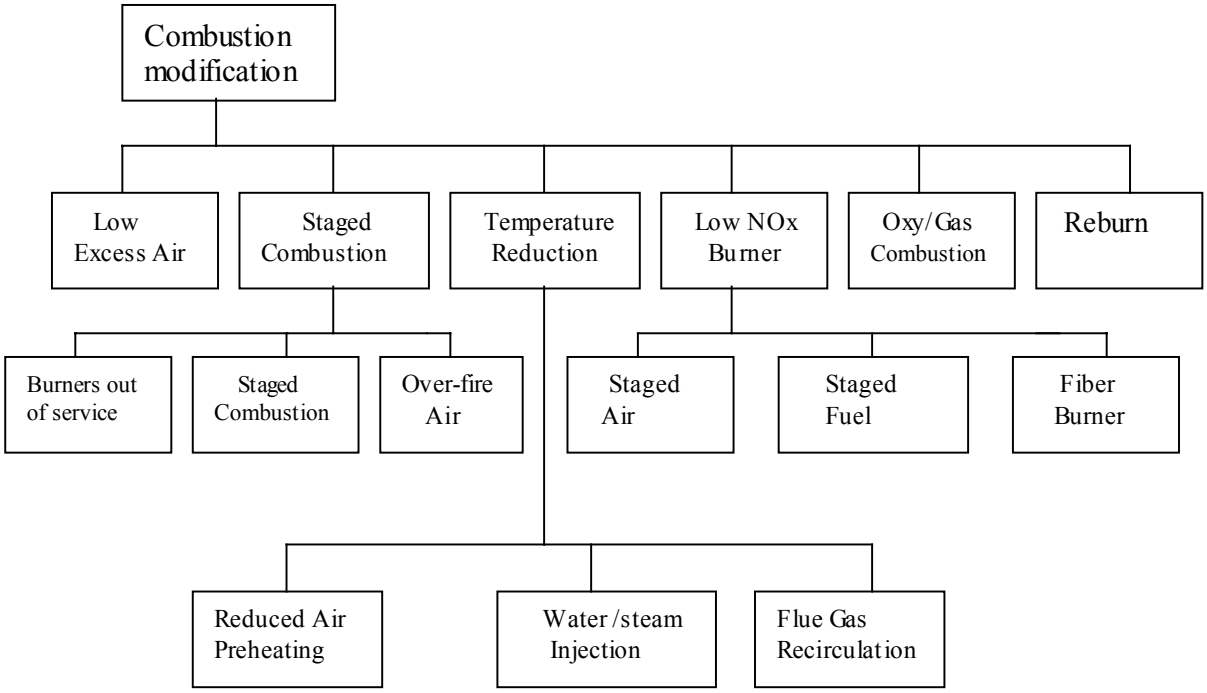

Figure 2.4 Combustion modification technologies for NOx control

Staged Combustion — Staged combustion processes significantly reduce NOx emissions. In the initial stage of combustion, the air supplied to the burners is less than the amount required to completely burn the fuel. During this stage, fuel-bound nitrogen is released but cannot be oxidized, so it forms stable molecules of harmless molecular nitrogen (N2). Other components of the fuel are also released without being fully oxidized. These include carbon particles and carbon monoxide. By adding a second stage, in the air-fuel mixture, the carbon and carbon monoxide can be burned, converting them to carbon dioxide.

Over-fire Air — Over-fire air is the air that is injected into the furnace above the normal combustion zone. Generally when Over-fire air is employed, the burners are operated at a lower than normal air-to-fuel ratio, which reduces NOx formation. Over-fire air, which is frequently

used in conjunction with low NOx burners, completes the combustion process at a lower temperature.

Flue Gas Recirculation — Flue Gas Recirculation, in which part of the flue gas is recirculated to the furnace, can be used to modify conditions in the combustion zone (lowering the temperature and reducing the oxygen concentration) to reduce NOx formation. Flue Gas Recirculation is also used as a carrier to inject fuel into a reburn zone to increase penetration and mixing.

Operational Modifications — Changing certain boiler operational parameters can create conditions in the furnace that will lower NOx production. Examples include burners-out-of-service (BOOS), low excess air (LEA), and biased firing (BF). In BOOS, selected burners are removed from service by stopping fuel flow, but airflow is maintained to create staged combustion in the furnace. LEA involves operating at the lowest possible excess air level without interfering with good combustion, and BF involves injecting more fuel to some burners (typically the lower burners) while reducing fuel to other burners (typically the upper burners) to create staged combustion conditions in the furnace.

Low NOx Burners (LNB) — Low NOx Burners are designed burners to control the mixing of fuel and air to achieve what amounts to staged combustion. This staged combustion reduces both flame temperature and oxygen concentration during some phases of combustion, in turn, reduces both thermal NOx and fuel NOx production. The most common LNB types achieve lower NOx emissions by "staging" the injection of either air or fuel in the burner region. Low NOx burners are classified as either a staged air or a staged fuel burner. Air staging is more common. As the name implies, the staged air burner gradually introduces combustion air to the fuel at various

regions along the flame front. These regions are typically referred to as the primary, secondary and tertiary (staged) air zones. The division of combustion air reduces the oxygen concentration in the primary burner combustion zone, lowering the amount of NO formed there and increasing the amount of NO-reducing agents formed in an oxygen deficient combustion zone. Secondary and tertiary air injections complete the combustion downstream of the primary zone, lowering the peak temperature and reducing thermal NOx formation. Aside from the basic staged air burner, there are other variations of staged air burners that incorporate internal recirculation of combustion products to aid in NOx reduction. Low NOx Burners are often coupled with over fire (secondary) air (OFA) injection to assure complete combustion. Low NOx burner employing air staging and fuel staging is shown in Figure 2.5.

Reburning — In the Reburning process, part of the boiler fuel input (typically 10-25%) is added in a separate reburn zone. The fuel-rich reducing conditions in this zone lead to the reduction of NOx formed in the normal combustion zone. OFA is injected above the reburn zone to complete combustion. Thus, with reburn there are three zones in the furnace: (1) a combustion zone with an approximately normal air-to-fuel ratio; (2) a reburn zone, where added fuel results in a fuel-rich condition; and (3) a burnout zone, where OFA completes the combustion. Coal, oil, or gas can be used as the reburn fuel.

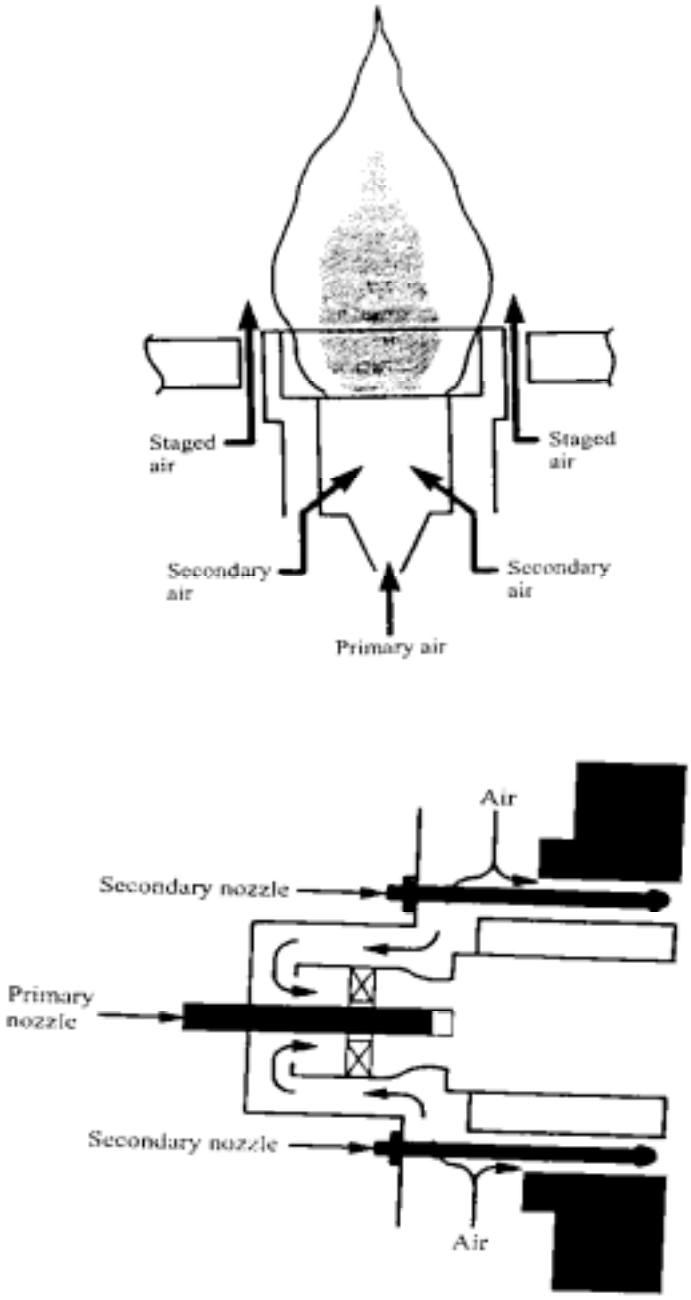

Figure 2.5 (a) Low NOx burner employing air staging (above)

(b) Low NOx burner employing fuel staging

Post-Combustion controls for NOx reduction

The post-combustion controls can be achieved by using selective non-catalytic reduction (SNCR) and selective catalytic reduction (SCR) as shown in Figure 2.6.

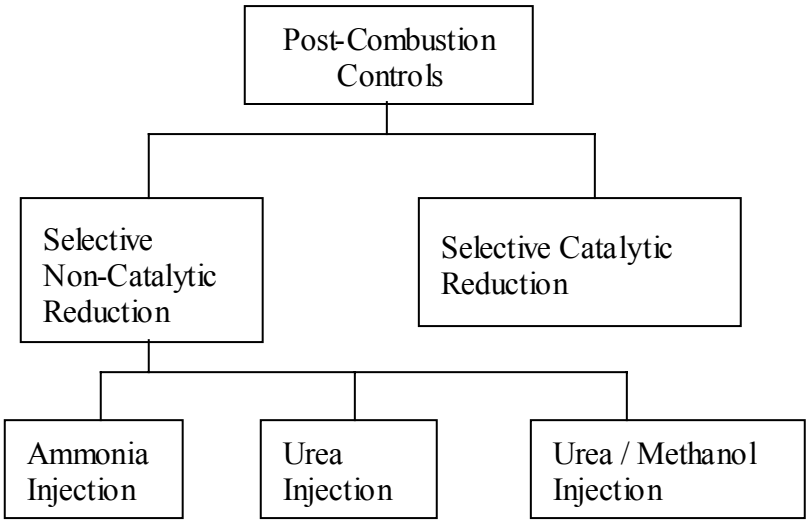

Figure 2.6 Post-combustion control technologies for NOx reduction

Selective Non-Catalytic Reduction (SNCR) — In this post control technique, a nitrogen containing additive, ether ammonia, urea, or cyanuric acid is injected and mixed with flue gases to affect chemical reduction of NO to N_2 without the aid of catalyst. Temperature is a critical variable, and operation within a relatively narrow range of temperatures is required to achieve large NO_x reductions.

Selective Catalytic Reduction (SCR) — In this technique, a catalyst is used in conjunction with ammonia injection to reduce NO to N_2. Effective reduction depends on the temperature range and is about 480 K to 780 K. Greater NOx reductions are possible but the costs of NO_x removal are generally the highest of all NO_x control techniques because of both the initial cost and the operating costs associated with catalyst replacement.

CHAPTER THREE

PROBLEM SETUP AND MODELING

The overall design of the studied boiler is shown in Figure 3.1. The model basically consists of four sections, burner, combustion chamber, saturating/superheating, and chimney (exhaust). The top view of the boiler is shown in Figure 3.2. The burner is provided with three inlets, two for air inlet and one for fuel inlet. Primary and secondary air enters the burner as shown in Figure 3.3 and Figure 3.4. The primary air enters with a swirl and is directed outward. The air entering around the outside periphery of the swirl air is defined as the secondary air. It contributes to a controlled expansion in the quarl section of the burner where it reacts with the unburned fuel from the center reaction to complete the combustion process. The fuel used is Methane, CH_4, which is burned in the combustion chamber and the flue gasses pass through the saturated and super-heater tubes and exhausted through the chimney.

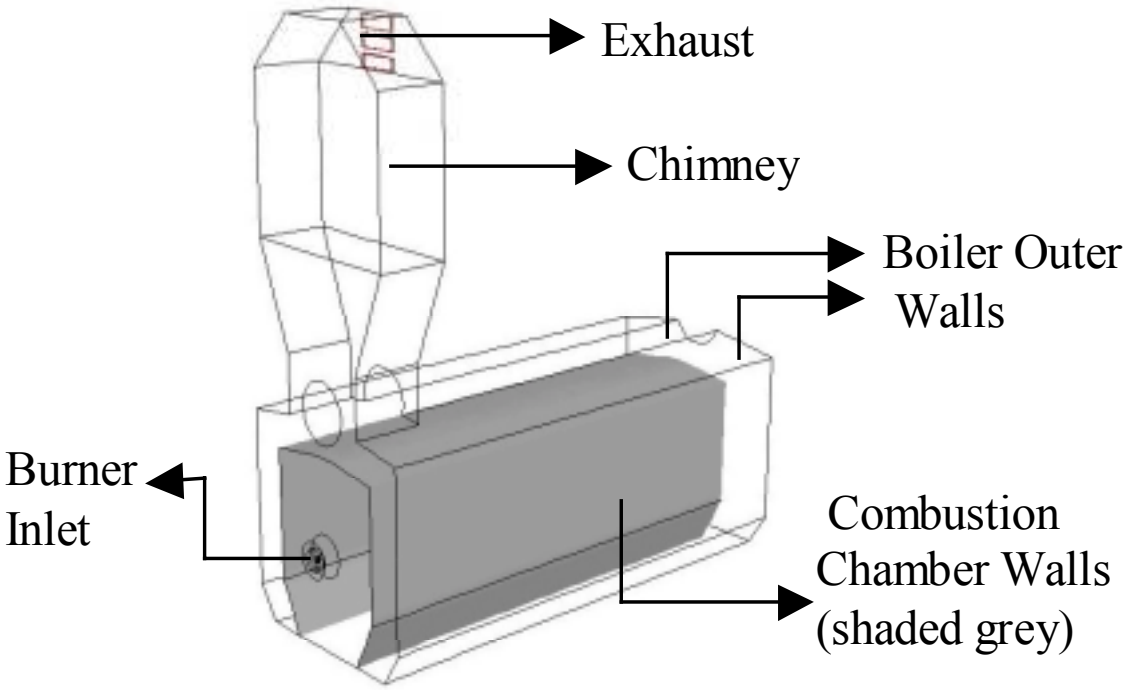

Figure 3.1 A 3-D view of the studied boiler (steam tubes are not shown)

The problem is modeled with the following general assumptions:

1. The flow is steady and incompressible.
2. Variable fluid properties.
3. Turbulent Flow
4. Instantaneous combustion with the chemical reaction much faster than the turbulence time scale.
5. The steam temperature is assumed as the tube wall temperature.

The full three-dimensional Navier-Stokes equations are employed with five species transport equations.

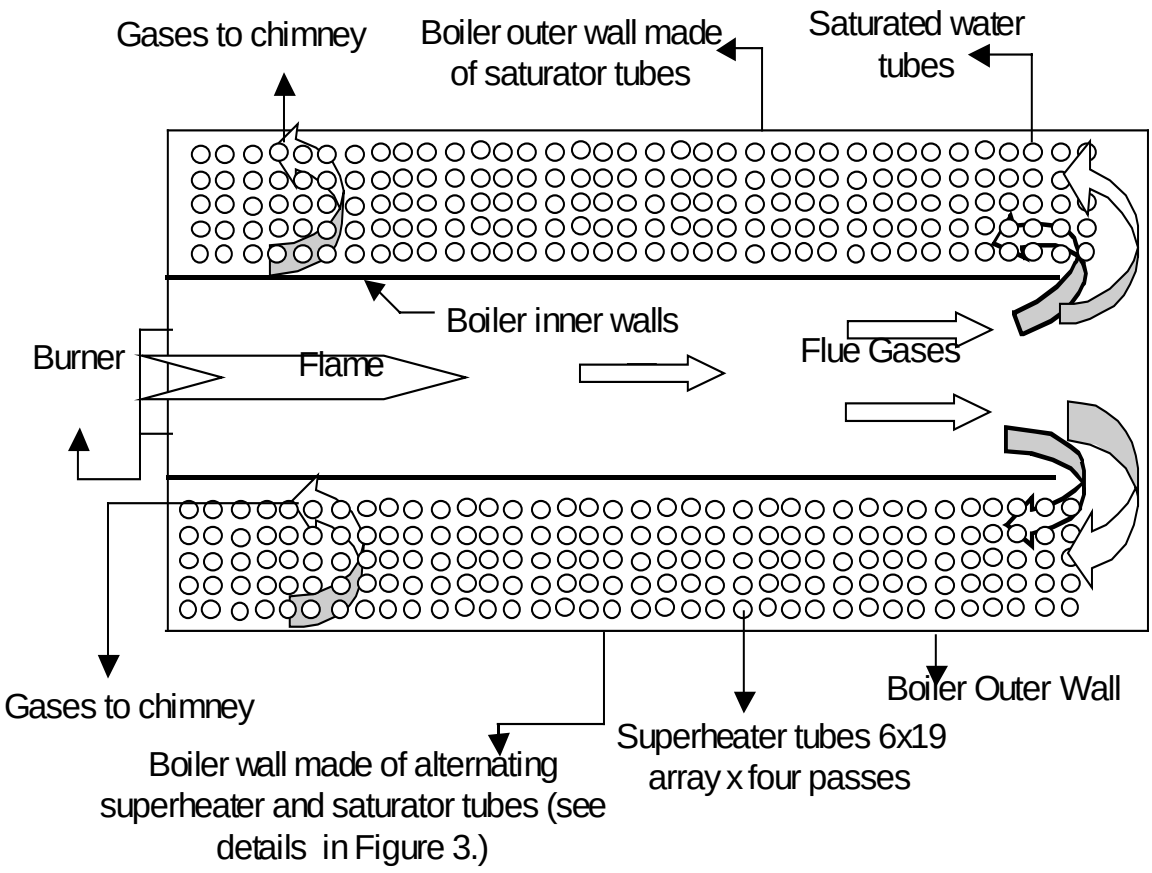

Figure 3.2 a) Top view of the horizontal mid plane of the boiler

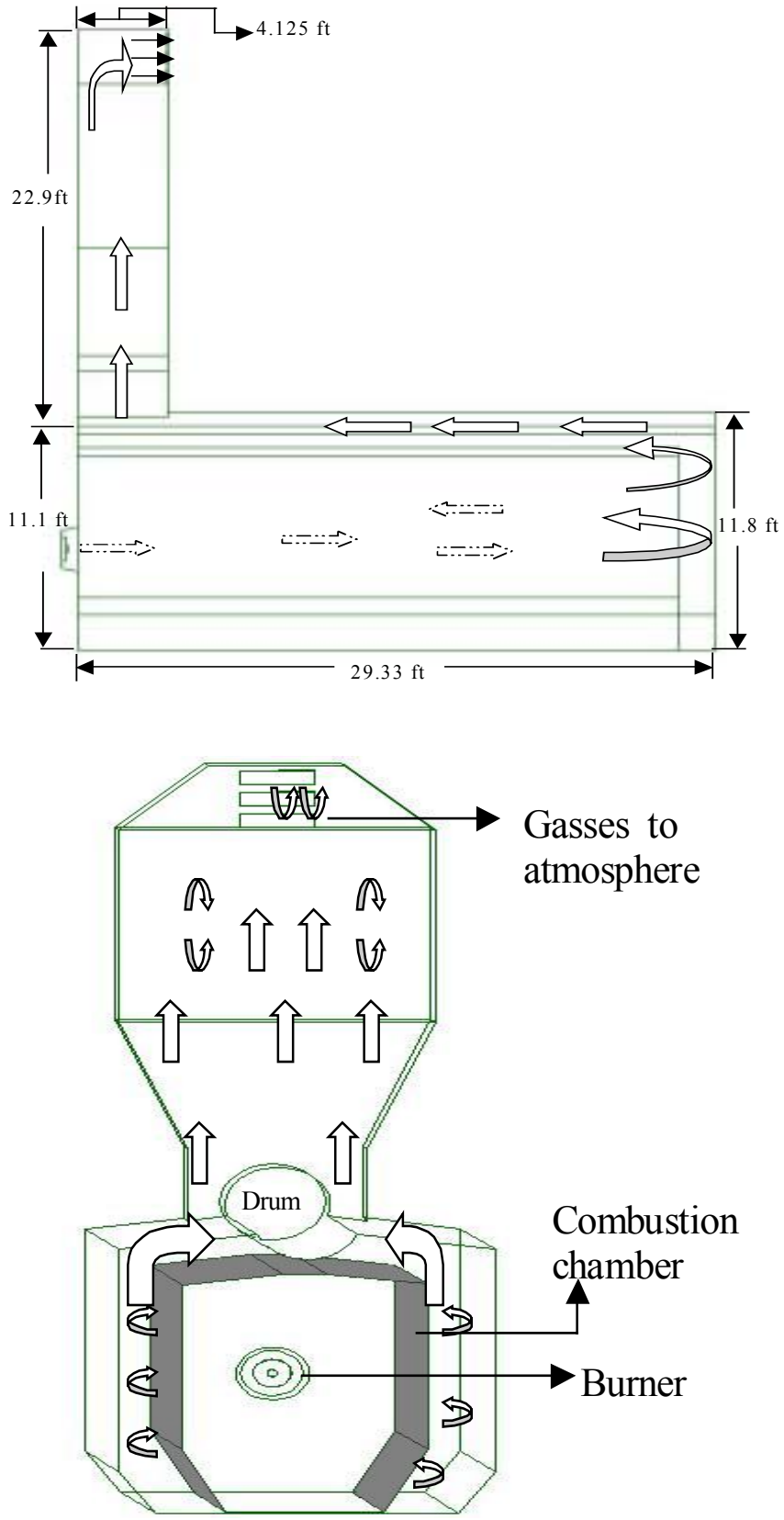

Figure 3.2 b) Side view of the boiler c) Compressed end view looking towards the burner

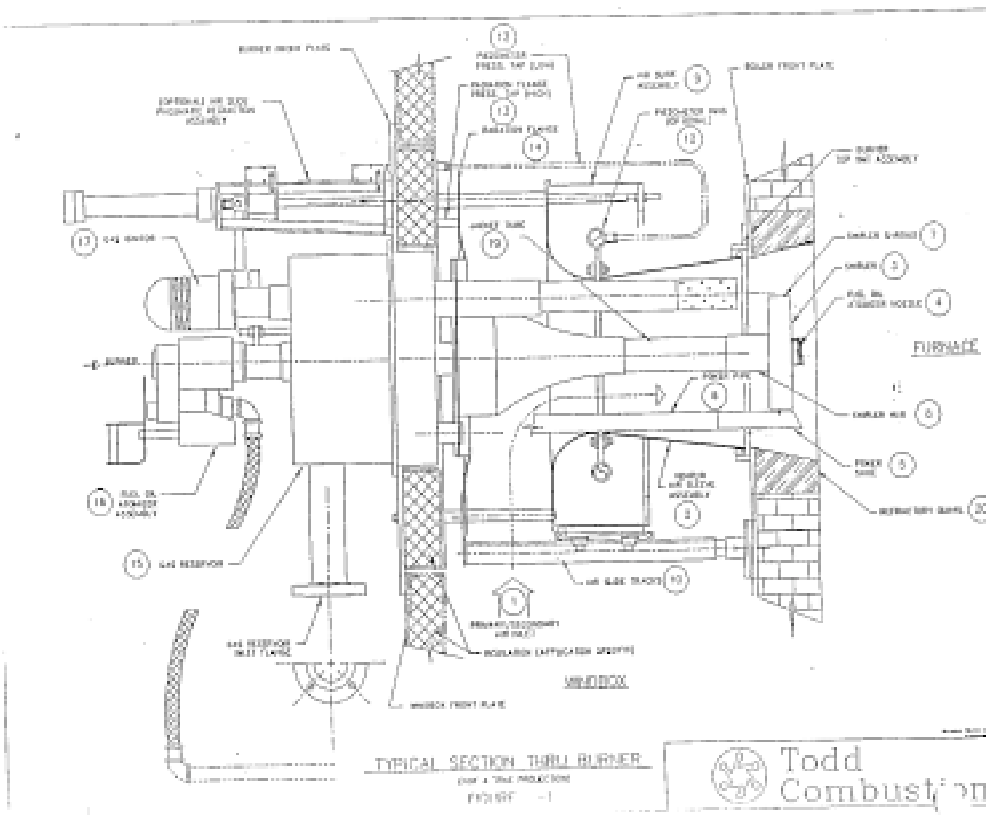

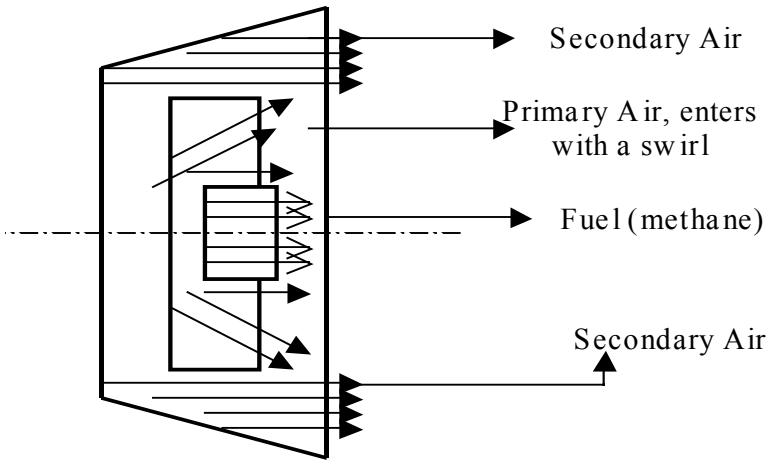

Figure 3.3. (a) Schematic of the burner geometry (b) Simulated burner geometry

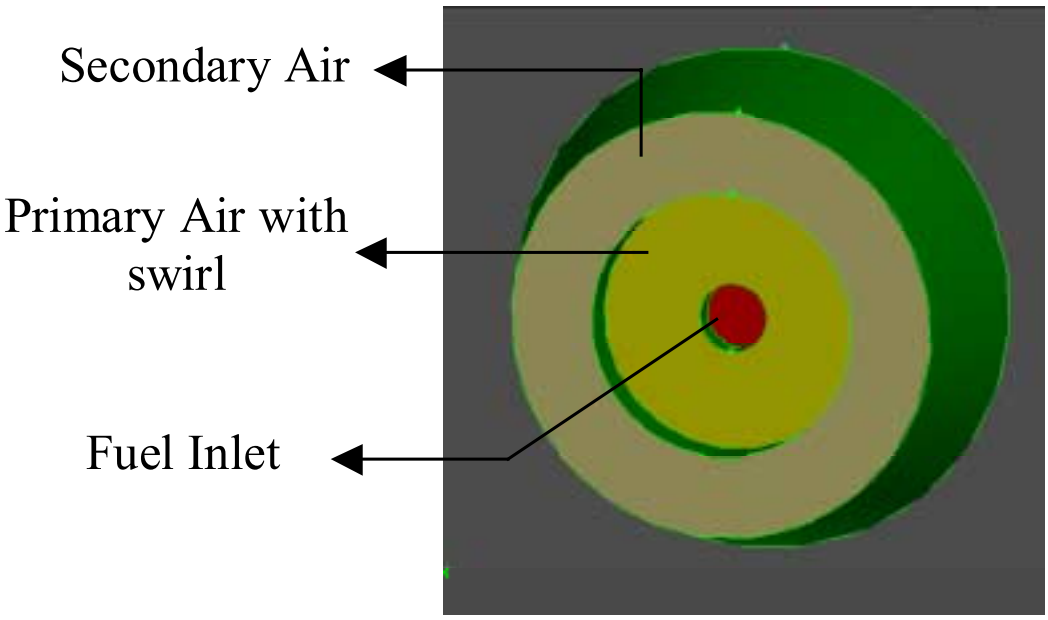

Figure 3.4. Computational model of the 3-D view of the burner exit

3.1 Governing Equations

The conservation equations for mass, momentum and energy conservation in general form are shown below.

$$\frac{\partial \rho}{\partial t} + \nabla \cdot (\rho \vec{v}) = 0 \tag{3.1}$$

$$\frac{\partial}{\partial t}(\rho \vec{v}) + \nabla \cdot (\rho \vec{v}\vec{v}) = -\nabla p + \nabla \cdot (\bar{\bar{\tau}}) + \rho \vec{g} + \vec{F} \tag{3.2}$$

$$\frac{\partial}{\partial t}(\rho E) + \nabla \cdot (\vec{V}(\rho E + p)) = \nabla \cdot \left(k_{eff} \nabla T - \sum_j h_j \vec{J}_j + (\bar{\bar{\tau}}_{eff} \cdot \vec{v}) \right) + S_h \tag{3.3}$$

$\bar{\bar{\tau}}$, the stress tensor is given by

$$\bar{\bar{\tau}} = \mu\left[(\nabla\vec{v} + \nabla\vec{v}^{T}) - \frac{2}{3}\nabla\cdot\vec{v}\cdot I\right] \tag{3.4}$$

where I is the unit tensor.

In energy equation E is given as

$$E = h - \frac{p}{\rho} + \frac{v^2}{2} \tag{3.5}$$

"h" is sensible enthalpy and for incompressible flow it is given as

$$h = \sum_{j} Y_j h_j + \frac{p}{\rho} \tag{3.6}$$

$$h_j = \int_{T_{ref}}^{T} c_{p,j} dT \tag{3.7}$$

T_{ref} is constant taken as 298.15 K

S_h in the energy equation (3.3) is the source term, which is provided by the net enthalpy formation rates from the species transport reactions

The boundary conditions are

Fuel inlet: Mass inlet condition , $\dot{m}_{fuel} = 0.855$ kg/s

Air inlet: $\dot{m}_{primary\ air} = 6.9$ kg/s, $\dot{m}_{secondary\ air} = 13.08$ kg/s

Outlet: Constant pressure outlet condition at P = 1 bar

Walls: Adiabatic or constant wall temperature

- Flow: No-slip condition at the walls; u = 0, v = 0, w = 0.
- Temperature: Walls at the surfaces inside the combustion chamber are covered by the saturating steam tubes at constant temperature at T = 526.68 K
- All the superheaters are set at the constant temperature at T = 672.03 K
- Saturator section: All walls set at T = 526.68 K
- Superheater section: Outer wall is at alternating saturator (T = 526.86 K) and superheater temperature (T = 672.03 K)
- Chimney walls: Adiabatic

3.2 Computational Domain

In view of the complex geometry of the boiler, the simulation is conducted in three stages.

Stage 1: In this stage of study, the computational domain includes the entire boiler but excludes water/steam tubes. The computational domain with all boundary conditions is shown in Figure 3.5.

Stage 2: In stage 2 of study, detailed simulation of the saturating and superheating regions is performed. Due to the large numbers of saturator and superheater tubes, the simulation is broken down into 33 sub-sections. Each sub-section includes 4x2x2 tubes. The geometry and boundary conditions are shown in Figure 3.6 and Figure 3.7. Figure 3.6 (b) shows the expanded view of

the saturating and superheating regions. Initially only combustion chamber part section, as shown in Figure 3.6 (a), is modeled and simulated. The outlet profile solution (velocity, temperature and species concentrations) of the combustor section is used as the inlet profile condition for the saturating/superheating regions (Figure 3.7). A total of 32 sub-sections of similar computational domain as shown in Figure 3.7 are simulated. Each uses the outlet profile solution of the previous sub-section as the inlet profile boundary condition. In this approach the inlet pressure information will be calculated and updated to satisfy overall mass and momentum conservation.

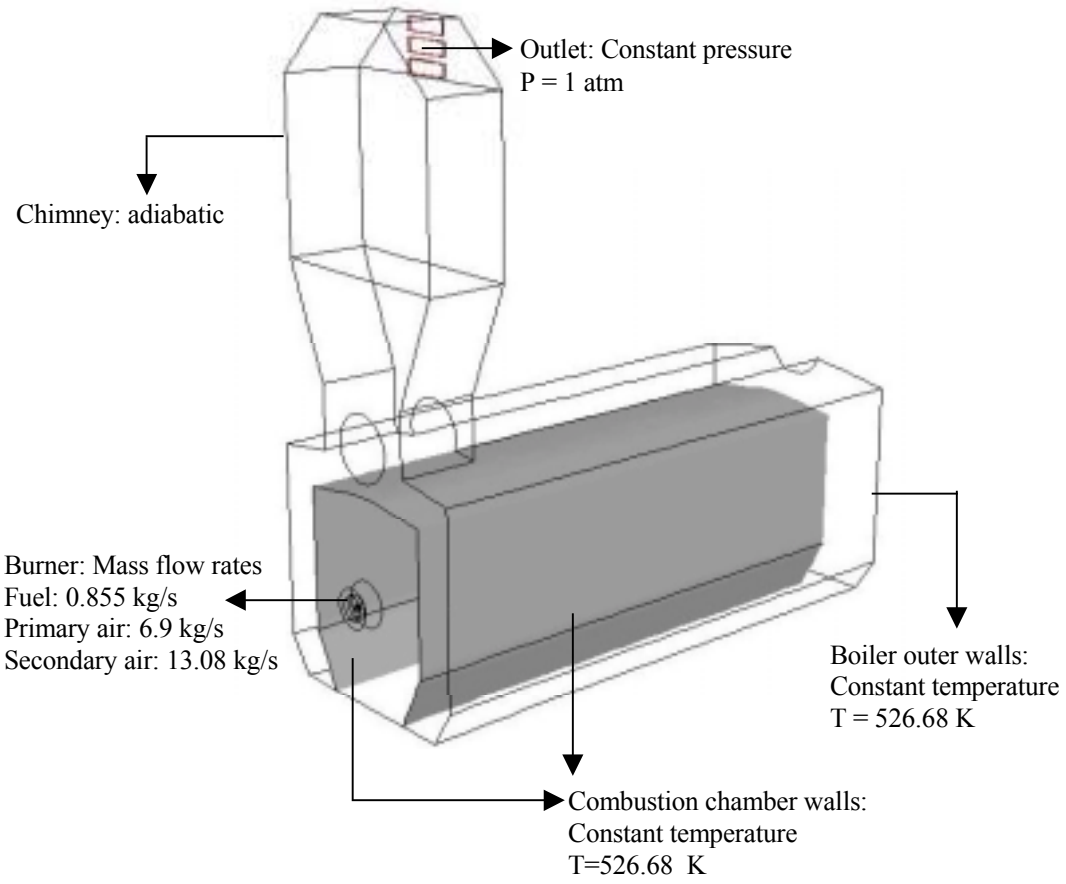

Figure 3.5 Computational domain and boundary conditions for stage 1: The entire boiler is employed as the computational domain excluding water/steam tubes.

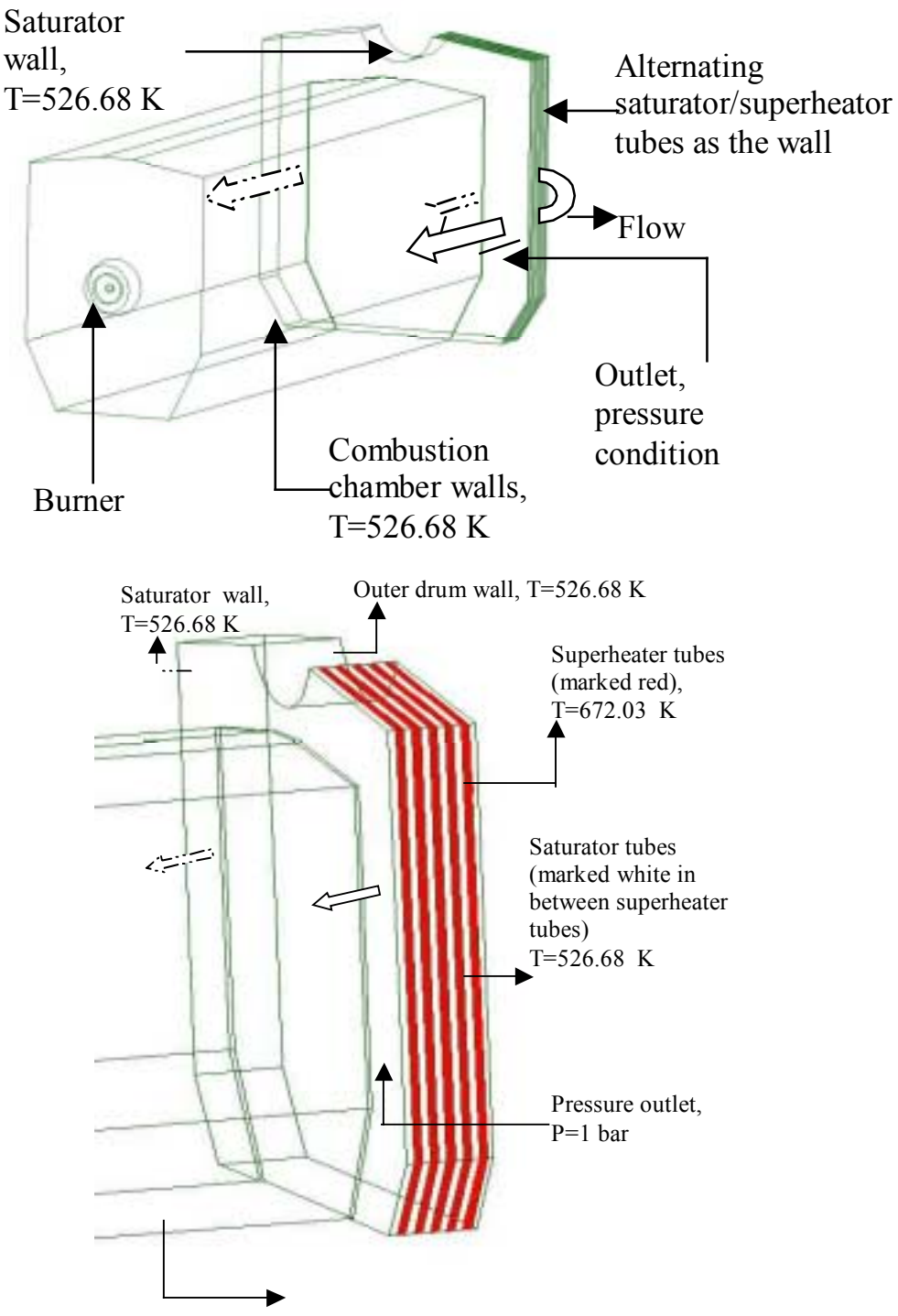

Figure 3.6 (a) Computational domain for combustion chamber with boundary conditions for stage-2 study (b) Computational sub-domain with boundary conditions for the saturating and superheating regions.

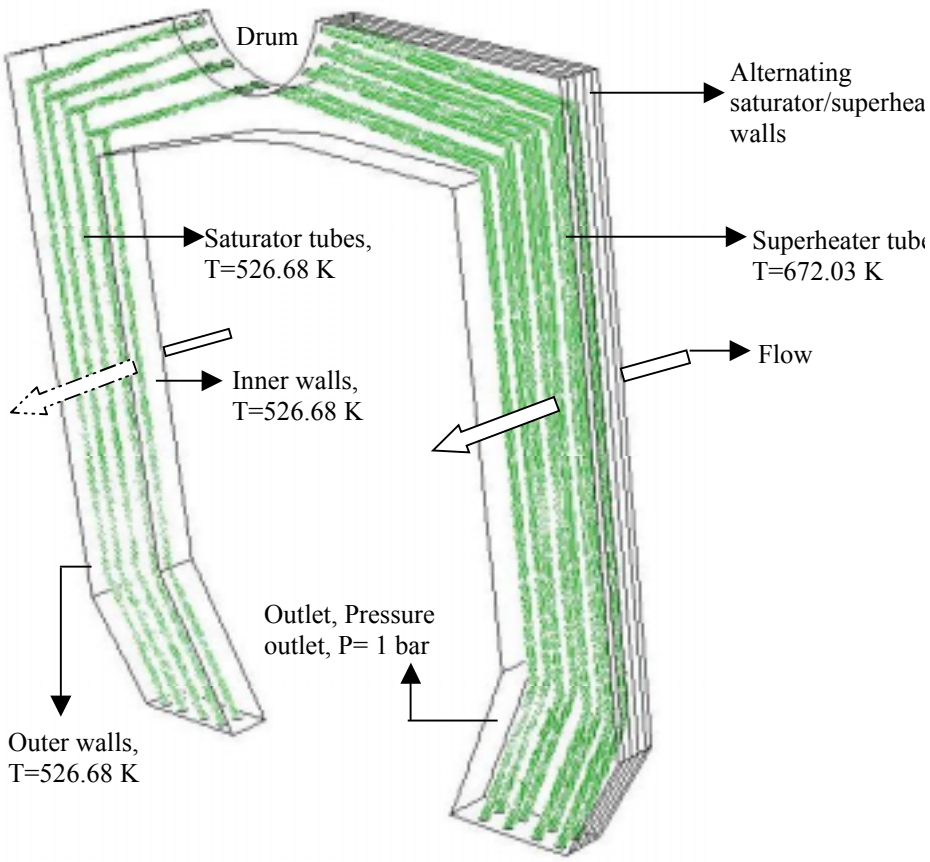

Figure 3.7 A representative computational sub-domain with boundary conditions for the saturating and superheating regions in stage-2 simulation

Stage 3: In this phase of study, the outlet results of stage 2 are used to calculate the flow in the chimney section. For this stage the computational domain and boundary conditions are shown in figure 3.8. The outlet profile (velocity, temperature and species concentration) solution of the last sub-section of stage 2 is taken as the inlet profile condition for this stage.

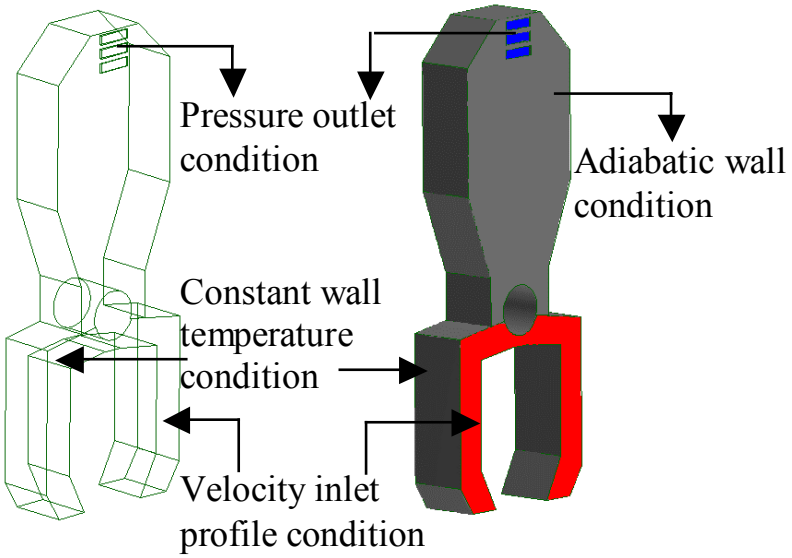

Figure 3.8 Computational domain with boundary conditions for the chimney section in stage-3 simulation

3.3 Turbulence Model

Turbulent flows are characterized by spectral broad-brand, randomly fluctuating velocity fields. These fluctuations mix transported quantities such as momentum, energy, and species concentration, and cause the transported quantities to fluctuate as well. Since these fluctuations can be of small scale and high frequency, they are too computationally intensive to simulate directly in practical engineering calculations. Instead, the instantaneous (exact) governing equations can be time-averaged, ensemble-averaged, or otherwise manipulated to remove the small scales, resulting in a modified set of equations that are computationally less expensive to solve. However, the modified equations contain additional unknown variables, and turbulence models are needed to determine these variables in terms of known quantities.

The following turbulence models are available in the public literature:

- Spalart-Allmaras model
- κ-ε models
    - Standard κ-ε model
    - Renormalization-group (RNG) κ-ε model
    - Realizable κ-ε model
- κ-ω models
    - Standard κ-ω model
    - Shear-stress transport (SST) κ-ω model
- υ^2-f model
- Reynolds stress model (RSM)
- Large eddy simulation (LES) model

In view of the complex flow field in the boiler, this study selects the standard κ-ε model due to its suitability for a wide range of wall-bound and free-shear flows. The standard κ-ε model is the simplest of turbulence two-equation model in which the solution of two separate transport equations allows the turbulent velocity and length scales to be independently determined. The κ-ε model is a semi-empirical model with several constants obtained from experiments.

All the three κ-ε models have similar forms, with major differences in the method of calculating the turbulent viscosity, the turbulent Prandtl numbers, and the generation and destruction terms in the k-ε equations.

The standard κ-ε model is a semi-empirical model based on model transport equations for the turbulence kinetic energy (κ) and its dissipation rate (ε). The model transport equation for κ is

derived from the exact equation, while the model transport equation for ε is obtained using physical reasoning and bears little resemblance to its mathematically exact counterpart.

The turbulence kinetic energy, κ, and its rate of dissipation, ε, are obtained from the following transport equations:

$$\frac{\partial}{\partial t}(\rho\kappa)+\frac{\partial}{\partial x_i}(\rho\kappa u_i)=\frac{\partial}{\partial x_j}\left[(\mu+\frac{\mu_t}{\sigma_k})\frac{\partial\kappa}{\partial x_j}\right]+G_k+G_b-\rho\varepsilon-Y_M+S_k \tag{3.8}$$

$$\frac{\partial}{\partial t}(\rho\varepsilon)+\frac{\partial}{\partial x_i}(\rho\varepsilon u_i)=\frac{\partial}{\partial x_j}\left[(\mu+\frac{\mu_t}{\sigma_\varepsilon})\frac{\partial\varepsilon}{\partial x_j}\right]+C_{1\varepsilon}\frac{\varepsilon}{\kappa}(G_k+C_{3\varepsilon}G_b)-C_{2\varepsilon}\rho\frac{\varepsilon^2}{\kappa}+S_\varepsilon \tag{3.9}$$

In these equations, G_k represents the generation of turbulence kinetic energy due to the mean velocity gradients and the Reynolds stress, calculated as

$$G_\kappa=-\rho\overline{u_i'u_j'}\frac{\partial u_j}{\partial x_i} \tag{3.10}$$

G_b represents the generation of turbulence kinetic energy due to buoyancy, calculated as

$$G_b=\beta g_i\frac{\mu_t}{Pr_t}\frac{\partial T}{\partial x_i} \tag{3.11}$$

where Pr_t is the turbulent Prandtl number and g_i is the component of the gravitational vector in the i-th direction. For standard κ-ε model the value for Pr_t is set 0.85 in this study.

β is the coefficient of thermal expansion and is given as

$$\beta = -\frac{1}{\rho}\left(\frac{\partial \rho}{\partial T}\right)_p \tag{3.12}$$

In equation (3.8), Y_M represents the contribution of the fluctuating dilatation in compressible turbulence to the overall dissipation rate, and is given as

$$Y_M = 2\rho\varepsilon M_t^2 \tag{3.13}$$

where M_t is the turbulent Mach number, given as

$$M_t = \sqrt{\frac{k}{a^2}} \tag{3.14}$$

where $a = \sqrt{\gamma RT}$ is the speed of sound.

The turbulent (or eddy) viscosity, μ_t, is computed by combining κ and ε as

$$\mu_t = \rho C_\mu \frac{\kappa^2}{\varepsilon} \tag{3.15}$$

$C_{1\varepsilon}$, $C_{2\varepsilon}$, $C\mu$, σ_κ, and σ_t are constants and have the following values

$$C_{1\varepsilon} = 1.44,\ C_{2\varepsilon} = 1.92,\ C_\mu = 0.09,\ \sigma_\kappa = 1.0,\ \sigma_t = 1.3 \tag{3.16}$$

These constant values have been determined from experiments with air and water for fundamental turbulent shear flows including homogeneous shear flows and decaying isotropic

grid turbulence. They have been found to work fairly well for a wide range of wall-bounded and free-shear flows. The initial values for κ and ε at the inlets and outlet are set as 1 m^2/s^2 and 1 m^2/s^3 respectively.

In general, turbulent flows are significantly affected by the presence of walls. Very close to the wall, viscous damping reduces the tangential velocity fluctuations, while kinematic blocking reduces the normal fluctuations and away from the wall the turbulence is increased by the production of turbulence kinetic energy. In the near-wall region the solution variables have large gradients, and the momentum and other scalar transports occur strongly. Therefore, accurate representation of the flow in the near-wall region is required for successful predictions of wall-bounded turbulent flows.

The κ-ε turbulence model used in this study is primarily valid for turbulent core flows (i.e., the flow in the regions somewhat far from walls). Wall functions are used to make this turbulence model suitable for wall-bounded flows. Wall functions are a collection of semi-empirical formulas and functions that link the solution variables at the near-wall cells and the corresponding quantities on the wall. The wall functions consists of the following:

- Laws of the wall for mean velocity and temperature and other scalars
- Equations for near-wall turbulent quantities

The law-of –the-wall for mean velocity gives

$$U^+ = \frac{1}{\kappa}\ln(Ey^+) \tag{3.17}$$

where $U^+ \equiv \frac{U_P C_\mu^{0.25} k_P^{0.5}}{\tau_w / \rho}$

$$y^+ \equiv \frac{\rho C_\mu^{0.25} k_P^{0.5} y_P}{\mu}$$

k = von Karman constant (=0.42)

E = empirical constant (=9.793)

U_P = mean velocity of the fluid at point P

k_P = turbulence kinetic energy at point P

y_P = distance from point P to the wall

μ = dynamic viscosity of the fluid

The logarithmic law for mean velocity is valid for y^+ > about 30 to 60

The law-of-the-wall for temperature is given

$$\begin{aligned} T^+ &\equiv \frac{(T_w - T_P)\rho c_p C_\mu^{0.25} k_P^{0.5}}{\dot{q}} = \Pr y^+ + 0.5\rho \Pr \frac{C_\mu^{0.25} k_P^{0.5}}{\dot{q}} U_P^2 \qquad (y^+ < y_T^+) \\ &= \Pr_t [\frac{1}{k} \ln(Ey^+) + P] + 0.5\rho \frac{C_\mu^{0.25} k_P^{0.5}}{\dot{q}} \{\Pr_t U_P^2 + (\Pr - \Pr_t) U_c^2 \qquad (y^+ > y_T^+) \end{aligned} \tag{3.18}$$

where P is computed using the formula

$$P = 9.24 \left[\left(\frac{P_r}{P_{rt}} \right)^{3/4} - 1 \right] \left[1 + 0.28 e^{-0.007 \Pr / \Pr_t} \right] \tag{3.19}$$

k_f = thermal conductivity of the fluid

ρ = density of fluid

c_p = specific heat of fluid

$\dot{q}$ = wall heat flux

T_p = temperature at the cell adjacent to the wall

T_w = temperature at the wall

Pr = molecular Prandtl number ($\mu c_p / \kappa_f$)

Pr_t = turbulent Prandtl number (=0.85 at the wall)

A = 26 (Van Driest constant)

κ = 0.4187 (von Karman constant)

E = 9.793 (wall function consatant)

U_c = mean velocity magnitude at $y^+ = y_T^+$

For κ-ε turbulence model, wall adjacent cells are considered to solve the κ-equation. The boundary condition for κ imposed at the wall is $\frac{\partial \kappa}{\partial n} = 0$, where "n" is the local coordinate normal to the wall. The production of kinetic energy, G_k, and its dissipation rate, ε, at the wall-adjacent cells, which are the source terms in κ equation, are computed on the basis of equilibrium hypothesis with the assumption that the production of κ and its dissipation rate assumed to be equal in the wall-adjacent control volume. The production of κ and ε is computed as

$$G_k \approx \tau_w \frac{\partial U}{\partial y} = \tau_w \frac{\tau_w}{\kappa \rho C_\mu^{0.25} k_P^{0.5} y_P} \qquad (3.20.a)$$

$$\varepsilon_P = \frac{C_\mu^{0.75} k_p^{1.5}}{\kappa y_P} \qquad (3.20.b)$$

3.4 Radiation Model

The radiative transfer equation for an absorbing, emitting, and scattering medium at position $\vec{r}$ in the direction $\vec{s}$ is given as

$$\frac{dI(\vec{r},\vec{s})}{ds} + (a+\sigma_s)I(\vec{r},\vec{s}) = an^2\frac{\sigma T^4}{\pi} + \frac{\sigma_s}{4\pi}\int_0^{4\pi} I(\vec{r},\vec{s}')\Phi(\vec{s}\cdot\vec{s}')d\Omega' \qquad (3.21.a)$$

where $\vec{r}$ is position vector

$\vec{s}$ is direction vector

$\vec{s}'$ is scattering direction vector

s is path length

a is absorption coefficient

n is refractive index

σ_s is scattering coefficient

I is radiation intensity, which depends on position $\vec{r}$ and direction $\vec{s}$

T is local temperature

Φ is phase angle

Ω' is solid angle

The Rosseland radiation model [7] is used in this study, which is valid for medium optical thickness. The radiative heat flux in a gray medium is approximated by the following equation

$$q_r = -\Gamma\nabla G \qquad (3.21.b)$$

where Γ is given as

$$\Gamma = \frac{1}{(3(a+\sigma_s) - C\sigma_s)} \qquad (3.21.c)$$

$$G = 4\sigma T^4 \qquad (3.21.d)$$

In Rosseland model it is assumed that the intensity is the black-body intensity at the gas temperature. Therefore substituting equation (3.21.d) into equation (3.21.b) gives

$$q_r = -16\sigma\Gamma T^3 \nabla T \tag{3.21.e}$$

3.5 Combustion Model

Modeling for combustion ranges from nonreacting to multiple reactions with multiple species, and finite rate kinetics. In this study, combustion of methane is modeled by a single-step reaction. The mixing and transport of chemical species is modeled by solving the conservation equations describing convection, diffusion, and reaction sources for each component species. The species transport equations are solved by predicting the local mass fraction of each species, Y_i, through the solution of a convection-diffusion equation for the i-th species. The species transport equation in general form is given as:

$$\frac{\partial}{\partial t}(\rho Y_i) + \nabla \cdot (\rho \vec{v} Y_i) = -\nabla \cdot \vec{J}_i + R_i + S_i \tag{3.22}$$

where R_i is the net rate of production of species i by chemical reaction. S_i is the rate of creation by addition from the dispersed phase plus any user-defined sources. $\vec{J}_i$ is the diffusion flux of species i, which arises due to concentration gradients. Mass diffusion for laminar flows is given as

$$\vec{J}_i = -\rho D_{i,m} \nabla Y_i \tag{3.23}$$

For turbulent flows, mass diffusion flux is given as

$$\vec{J}_i = -\left(\rho D_{i,m} + \frac{\mu_t}{Sc_t} \right) \nabla Y_i \tag{3.24}$$

where Sc_t is the turbulent Schmidt number given as $\frac{\mu_t}{\rho D_t}$, where μ_t is the turbulent viscosity and D_t is the turbulent diffusivity.

The reaction rate that appears as source term in equation (3.22) is given by the turbulence-chemistry interaction model called the eddy-dissipation model. The overall rate of reaction for most fast burning fuels is controlled by turbulent mixing. The net rate of production of species i due to reaction r, $R_{i,r}$, is given by the smaller of the two given expressions below:

$$R_{i,r} = \nu'_{i,r} M_{w,i} A\rho \frac{\varepsilon}{\kappa} \min_R \left(\frac{Y_R}{\nu'_{R,r} M_{w,R}} \right) \tag{3.25}$$

$$R_{i,r} = \nu'_{i,r} M_{w,i} AB\rho \frac{\varepsilon}{\kappa} \frac{\sum_P Y_P}{\sum_j^N \nu''_{j,r} M_{w,j}} \tag{3.26}$$

where Y_P is the mass fraction of any product species, P

Y_R is the mass fraction of a particular reactant, R

A is an empirical constant equal to 4.0

B is an empirical constant equal to 0.5

$\nu'_{i,r}$ is the stoichiometric coefficient for reactant “i” in reaction “r”.

$\nu''_{j,r}$ is the stoichiometric coefficient for product “j” in reaction “r”

In the above equations (3.25) and (3.26), the chemical reaction rate is governed by the large-eddy mixing time scale, $\frac{\kappa}{\varepsilon}$, and an ignition source is not required. This is based on the assumption that the chemical reaction is much faster than the turbulence mixing time scale, so the actual chemical reaction is not important.

In this study, methane (CH_4) is used as fuel. The complete stoichiometric combustion equation is given below:

$$CH_4 + 2(O_2 + 3.76\ N_2) \rightarrow CO_2 + 2H_2O + 7.52\ N_2 \quad (3.27)$$

3.6 Modeling and Calculation of NO_x Emissions

NOx emission consists of mostly nitric oxide (NO). Less significant are nitrogen oxide, NO_2 and nitrous oxide (N_2O). NOx is a precursor for photochemical smog, it contributes to acid rain, and causes ozone depletion. Thus, NOx is a pollutant.

To predict NOx emission, transport equation for nitric oxide (NO) concentration are solved. With fuel NOx sources, an additional transport equation for an intermediate species (HCN or NH_3) are solved. Since NOx concentrations generated in a combustion system are generally low, NOx chemistry has negligible influence on the predicted flow fields, and species concentrations. Therefore, the calculation of NOx concentrations can be post-processed after the thermal flow and major species concentrations are computed.

The NOx transport equations are solved based on a given flow field and combustion solution. NOx is post processed from a combustion simulation, thus an accurate combustion solution becomes a prerequisite of NOx production. For example, thermal NOx production

doubles for every 90 K temperature increase when the flame temperature is about 2200 K. Accurate prediction of NOx parametric trends can cut down on the number of laboratory tests, allow more design variations to be studied, shorten the design cycle, and reduce product development cost.

In laminar flames, and at the molecular level within turbulent flames, the formation of NOx can be attributed to four distinct chemical kinetic processes: thermal NOx formation, prompt NOx formation, fuel NOx formation, and reburning. Thermal NOx is formed by the oxidation of atmospheric nitrogen present in the combustion air. Prompt NOx is produced by high-speed reactions at the flame front, and fuel NOx is produced by oxidation of nitrogen contained in the fuel. The reburning mechanism reduces the total NOx formation by accounting for the reaction of NO with hydrocarbons.

The mass transport equation for the NO species is solved taking into account convection, diffusion, production and consumption of NO and related species. The effect of residence time in NOx mechanisms, a Lagrangian reference frame concept, is included through the convection terms in the governing equations written in the Eulerian reference frame. For thermal and prompt NOx mechanisms, only the NO species transport equation is needed which is given as

$$\frac{\partial}{\partial t}(\rho Y_{NO}) + \nabla \cdot (\rho \vec{v} Y_{NO}) = \nabla \cdot (\rho D \nabla Y_{NO}) + S_{NO} \tag{3.28}$$

Thermal NOx

The formation of thermal mechanism dominates in high-temperature combustion over a fairly wide range of equivalence ratios. The formation of thermal NOx is determined by a set of

highly temperature-dependent chemical reactions known as the extended Zeldovich mechanism described

$$O + N_2 \underset{k_1 r}{\overset{k_1 f}{\Leftrightarrow}} NO + N \tag{3.29}$$

$$N + O_2 \underset{k_2 r}{\overset{k_2 f}{\Leftrightarrow}} NO + O \tag{3.30}$$

$$N + OH \underset{k_3 r}{\overset{k_3 f}{\Leftrightarrow}} NO + H \tag{3.31}$$

The net rate of formation of NO via extended Zeldovich mechanism reactions described above from equations (3.29) to (3.31) is given by

$$d[NO] / dt = K_{1f}[O][N_2] + K_{2f}[N][O_2] + K_{3f}[N][OH] - K_{1r}[NO][N] - K_{2r}[NO][O] - K_{3r}[NO][H] \tag{3.32}$$

Where all concentrations have units of gmol/m^3. In order to calculate the formation rates of NO and N, the concentrations of O, H, OH are required. The rate constants for these reactions have been measured in numerous experimental studies. The expressions for the rate coefficients for above reactions are:

$$K_{1f} = 1.8*10^{11} \exp [-38{,}370/T\ (K)] \quad m^3 / kmol\text{-}s, \tag{3.33}$$

$$K_{1r} = 3.8*10^{10} \exp[-425/T\ (K)] \quad m^3 / kmol\text{-}s, \tag{3.34}$$

$$K_{2f} = 1.8*10^{7} \exp [-4{,}680/T\ (K)] \quad m^3 / kmol\text{-}s, \tag{3.35}$$

$$K_{2r} = 3.8*10^{6} \exp[-20{,}820/T\ (K)] \quad m^3 / kmol\text{-}s, \tag{3.36}$$

$$K_{3f} = 7.1*10^{10} \exp [-450/T\ (K)] \quad m^3 / kmol\text{-}s, \tag{3.37}$$

$$K_{3r} = 1.7*10^{11} \exp[-24{,}560/T\ (K)] \quad m^3 / kmol\text{-}s \tag{3.38}$$

Where K_{1f} is forward reaction rate for reaction 1 and K_{1r} is the backward reaction rate for reaction 1 and in a similar manner for reactions 2 and 3.

The rate of formation of NOx is significant only at high temperatures because fixation of nitrogen requires the breaking of the strong N_2 triple bond. A quasi-steady state can be established for a fuel-lean flame, where the rate of consumption of free nitrogen atoms becomes equal to the rate of its formation. This assumption is valid for most combustion cases except in extremely fuel-rich combustion conditions. In quasi-steady state the NO formation rate is predicted by the following equation:

$$\frac{d[NO]}{dt} = 2k_1[O][N_2]\frac{\left(1 - \frac{k_{-1}k_{-2}[NO]^2}{k_1[N_2]k_2[O_2]}\right)}{\left(1 + \frac{k_{-1}[NO]}{k_2[O_2] + k_3[OH]}\right)} \tag{3.39}$$

where the sub-scripts , negative is for backward reaction and positive is for forward reaction and the number (1,2,3) stands for the reaction number in the Zeldovich mechanism (Eq. 3.29, 3.30, and 3.31).

From the above equation it is clear that the rate of formation of NO will increase with increasing oxygen concentration. The O-atom concentration is calculated by the equations given below

- For the equilibrium assumption

$$[O] = 3.97 \times 10^5 T^{-1/2} [O_2]^{\frac{1}{2}} e^{-31090/T} \tag{3.40}$$

- For a partial equilibrium assumption

$$[O] = 36.64\, T^{1/2} [O_2]^{\frac{1}{2}} e^{-27123/T} \tag{3.41}$$

- Using the local O_2-species mass fraction.

The source term due to thermal NO_x formation in equation (3.28) is calculated as

$$S_{thermal,\,NO} = M_{w,\,NO} \frac{d[NO]}{dt} \tag{3.42}$$

where $M_{w,\,NO}$ is the molecular weight of NO, and $\frac{d[NO]}{dt}$ is computed from Equation (3.39)

Prompt NO_x

During combustion of hydrocarbon fuels, the NOx formation rate can exceed that produced from direct oxidation of nitrogen molecules (i.e., thermal NOx). Prompt NOx can be formed in a significant quantity in some combustion environments, such as in low-temperature, fuel-rich conditions and where residence times are short. Surface burners, staged combustion systems, and gas turbines can create such conditions.

The formation of prompt NOx is governed by a set of equations known as Fenimore mechanism given below:

$$CH + N_2 \Leftrightarrow HCN + N \tag{3.43}$$

$$C + N_2 \Leftrightarrow CN + N \tag{3.44}$$

$$N + O_2 \Leftrightarrow NO + O \tag{3.45}$$

$$HCN + OH \Leftrightarrow CN + H_2O \quad (3.46)$$

$$N + OH \Leftrightarrow NO + H \quad (3.47)$$

The scheme of Fenimore mechanism is that hydrocarbon radicals react with molecular nitrogen to form amines or cyano compounds. The amines and cyano compounds are then converted to inverted compounds that ultimately form NO.

In prompt NOx mechanism, reaction (3.43) is of primary importance. The majority of the NOx at the flame base is prompt NOx formed by the CH reaction and the prompt NOx formation rate is given as

$$\frac{d[NO]}{dt} = k_0[CH][N_2] \quad (3.48)$$

The prediction of prompt NOx formation within the flame requires coupling of the NOx kinetics to an actual hydrocarbon combustion mechanism. Hydrocarbon combustion mechanisms involve many steps and, as mentioned previously, are extremely complex and costly to compute. The rate for most hydrocarbon is given as

$$\frac{d[NO]}{dt} = fk'_{pr}[O_2]^a[N_2][FUEL]e^{-E'_a/RT} \quad (3.49)$$

where "a" is the oxygen reaction order, R is the universal gas constant.

$k_{pr} = 1.2 \times 10^7 (RT/p)^{a+1}$ and

$E_a = 60$ kcal/gmol

The source term due to prompt NOx mechanism in equation (3.28) is given as

$$S_{prompt\ ,NO} = M_{w,NO} \frac{d[NO]}{dt} \tag{3.50}$$

where $M_{w,\ NO}$ is the molecular weight of NO, and $\frac{d[NO]}{dt}$ is computed from Equation (3.49). In above equation (3.49) f is a correction factor and is given as

$$f = 4.75 + 0.0819\ n - 23.2\phi + 32\phi^2 - 12.2\phi^3 \tag{3.51}$$

where n is the number of carbon atoms per molecule for the hydrocarbon fuel, and ϕ is the equivalence ratio which is defined as

ϕ = (Actual air-fuel ratio) / (stoichiometric air-fuel ratio)

CHAPTER FOUR

COMPUTATIONAL METHOD

4.1 Fluent Background

In the past two decades, because of the continuous increase of computer speed, computational fluid dynamics (CFD) technique has become a widely used tool in engineering, biomedical, and environmental research and development. This study uses the commercial code FLUENT (version 6.1.22) as the simulation tool.

FLUENT is a finite volume CFD code for solving transport equations of mass, momentum, energy conservation, and species concentrations. FLUENT software is used for simulation, visualization, and analysis of fluid flow, heat and mass transfer, and chemical reactions. The organizational program structure of FLUENT package is shown below:

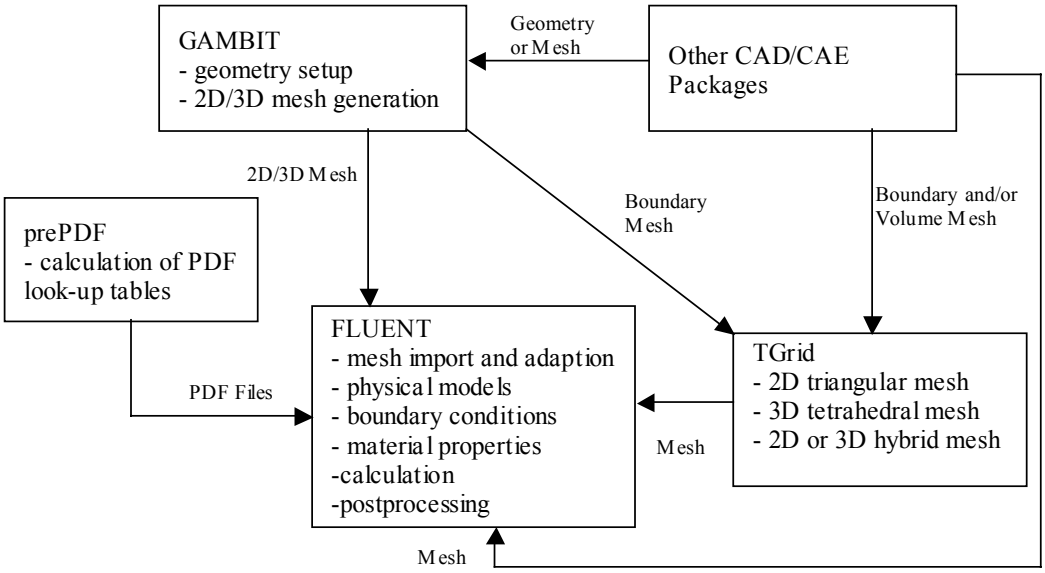

Figure 4.1 Organizational program structure of FLUENT

4.2 Solution Methodology

Fluent employs the finite-volume method to discretize the partial differential equations. The following general steps are taken for modeling fluid flow and heat transfer

- Pre-processing , done using Gambit
    - Defining geometry
    - Grid or Mesh
    - Boundary Conditions
- Processing
    - Solving equations, using appropriate choices for solution parameters
- Post-processing
    - Analyzing results

Pre-processing

The pre-processing phase of a problem includes all the steps from the initial problem definition through the beginning of computation. At this phase, the scope of the geometry to be studied is considered. This includes geometry creation, mesh generation, model selection, fluid property specification, and enabling and setting up the models.

Processing

The processing phase is the phase where the calculations begin, after generating the mesh and setting up the problem for solution. The processing phase includes the steps of solving the equations, observe the progress of the CFD code toward convergence and perhaps adjust under-relaxation factors and adapt the grid. It is always the stated goal to obtain a solution that is grid-independent.

Post-processing

The post-processing phase includes the necessary outputs for the analyst to understand the results of the simulation. The outputs necessary are the x-y plots (e.g., temperature vs. position along the burner centerline), contour plots, velocity vectors plots, streamline plots, and combinations and animations of these outputs. The production of these different sorts of outputs becomes very important in communicating the results of a simulation. In addition to still images, animations can be effectively used to illustrate CFD results. Animated velocity vectors and streamlines can illustrate the path of the fluid flow in internal and external flow problems.

4.3 Computational Grid

Geometry modeling is based on constructing a mesh for the studied boiler. In the model burner inlets are defined with circular shapes with the same effective areas as the real burner, to get the same incoming velocities. Three-dimensional tetrahedral mesh is used for meshing the entire boiler. Figure 4.2 illustrates the model geometry with computational grid for the current study. In this study boundary layer is not important in the combustion chamber and exhaust chimney sections but is important in the saturating/superheating sections. Wall function is used to link the solution variables at the near-wall cells and the corresponding quantities on the wall. The wall boundary conditions for the solution variables, including mean velocity, temperature, species concentration, k, and ε, are all taken care of by the wall functions.

4.4 Combustion Model

The combustion model consists of the following sub-models:

- Three-dimensional flow is described by the Navier-Stokes equations
- Turbulence is accounted by the standard κ-ε model with wall-functions
- Combustion is described by the conserved scalar approach to high temperature species-transport combustion
- Chemistry is described with one-step global reactions.
- Properties of the gas mixture are composition and temperature dependant.

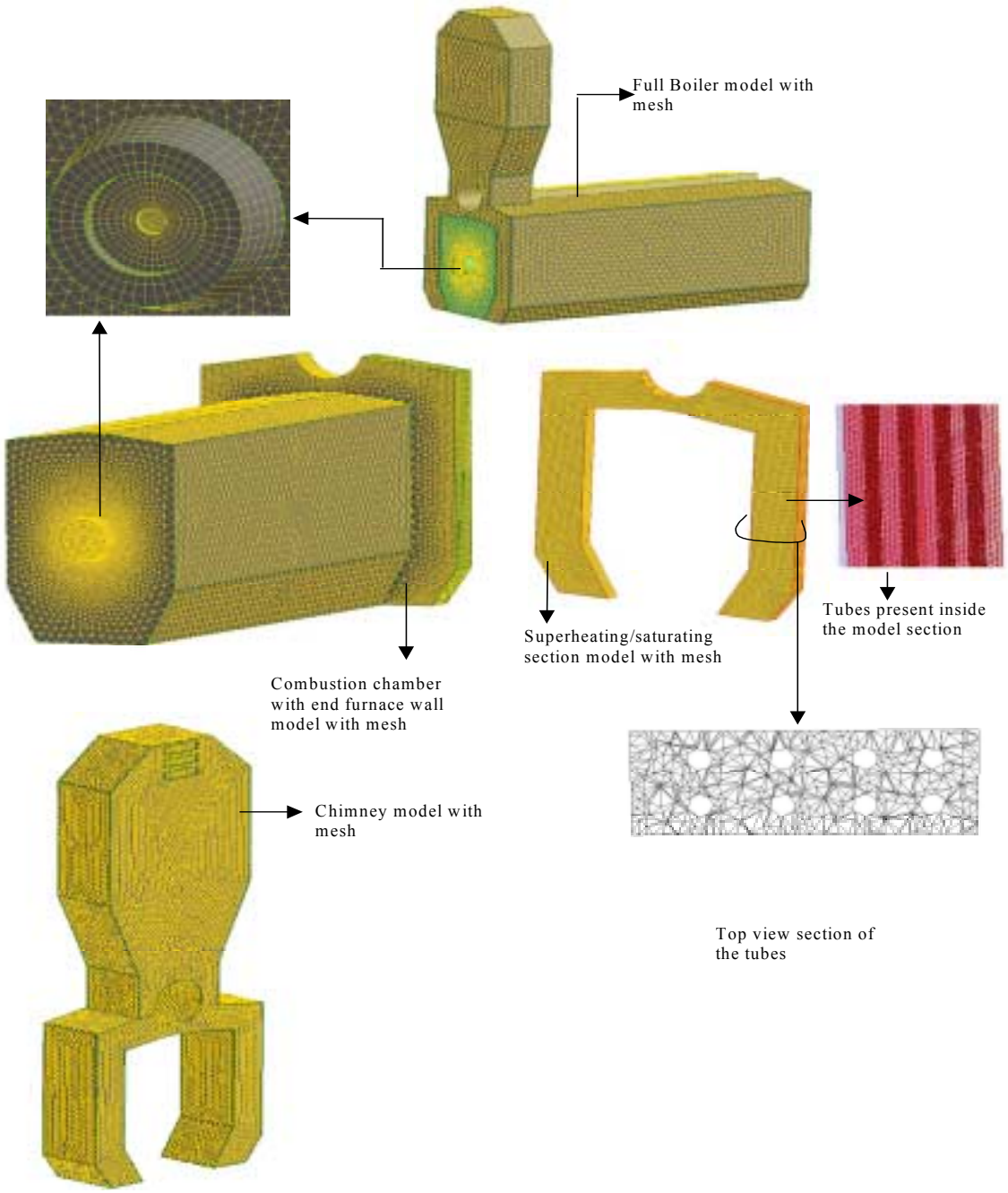

Figure 4.2 Computational model of the studied boiler showing different sections with meshes

4.5 Numerical Procedure

The numerical procedure consists of the following problem solving steps:

1. Creating and meshing the geometry model using Gambit
2. Importing the geometry model to FLUENT solver
3. Selecting the appropriate solver formulation
4. Choosing the physical models to be solved
5. Specifying the material properties
6. Specifying the initial boundary conditions
7. Calculating the solution
    - (i) Solve the continuity, momentum and κ-ε turbulence equation using the SIMPLE algorithm (pressure-predictor-correction method)
    - (ii) Obtain the velocity, pressure and turbulence distribution
    - (iii) Solve the energy equation and calculate the temperature distribution
    - (iv) Calculate the species production using the eddy-dissipation model
    - (v) Transfer the species production to the source terms of the species transport equations
    - (vi) Solve the species transport equation to obtain species concentration distribution and enthalpy formation
    - (vii) Transfer the enthalpy formation energy to the source term of the energy equation
    - (viii) Update the continuity with new distribution of mass from the solution of species of transport equation (step (vi))
    - (ix) Return to (i) and reiterate until convergence is achieved.
8. Post-processing the results

The geometry is created and meshed using GAMBIT. Three-dimensional tetrahedral mesh is used for meshing the studied boiler model. After creating and meshing, the model is imported and read in FLUENT.

FLUENT provides three different solver formulations: segregated, coupled implicit, and coupled explicit. In the segregated formulation, the governing equations are solved sequentially, i.e. segregated from one another; while in the coupled solver formulation the governing equations are solved simultaneously, i.e. coupled together. The implicit and explicit coupled solvers differ in the way that they linearize the coupled equations. In this study segregated solver formulation is used to solve the governing integral equations for the conservation of mass and momentum, energy, turbulence and chemical species. A control-volume-based technique is used to convert the governing equations to algebraic equations, which are solved numerically using the implicit method.

The governing equations are non-linear, therefore to obtain converged solution several iterations of the solution loop must be performed. Each iteration consists of the following steps:

(i) Fluid properties are updated first, based on the current solution or on the initialized solution

(ii) To obtain updated velocity field, the u, v, and w momentum equations are solved using the current values of pressure and face mass fluxes.

(iii) Equation for the pressure correction is calculated from the continuity equation and the linearized momentum equations, since the velocities obtained in above step may not satisfy the continuity equation.

(iv) The pressure correction equation obtained from above step is solved to obtain the necessary corrections to the pressure and velocity fields and face mass fluxes such that the continuity equation is satisfied

(v) Appropriate equations for scalars such as turbulence, energy, and species are solved using the updated values of the other variables.

(vi) The equation is checked for convergence.

The above steps are continued till the convergence criteria are obtained. The above steps can be shown by a flow chart as shown in Figure 4.3.

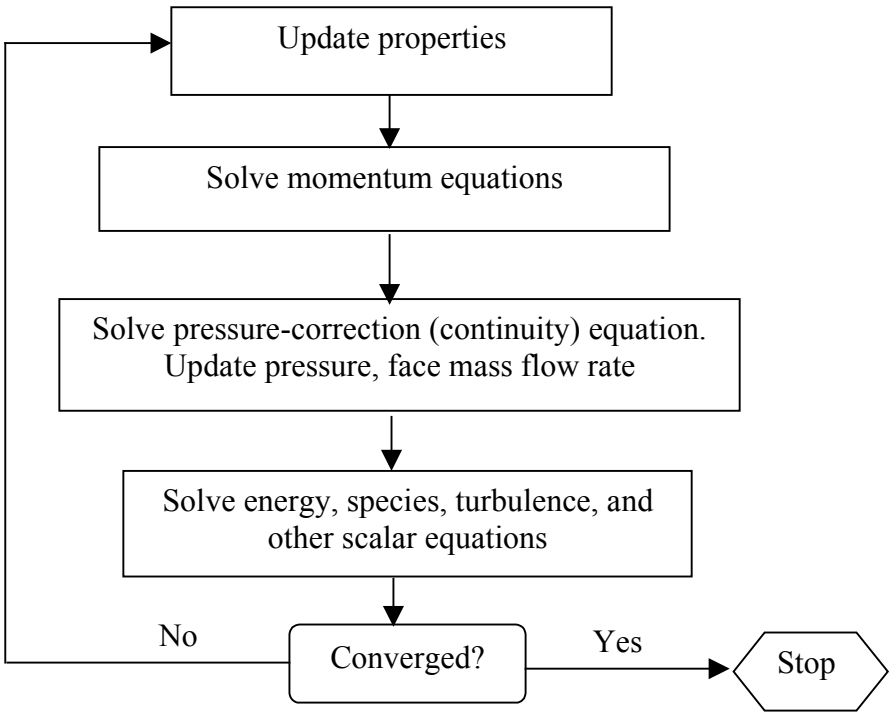

Figure 4.3 Flow chart showing the segregated solution method

In this simulation, segregated solver is used which employs implicit pressure-correction scheme. The SIMPLE algorithm is used for coupling the pressure and velocity. The momentum, energy, turbulence and species equations are discretized using the first order upwind scheme.

A generalized finite-rate chemistry model is used to analyze the combustion using a one-step global reaction mechanism, assuming complete conversion of the fuel to CO_2 and H_2O. FLUENT provides five approaches to reaction modeling: generalized finite-rate model, non-premixed combustion model, premixed combustion model, partially premixed combustion model, and composition PDF (Probability Density Function) Transport model. In this study generalized finite-rate combustion model is used to solve the species transport equations. The reaction rates are computed from the eddy dissipation model. The eddy-dissipation model computes the rate of reaction under the assumption that chemical kinetics are fast compared to the rate at which reactants are mixed by turbulent fluctuations. Basically FLUENT provides three finite-rate formulations for reaction rates: Laminar finite-rate model, eddy-dissipation model, and eddy-dissipation-concept (EDC) model. In eddy-dissipation reaction model the reaction rates are controlled by the turbulence.

In the present study methane-air combustion is simulated. The methane-air mixture consists of 5 species (CH_4, CO_2, H_2O, O_2 and N_2). The specific heat of the species is temperature dependant and is defined as a piecewise-polynomial function of temperature. The physical properties are defined for the mixture material and the constituent species. The flow and thermal variables are defined by the boundary conditions on the boundaries of the studied model. Mass-flow inlet conditions are applied at the three inlets in the burner. Pressure outlet boundary condition is applied at the outlet and the walls are treated as constant wall temperature or

adiabatic wall temperature. The walls are stationary with no-slip conditions applied on the wall surface.

Convergence

The solution convergence is obtained by monitoring the continuity, momentum, energy, turbulence and species equations separately. An order of 10^{-6} is used for convergence. The temperature distribution is determined after a converged solution is achieved.

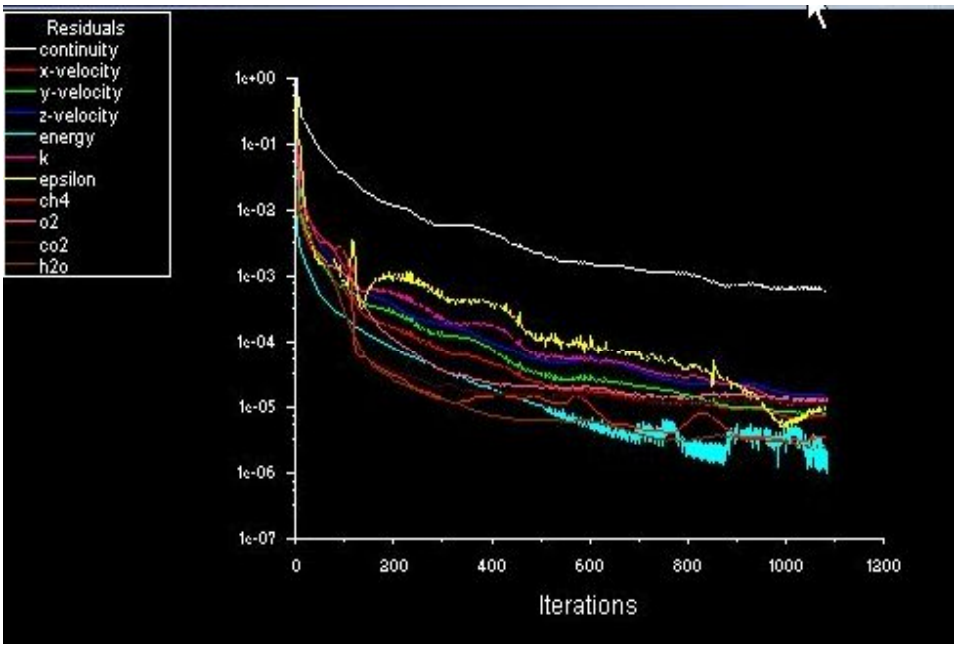

Figure 4.4 Plot showing iterations of converged residuals

Mass and Energy Conservation

The energy conservation is made by enforcing the thermal energy transfer out of the domain equal to that of into the domain. The net transport of energy at inlets consists of both the convection and diffusion components. The convection component is fixed by the inlet

temperature specified. The diffusion component depends on the gradient of the computed temperature field. The procedure for energy balance is given in Appendix-C.

4.6 Grid Independent Study

Grid independent study was conducted using a coarse grid (22424 grid points), a medium-density grid (95845 grid points) and a fine grid (198751 grid points) for the entire boiler. The contour temperature plots on the central horizontal plane y=0 for the three grids is shown in Figure 4.5. It can be seen that for both coarse grid and studied grid the peak temperature is of order 1,630 K and for fine grid the temperature is of order 1,640 K. The flow distribution is almost same for all the grids. The outlet exit temperature for all the grid cases is of order 560 K. The velocity, temperature and the methane and carbon dioxide concentrations at selected axial planes for the three grids are shown in Figure 4.6 and Figure 4.7. The species mass-fraction, temperature and pressure losses at the outlet for the three grids are shown in Table 4.1. It can be seen from the table that all the variables are almost identical between the results of the medium grid and fine grid. Although the solution is still changing between the medium and the fine grid cases the difference is small, to obtain results with reasonable time frame, therefore the medium density grid is used for this study.

Variable	Coarse Grid (22424 grid points)	Medium Grid (95845 grid points)	Fine Grid (198751 grid points)
Mass weighted average temperature at the outlet(K)	730.64	746.72	732.96
Peak temperature in the domain (K)	1630	1630	1640
Total pressure losses (Pascal)	4617.61	4282.69	4132.08
Outlet mass-fraction of CH_4	0	0	0
Outlet mass-fraction of O_2	0.056413464	0.056017853	0.055890907
Outlet mass-fraction of CO_2	0.1128673	0.11312288	0.11321723
Outlet mass-fraction of H_2O	0.092403255	0.09261018	0.092690654
Outlet mass-fraction of N_2	0.30602559	0.37207656	0.34881523

Table 4.1 Variables for three different grids

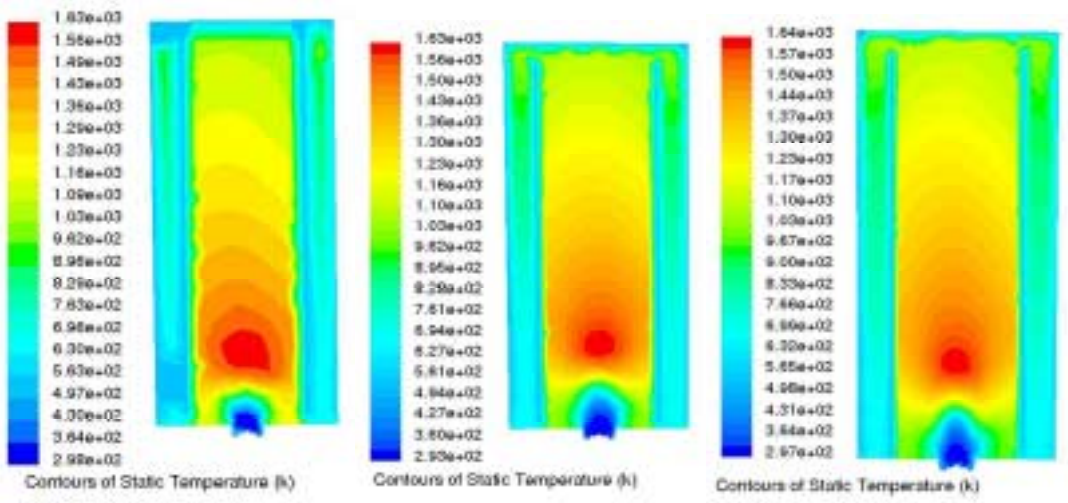

(a) (b) (c)

Figure 4. 5 Contours of temperature on horizontal plane y=0 for different meshing
a) Coarse mesh b) Medium mesh c) Fine mesh

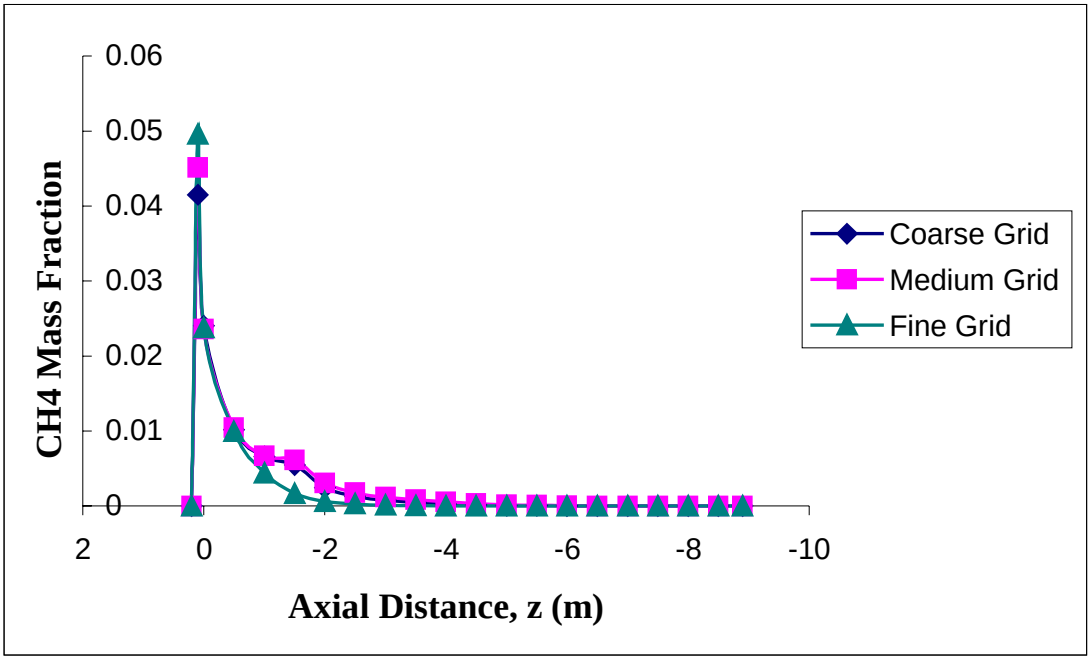

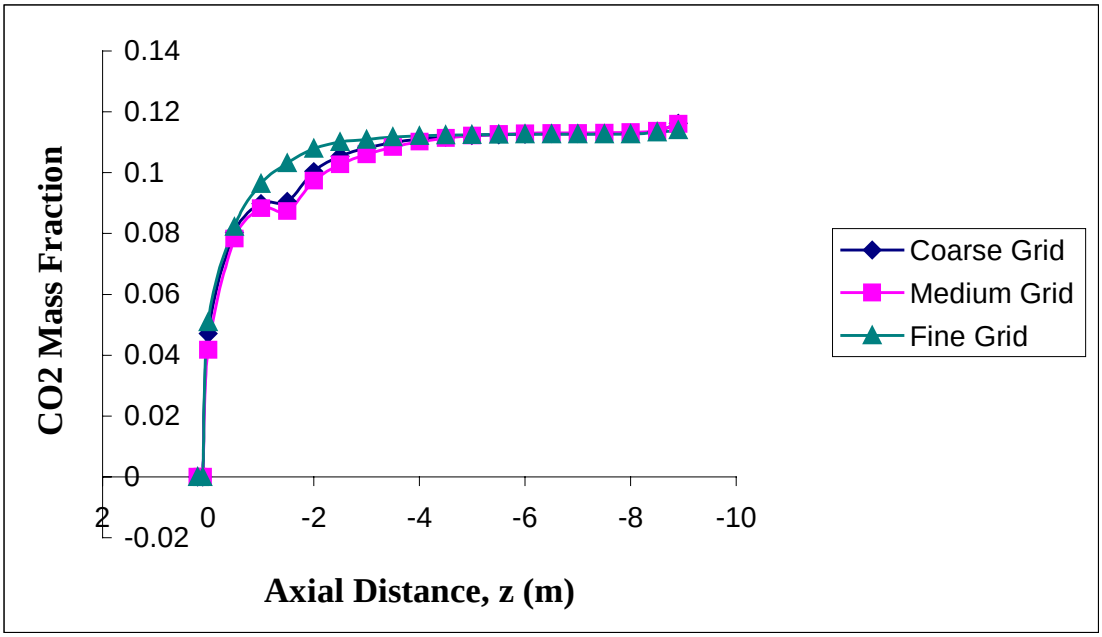

Figure 4.6 Concentrations of CH_4 and CO_2 at different axial planes for different grids

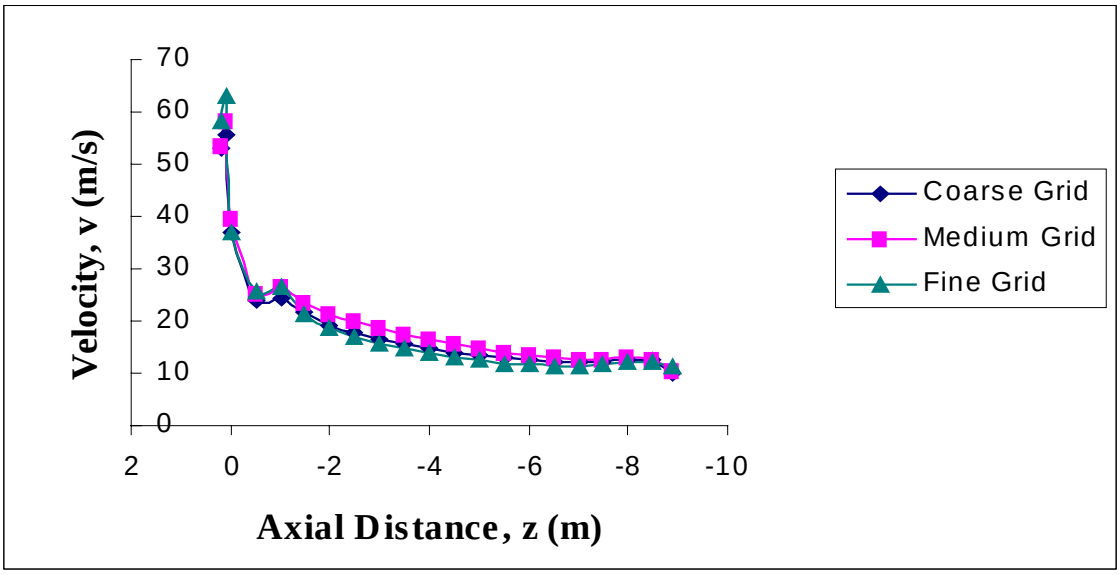

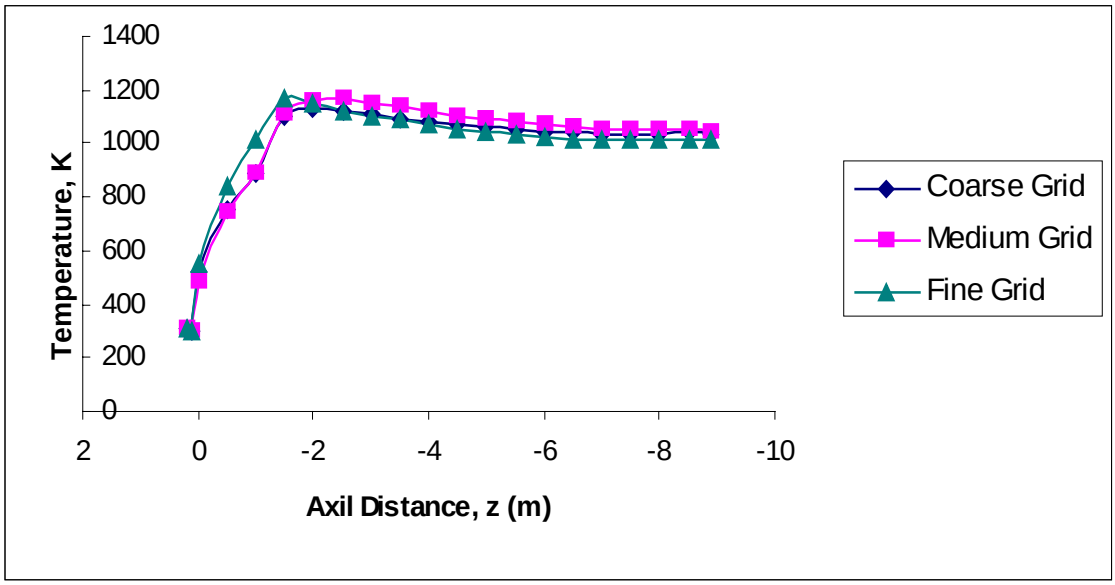

Figure 4.7 Profiles of velocity and temperature at different axial planes for different grids

CHAPTER FIVE

RESULTS

This study illustrates the analysis of simulation of combustion and thermal flow behavior inside an industrial boiler. The simulation is conducted in two stages. In the first stage the entire boiler with combustion chamber and furnace is considered. The flow and temperature distribution is simulated without the inclusions of superheater and saturator tubes located amid the flow path. In the second stage of the simulation, the boiler is divided into three main sections. The first main section consists of only the combustion chamber where the fuel is burned. The second main section which are further divided into 31 sub-sections including superheater and saturator tubes sections. The last main section consists of the chimney exhaust.

The flow distribution inside the entire boiler is simulated in the first stage of study. A mesh with approximately 95,845 grid points is used for the simulation. The grid incorporated the fuel inlet duct for injecting the natural gas, the primary inlet duct for injecting the swirling air stream and the secondary inlet duct for injecting the uniform air stream. Figure 5.1 shows the velocity vector distribution for the three inlets, where the primary air enters with a swirl. The swirling flow is used for enhance mixing for a complete combustion of air and fuel and for stabilizing the flame front. The swirl induces a recirculation zone along the centerline of the combustion chamber downstream from the burner outlet. The mass weighted average velocities

for the three inlets are given in Table 5.1. The total air supplied is 19.98 kg/s, which is at 35 % more air than the stoichiometric value.

Variables	Average Velocities (m/s)
Fuel Inlet	157.49
Primary Air Inlet	75.22
Secondary Air Inlet	57.95

Table 5.1 Average velocities at the burner inlets

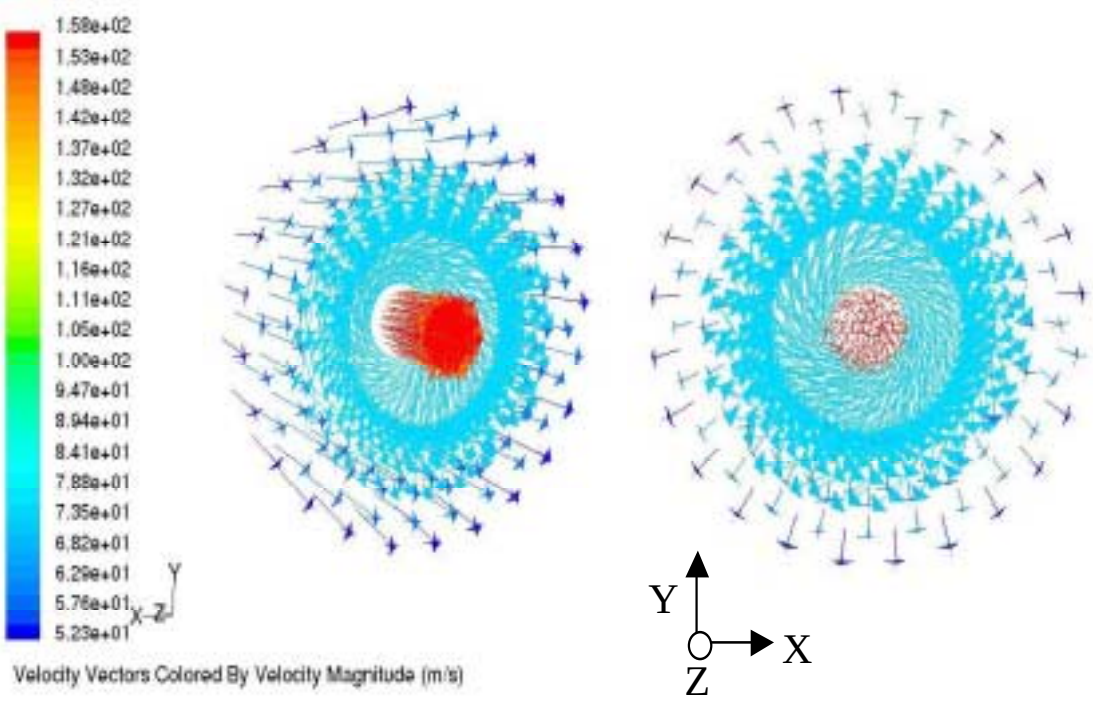

Figure 5.1 Velocity vectors for the three inlets in the burner

a) 3-D velocity profile b) A cross-sectional view

The temperature distributions on the vertical center-plane at x=0 and on the horizontal plane at y=0 are shown in Figure 5.2 and Figure 5.3, respectively. The temperature contour clearly shows the peak temperature is at about 1,630 K occurs at about 1/4 of the boiler length and is less than the adiabatic flame temperature 2,226 K for methane combustion. Both Figures 5.2 and 5.3 show the flame propagation and the mixing and chemical reactions occurring closer to the inlet. The horizontal plane in Figure 5.3 shows that the hot flames turn around 180 degrees at the end and enters into the super-heater section at the right passage. This flame is at about 1,100 K, which is higher than the yield temperature of the superheater tube material (SA-213-T12, temperature of yield at 1050 F). This imposes a risk to the integrity of the superheater tube wall. Due to this high temperature flow, the first few rows of the super-heater tubes near the end furnace wall are subjected to the risk of rupture.

Compositions of temperature distribution on different horizontal planes and vertical planes are shown in Figures 5.4 and 5.5, respectively. From these two figures, it can be clearly seen that the combustion starts as a ring, then propagates both inward and outward radially as well as longitudinally like a cone.

The flow-fields on the center horizontal and vertical planes in Figure 5.6 and 5.7 show the flow passes from the combustion chamber through the superheater section and finally through the chimney and is exhausted to the atmosphere. Figure 5.6 shows that the flame impinges on the combustion chamber sidewalls at 1/3 of the combustion chamber length. Figure 5.3 shows that the temperature of this impinging flame is about 1500 K. Care must be taken to frequently examine this hot region in the real boiler. Figure 5.6 shows that the flow separates at

the 180-degree turn at the end. These separations will induce total pressure losses and requires more fan power to drive the flow through the boiler. Figure 5.7 shows the flow is characterized by a flame jet spreading over the combustion chamber surfaces, top and bottom with a temperature of about 1250 K at about 1/3 of the chamber length. A recirculation zone is seen surrounding the flame near the burner. Figure 5.8 shows profile of mass-weighted average temperature at selected axial planes. It can be seen from the figure that maximum temperature is observed at about $1/3^{rd}$ of the combustion chamber length.

Figure 5.9 and Figure 5.10 shows the species (CH_4, O_2, CO_2, and H_2O) concentrations in vertical plane at x=0 and horizontal plane at y=0, respectively. These two figures show that the fuel (methane) is completely burned near the burner. The figures show that methane diffuses rapidly toward the flame front, where it is almost completely consumed, but a very small amount diffuses and convects outward from the leading edge of the flame. The figures show the oxygen depletes in the core of the flame jet and maintains higher oxygen concentrations in the recirculation zones. Downstream of the oxygen-depleted region, the oxygen mass fraction exhibits an increase due to replenish by advection/diffusion from the surrounding air. The figures also reveal that large quantities of H_2O and CO_2 are produced soon after the methane has been consumed. The mass fractions of H_2O and CO_2 are low near the burner region with higher values further downstream.

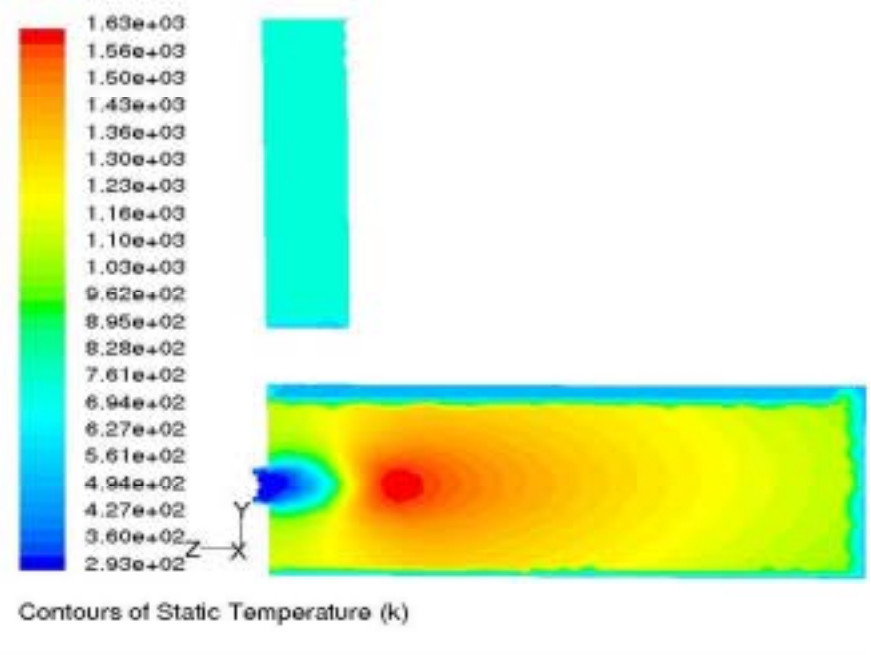

Figure 5.2: Contours of static temperature on the vertical plane at x=0

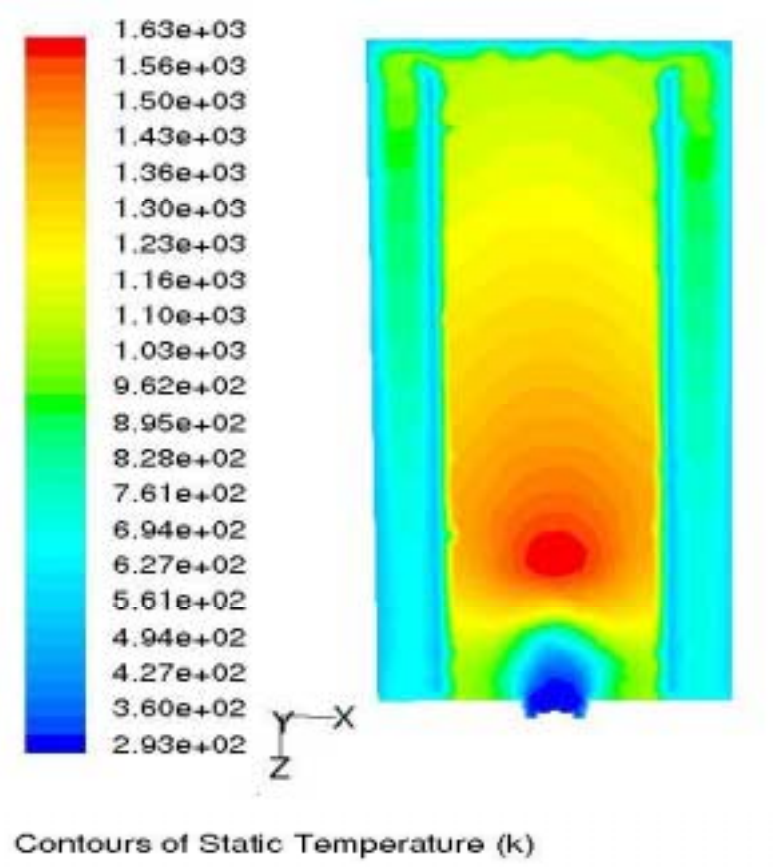

Figure 5.3 Contours of static temperature on the horizontal plane at y=0

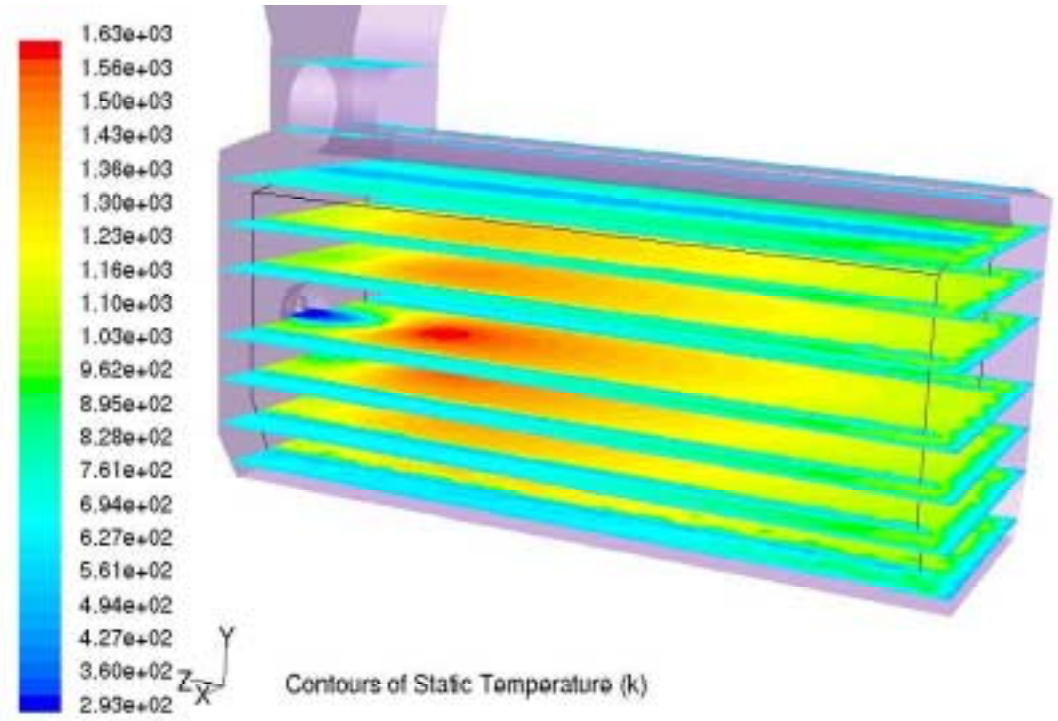

Figure 5.4 Contour temperature profile distribution on different horizontal y-planes

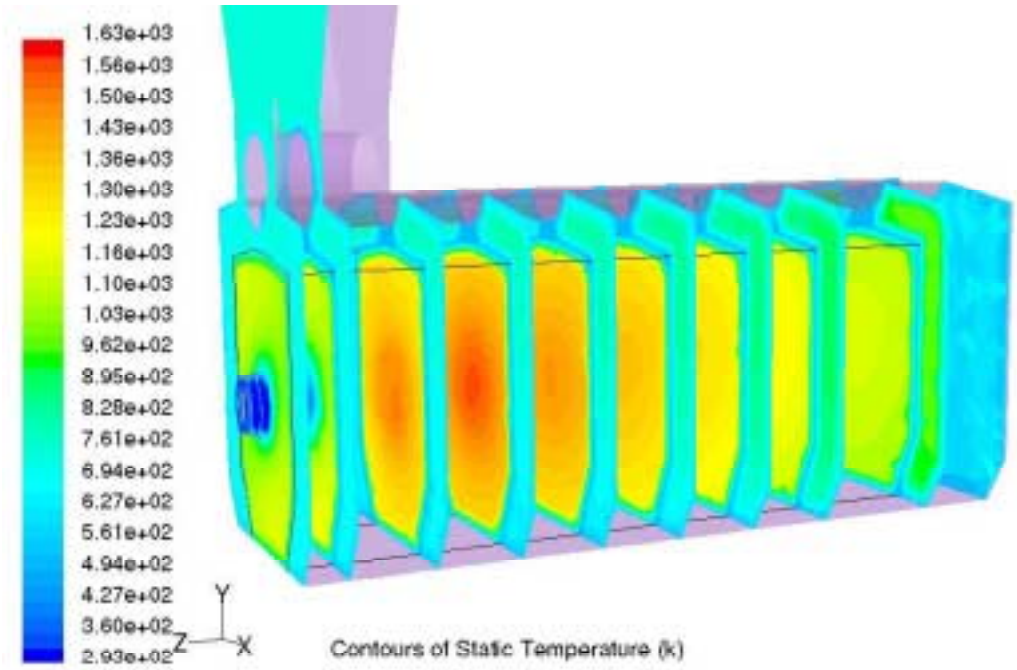

Figure 5.5 Contour temperature profile distribution on different vertical z-planes

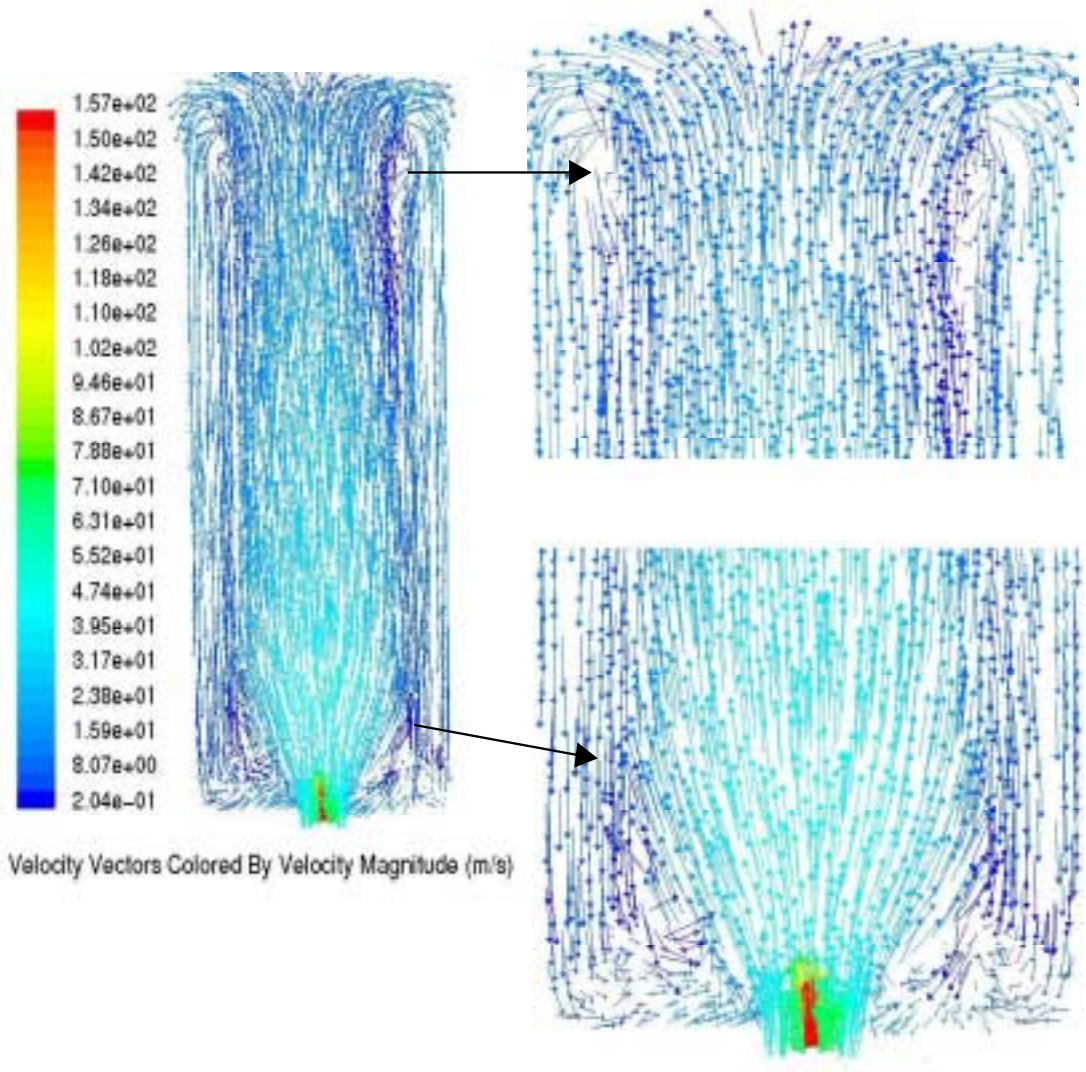

Figure 5.6 Vector plot of velocity on the horizontal plane at y=0

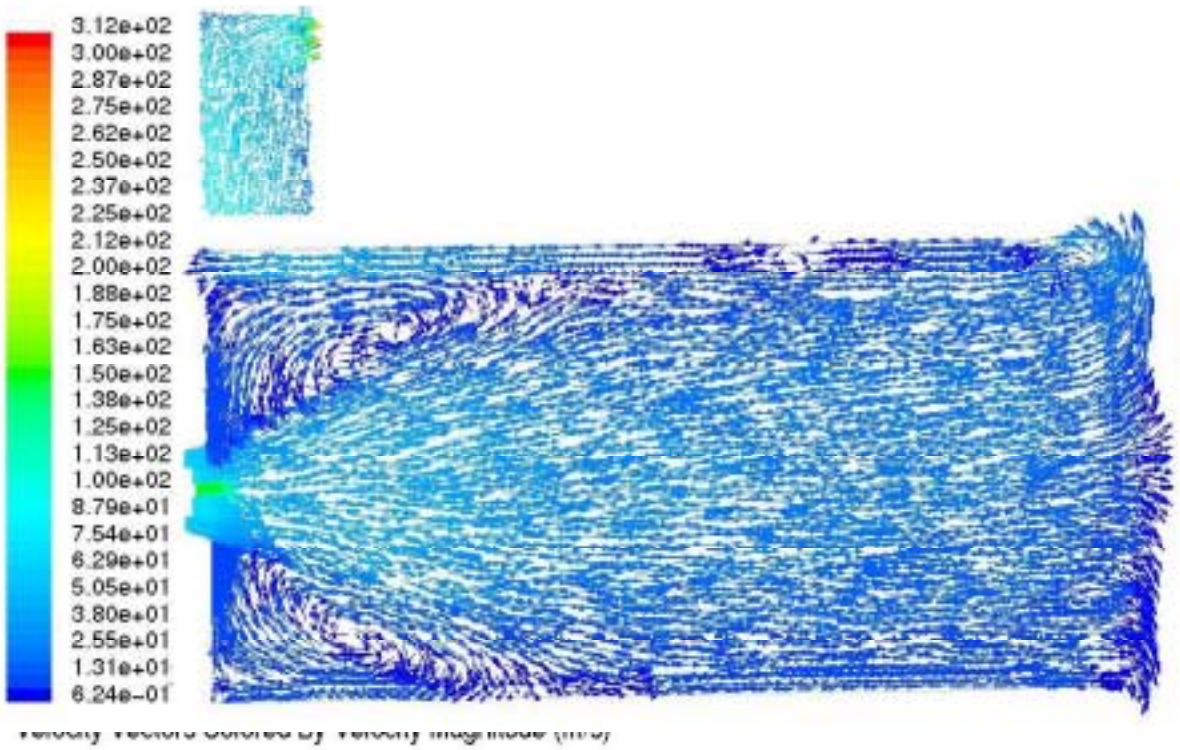

Figure 5.7 Vector plot of velocity on the vertical plane at x=0

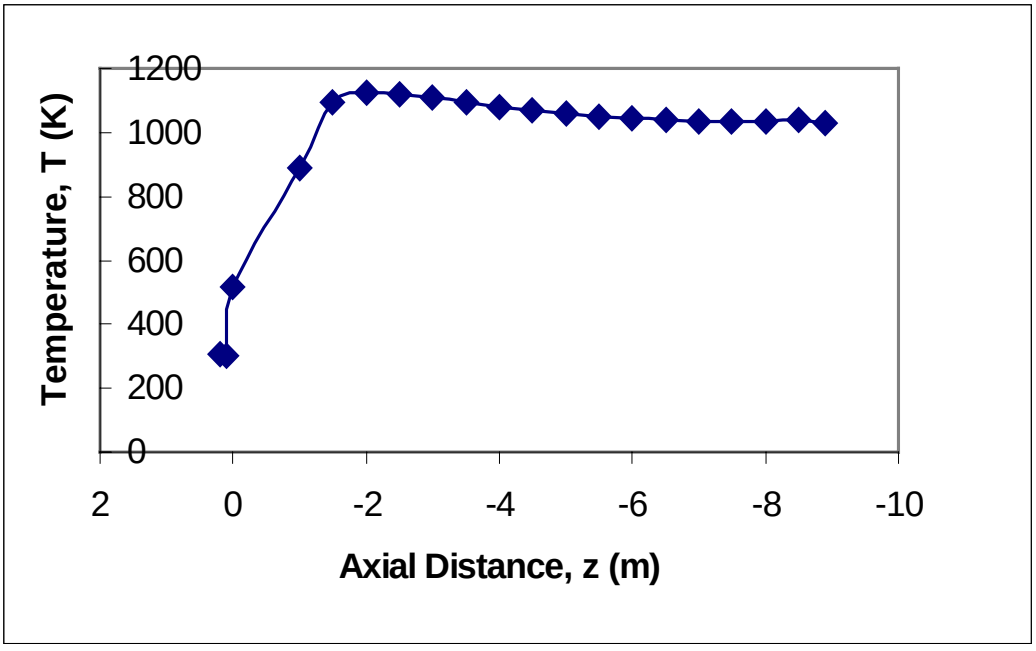

Figure 5.8 Profile of mass-weighted average temperature on selected axial distances

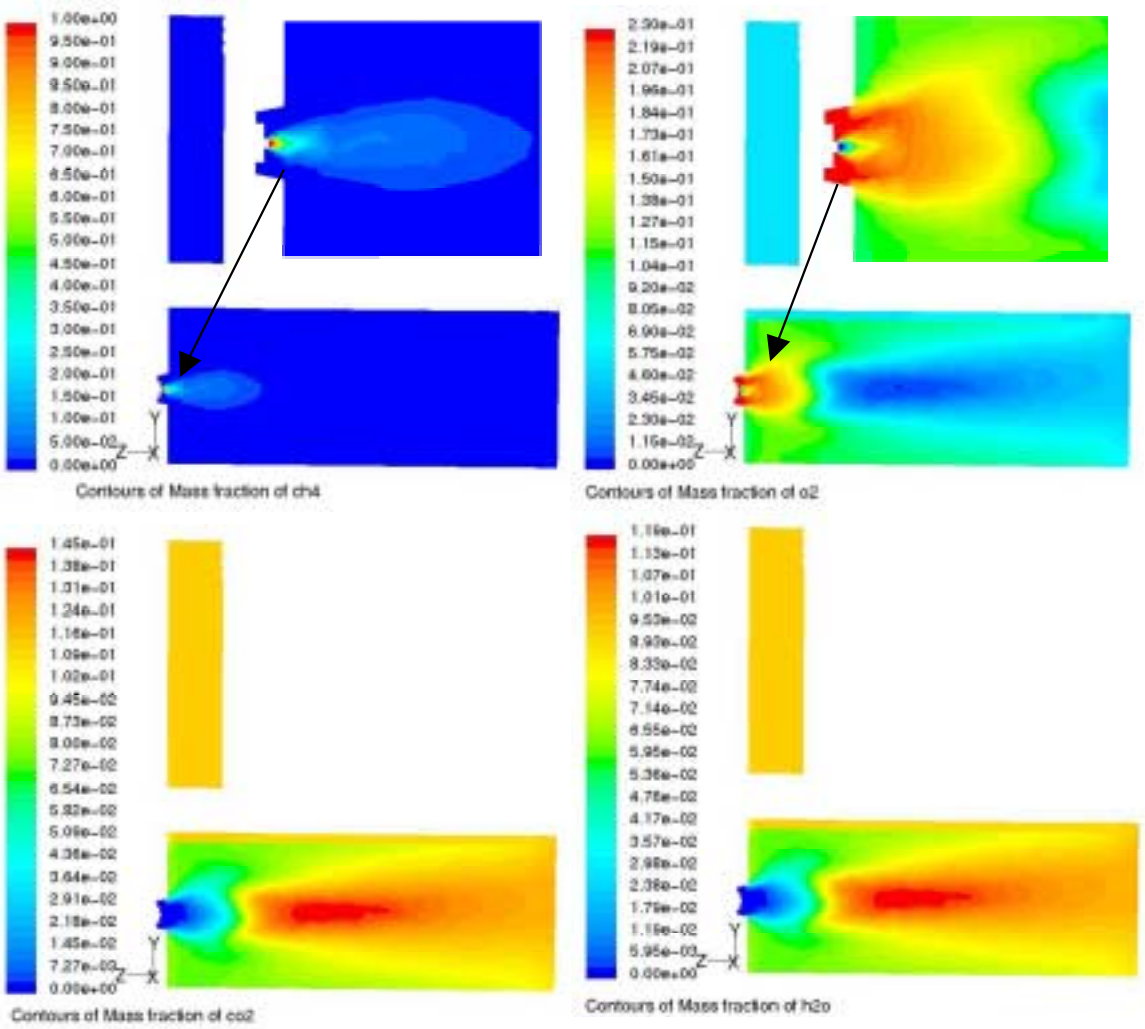

Figure 5.9 Contours of mass fraction of CH_4, H_2O, O_2, CO_2, and N_2 on plane x=0

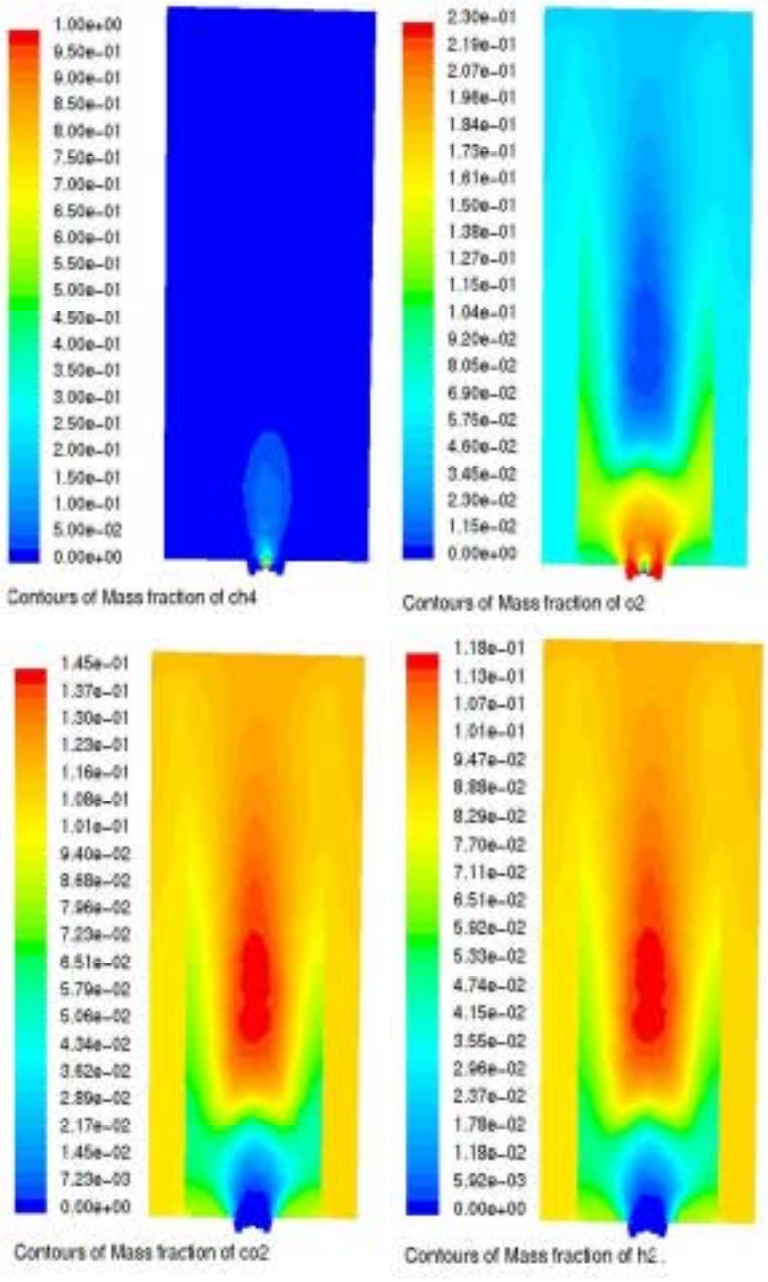

Figure 5.10 Contours of mass fraction of CH_4, H_2O, O_2, CO_2, and N_2 on plane y=0

Profiles for CH_4 concentrations, O_2 concentrations and H_2O concentrations and CO_2 concentrations, at selected axial locations are presented in Figure 5.11 (a) and Figure 5.11 (b), respectively. The profiles clearly show the decrease in methane concentrations, oxygen concentrations and nitrogen concentrations while the concentrations of CO_2 and H_2O are increased going further downstream.

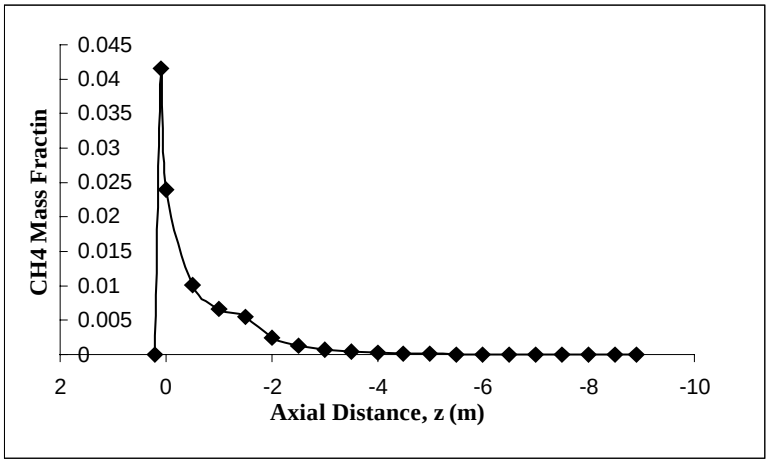

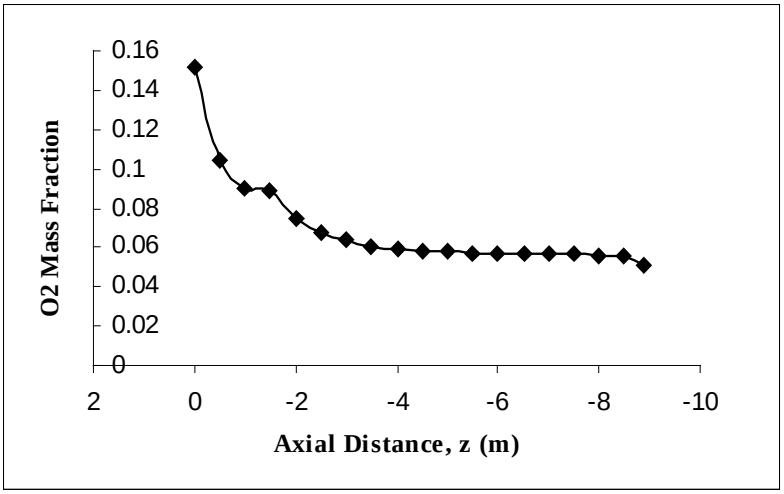

Figure 5.11 (a) Profiles of CH_4 and O2 concentrations along selected axial distances

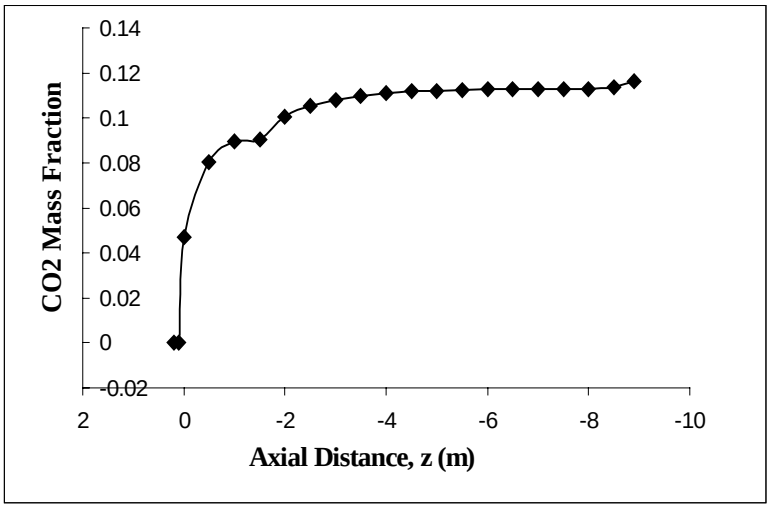

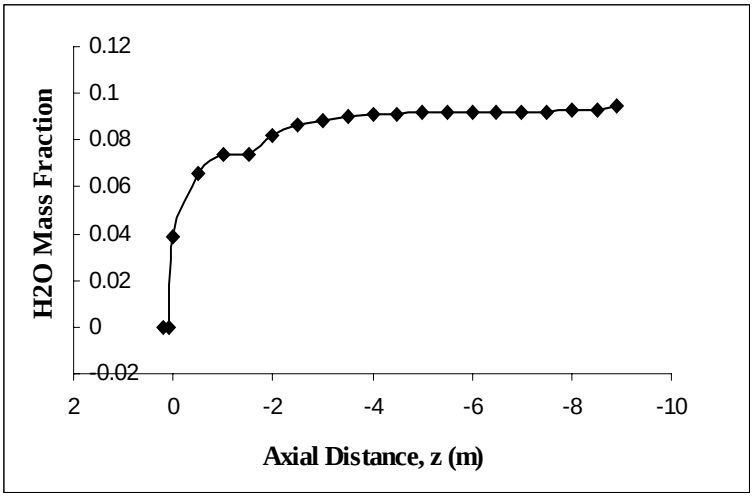

Figure 5.11 (b) Profiles of CO2 and H_2O concentrations along selected axial distances

In the second stage of this study, the second main section containing the saturator and superheater tubes is specifically zoomed in for a detailed simulation. This second main section is divided into thirty-one sub-sections. The outlet solution of the first main section (the combustion chamber) is used as the inlet condition for the first sub-section of the second main section. The first main section is simulated without downstream sections. The interface between the first and the second main sections is set at a constant pressure.

The temperature profile of the first section is shown in Figure 5.12. The figure shows the contour temperature profile on the vertical center plane x=0. Figure 5.13 shows the contour temperature profile on the horizontal center plane x=0. The figure shows the peak temperature is 1640 K, which is 10 K higher than in Figure 5.2 and Figure 5.3 when the entire boiler is simulated without the tubes. This difference is due to the disconnection of the downstream section from the first section. In the second-stage of simulation, a fine mesh is used near the outlet of the first section. Figure 5.13 shows that the flame shifts towards the right side (near the superheater tube section). This shift is believed to be induced by the clockwise swirl motion imposed by the burner.

The contour temperature profile at outlet of the first section is taken as the inlet profile condition of sub-section 1 of the main second stage as shown in Figure 5.14. High temperature of about 1000 K is seen near the center of the flow passage. This could be the region where the material of the superheater tubes may subject to extreme high thermal load and prone to rupture. Near the inner wall, the temperature is reduced to about 970 K due to the separation bubble, which serves as a buffer zone to protect the inner wall from the hot flue gases.

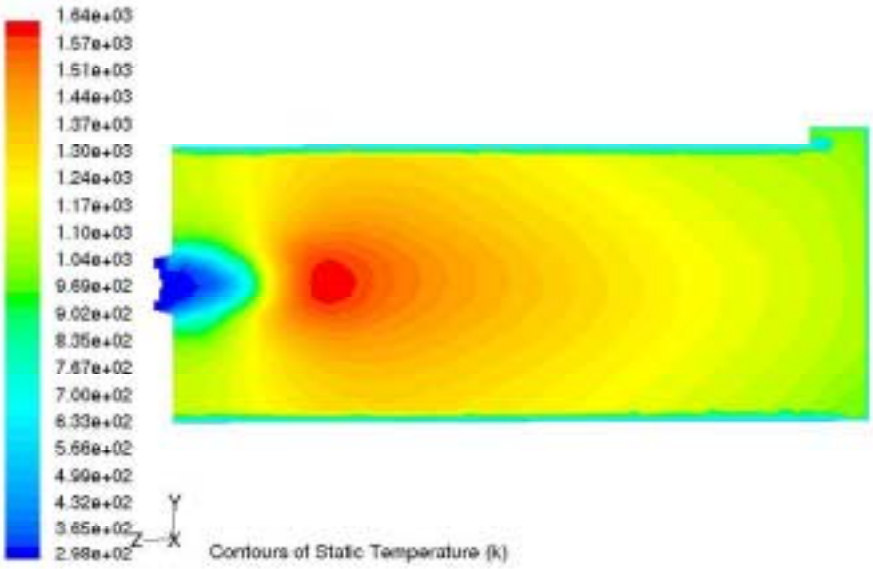

Figure 5.12 Contour temperature profile on the vertical center plane x=0 in the second stage simulation

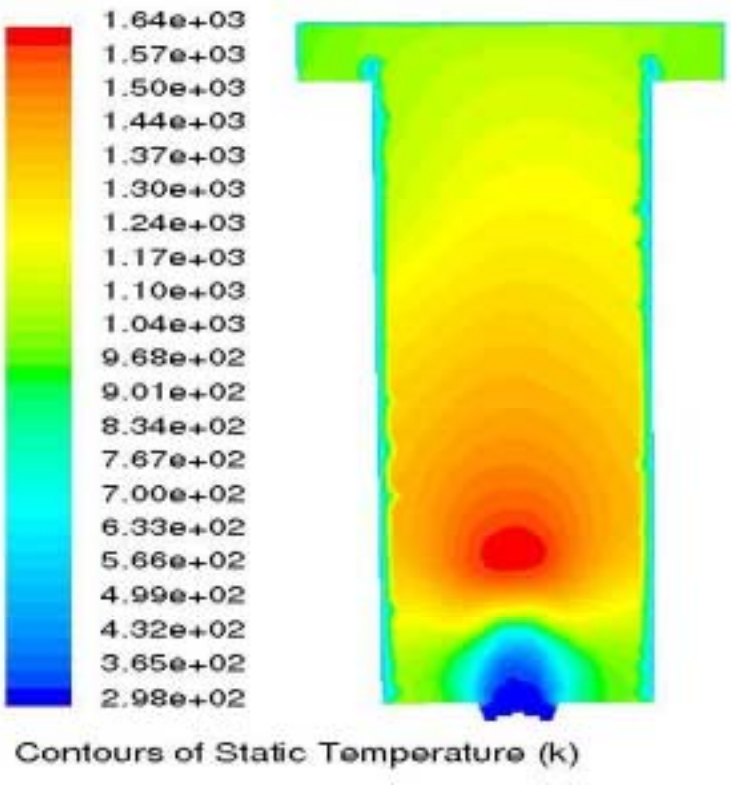

Figure 5.13 Contour temperature profile on the horizontal center plane y=0 in the second stage simulation

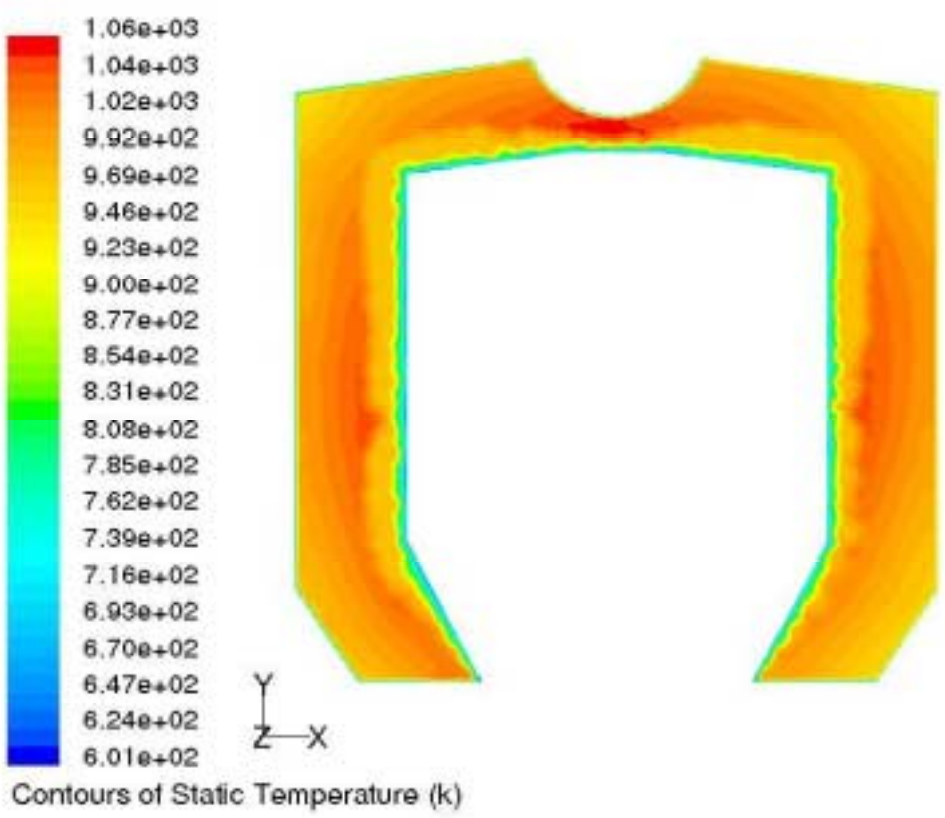

Figure 5.14 Contour temperature plot at outlet of first section of the second stage

Figure 5.15 shows temperature distribution on different selected horizontal y-planes. The flow between the superheater tubes is shown in the expanded view in Figure 5.15. A Recirculation can be seen near the inner wall due to low pressure area created by flow separation while taking a 180 degree sharp turn from the combustion chamber to enter into the saturator and superheater tubes section. The path lines of velocity vector colored by velocity magnitude near the superheater tubes inside the section model are shown in Figure 5.16.

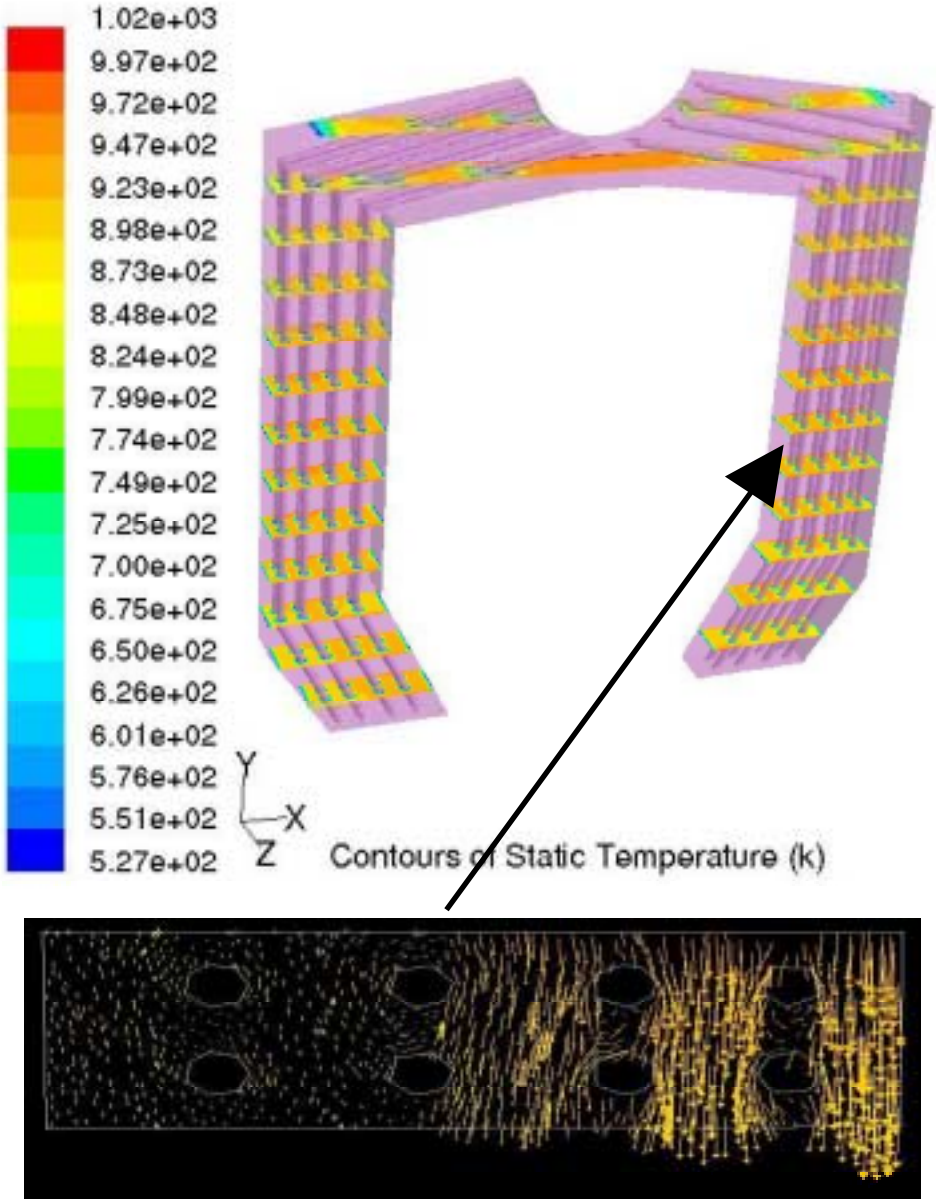

Figure 5.15 Temperature contour plots on different y planes

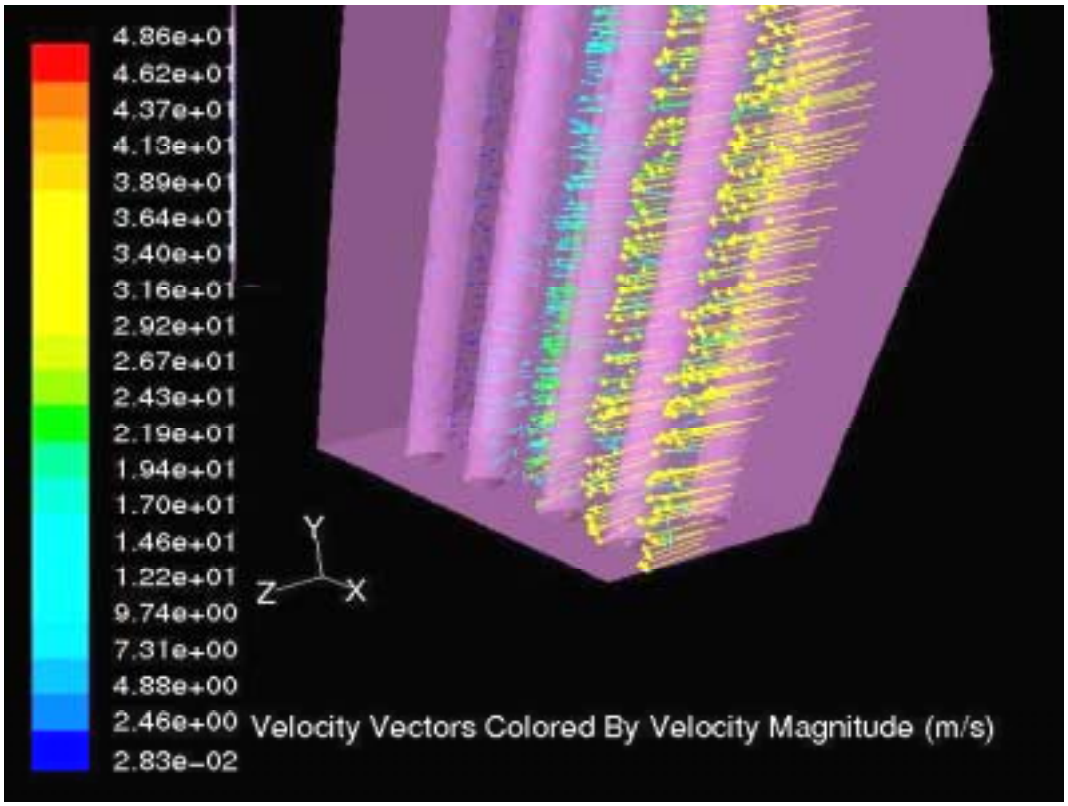

Figure 5.16 Velocity vectors inside the first sub-section of the superheater section

The outlet profile conditions for velocity, temperature and species mass-fraction of sub-section 1 is taken as the inlet profile condition for the next sub-domain (sub-section-2) and the simulation is carried until the calculation of the last sub-domain in the second main section is completed. The temperature contour plots of the entire second main section on the horizontal center-plane y = 0.3 is shown in Figure 5.17 (a). The profiles of mass-weighted average total pressure and temperature of the entire 31 sub-sections of second stage, on the horizontal plane at y=0.3 are shown in Figure 5.17 (b). The plots show decreasing temperature distribution due to heat losses to saturator and superheater tubes. The pressure drop due to the steam tubes is about 1055 Pascal. The compositions of velocity, temperature, and pressure at inlet and outlet boundaries are shown in Table 5.2.

Sub-section No./Variable	Pressure (Pascal)		Temperature (K)		Velocity (m/sec)	
	Inlet	Exit	Inlet	Exit	Inlet	Exit
Sub-section-1	791.8138	556.6385	1002.9	977.69	34.74	33.37
Sub-section-2	654.7561	548.7185	966.62	946.96	33.61	33.13
Sub-section-3	603.5862	525.4882	945.52	915.69	33.18	32.42
Sub-section-4	594.4885	472.1365	913.88	886.46	33.13	30.73
Sub-section-5	558.7462	431.5822	884.42	859.16	32.18	29.38
Sub-section-6	469.9282	351.3801	857.61	835.35	29.42	26.51
Sub-section-7	428.225	323.8613	833.83	812.38	28.1	25.45
Sub-section-8	394.1101	299.3905	810.95	789.67	26.99	24.47
Sub-section-9	364.2005	277.3013	788.96	768.42	25.97	23.55
Sub-section-10	337.17	263.3513	767.69	747.67	25	22.95
Sub-section-11	313.6561	257.8721	747.12	727.47	24.11	22.71
Sub-section-12	290.0861	240.9013	727.12	707.86	23.11	21.95
Sub-section-13	277.8022	215.4888	707.77	688.16	22.62	20.76
Sub-section-14	265.5018	206.8578	688.36	668.61	22.06	20.34
Sub-section-15	256.0261	200.4002	668.96	649.7	21.61	20.02
Sub-section-16	249.0865	195.2288	650.03	631.14	21.27	19.76
Sub-section-17	243.8001	190.7105	631.52	613.11	21.01	19.53
Sub-section-18	238.8465	186.6312	613.42	595.47	20.77	19.32
Sub-section-19	233.9258	182.405	595.79	578.28	20.54	19.1
Sub-section-20	224.9218	176.3442	578.52	561.41	20.06	18.78
Sub-section-21	223.1105	174.0978	562.39	560.93	19.97	18.66
Sub-section-22	215.0545	171.4952	561.08	544.15	19.67	18.52
Sub-section-23	209.3082	165.62	544.79	527.93	19.42	18.2
Sub-section-24	206.6245	159.3113	528.7	512.05	19.33	17.85
Sub-section-25	198.4113	152.2513	512.97	496.91	18.95	17.45
Sub-section-26	190.0413	146.205	497.62	481.77	18.55	17.1
Sub-section-27	181.7298	139.7792	482.74	467.32	18.14	16.72
Sub-section-28	173.6665	133.6613	468.24	453.24	17.73	16.35
Sub-section-29	165.9245	127.8401	454.09	439.46	17.33	15.99
Sub-section-30	158.5518	122.1485	440.26	426.03	16.94	15.63
Sub-section-31	151.3813	116.8921	426.76	412.91	16.55	15.29

Table 5.2 Mass weighted pressure, temperature and velocity compositions at inlets and outlets for all the 31 sub-sections in the saturator/superheater section.

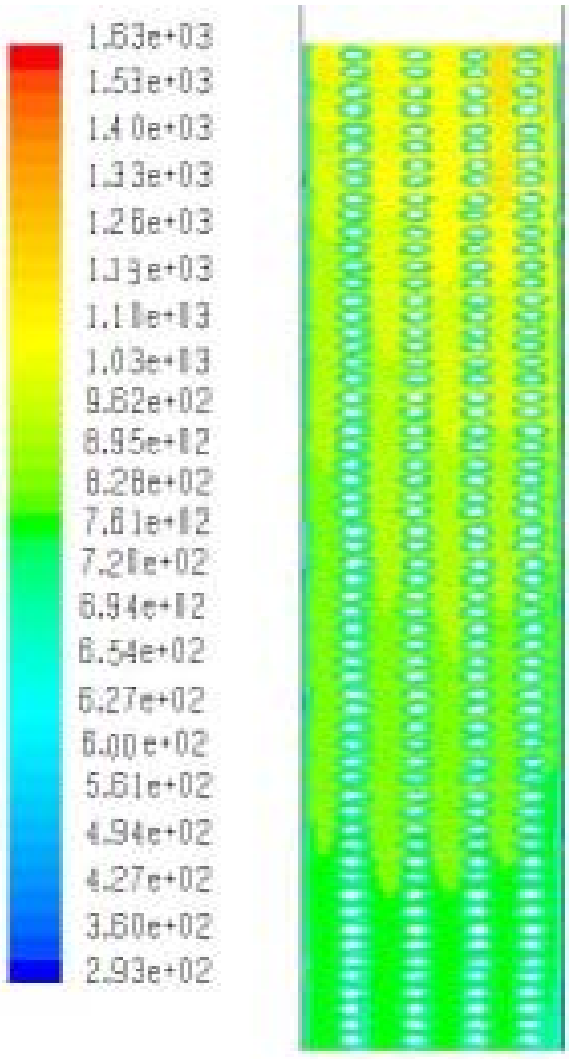

Figure 5.17 (a) Temperature contour plot of the superheater tubes section including all the 31 sub-sections on the horizontal plane at y=0.3

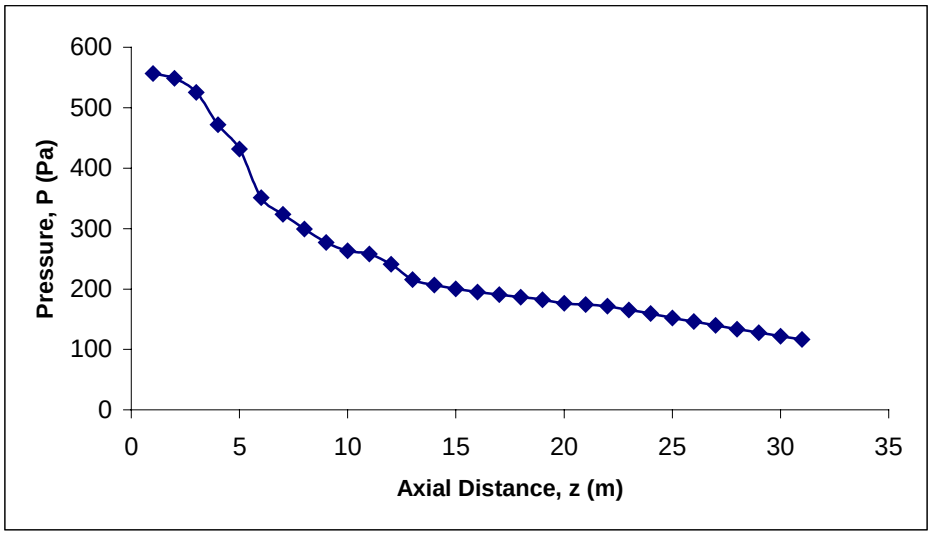

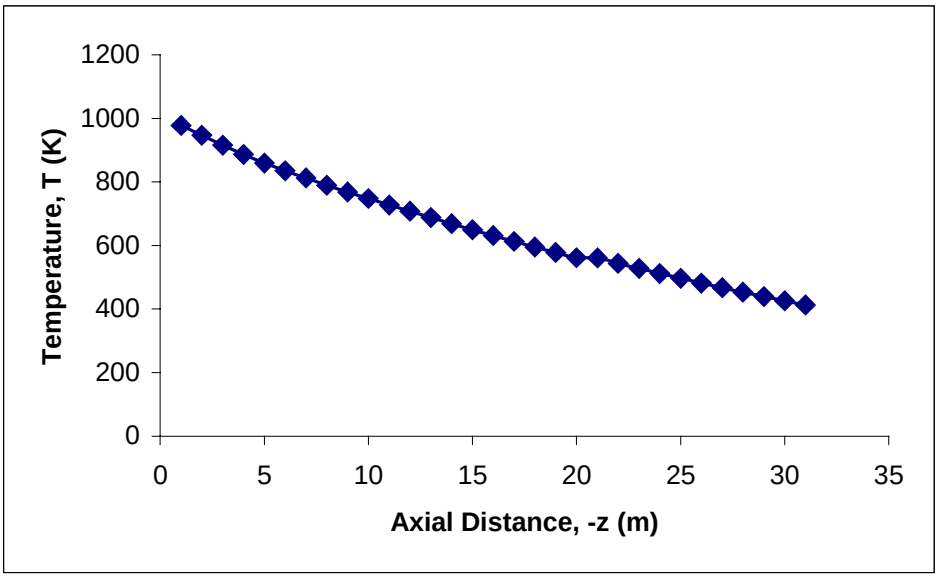

Figure 5.17 (b) Profiles of mass-weighted average total pressure and temperature of all the 31 sub-sections on the horizontal plane at y=0.3

In the third stage of study, the simulation is conducted focusing the chimney (exhaust) region. The outlet of sub-section 31 of section-2 is taken as the inlet condition for the main section-3. Peak temperature in the order of 580 K exists at the outlet of the superheater section. In the saturator section the peak temperature is lower at about 460 K. This is reasonable because more energy is transferred to the saturator. Also since the saturator tube walls are maintained at a lower temperature than the superheater tube walls, the hot gasses loose more energy to the saturator tubes than to the superheater tubes. There is total pressure loss due to the saturator and superheater tubes.

Figures5.18 and 5.19 shows the static pressure distribution on different x-planes and y-planes, respectively. The flue gasses with high pressure pass through the steam drum where its velocity is increased due to a sudden convergent section in the flow area.

Contours of static pressure, static temperature and velocity at the outlet are shown in Figure 5.20. The outlet static temperature is of order 465 K. The hot flue gasses loose energy to the walls covered by saturator tubes below the steam drum and finally passing through the chimney and exhausted to the atmosphere. The temperature is reduced from the order of 580 K to the order of 465 K**.** The exhaust temperature is high; a lot of useful energy is wasted. In the actual exhaust section, an economizer is installed to recover this energy. Due to the limited scope of this study, the economizer is not considered in this study. A infrared thermography inspection of the boiler was conducted recently. It is interesting to see that the actual infrared image shows the chimney exhaust gases at temperature about 360 F (455 K), which are close to the CFD results at 465 K. Figure 5.21 shows the exhaust outlet temperature for the simulated boiler and

the infrared thermography inspection of the boiler. Figure 5.22 shows the path lines colored by velocity magnitude. It is observed that the hot gases have a large re-circulation zone in the chimney section before leaving the atmospheric outlet. Figure 5.23 and Figure 5.24 show the vector distribution colored by velocity magnitude at selected planes. The plots clearly show the flow distribution, the flue gases heading towards the chimney and finally to the atmosphere.

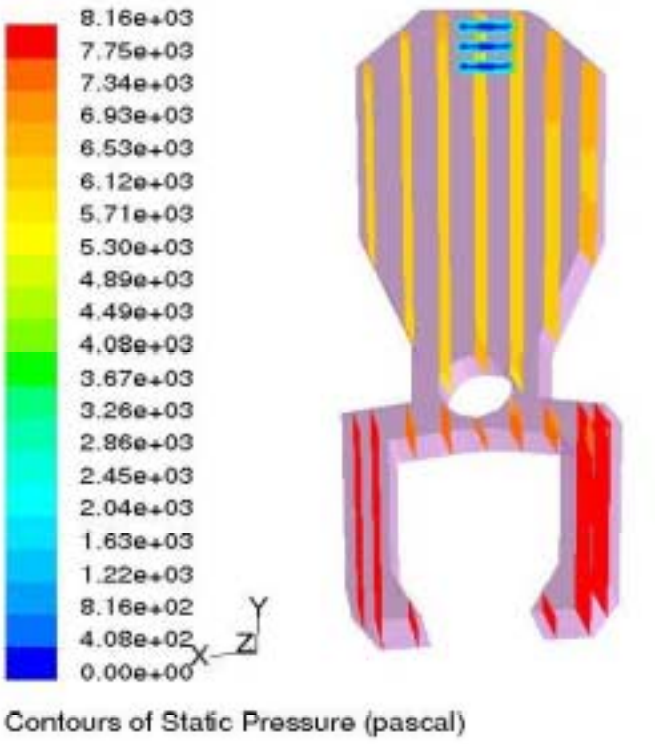

Figure 5.18 Contour plot of static pressure on different x-planes

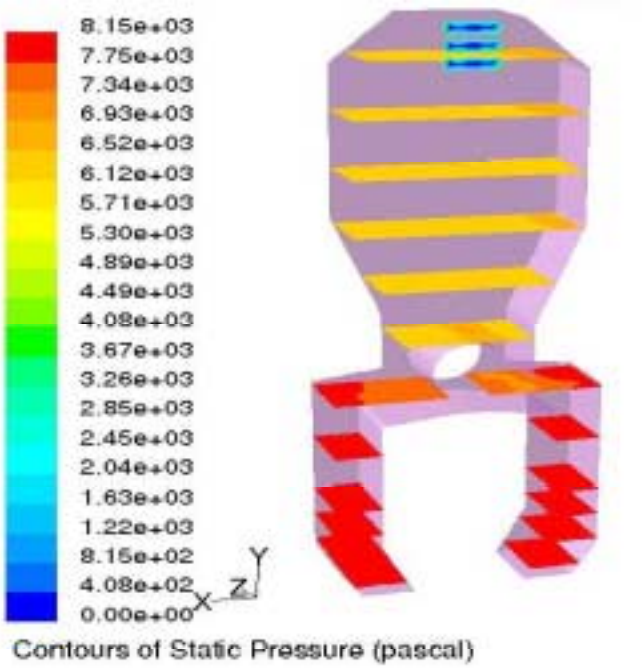

Figure 5.19 Contour plot of static pressure on different y-planes

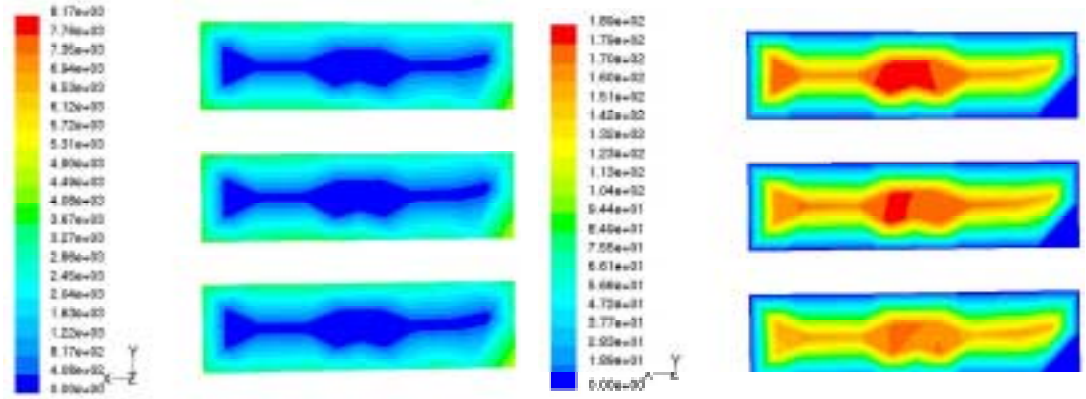

Figure 5.20 Contour plots of static pressure and velocity at the outlet of the boiler chimney

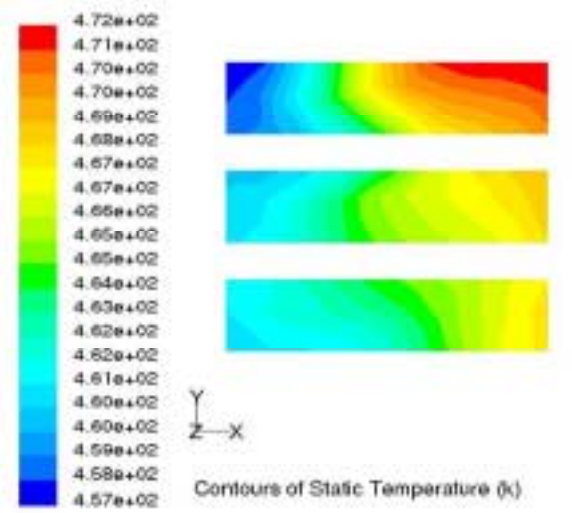

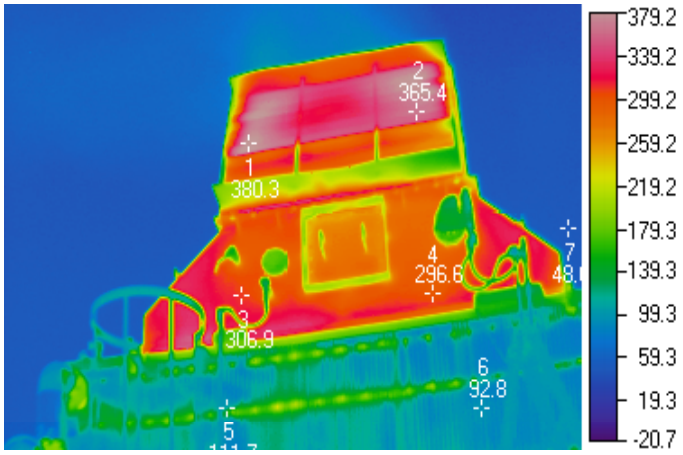

Figure 5.21 Contour plots of static temperature at the outlet of the boiler chimney

(a) simulated boiler chimney outlet, temperature is in (K)

(b) Infrared thermography inspection of the boiler, temperature unit is in (F)

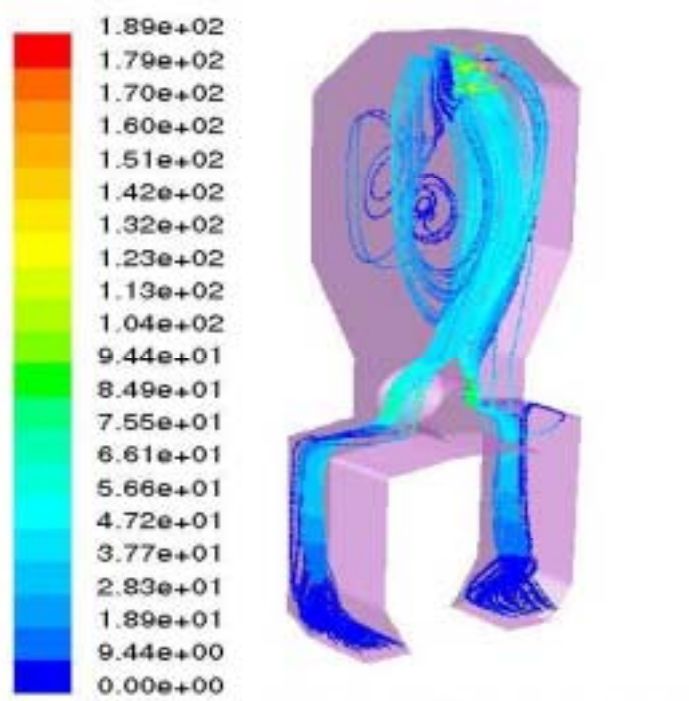

(a)

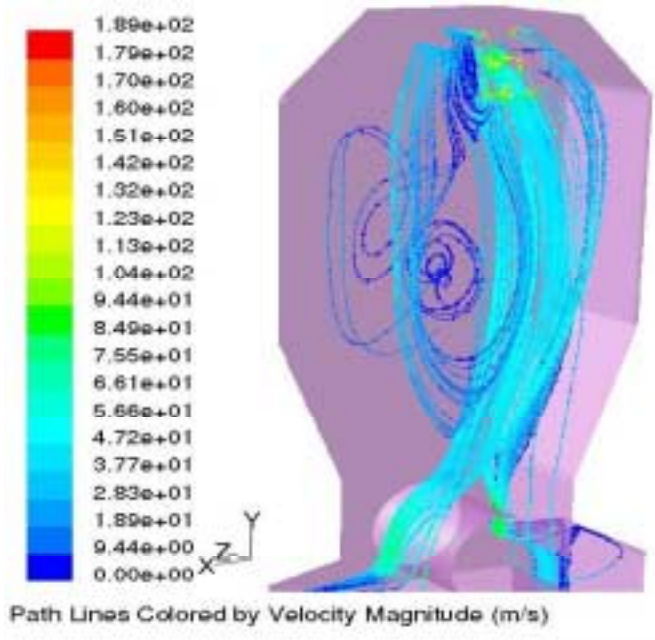

(b)

Figure 5.22 Path lines colored by velocity magnitude on z-plane
a) The entire section model b) Expanded view

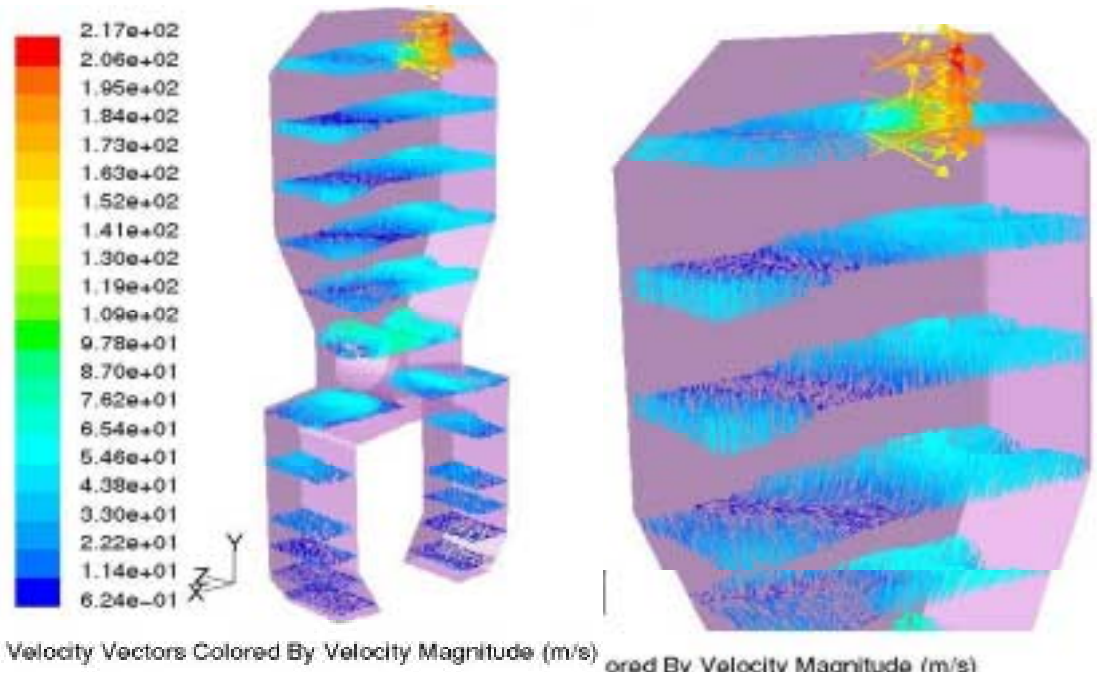

(a)

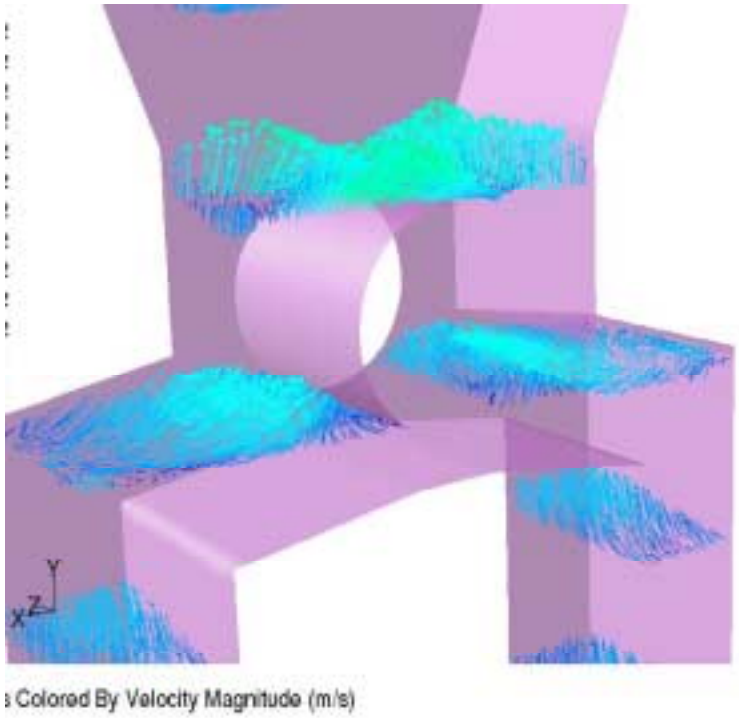

(b)

Figure 5.23 Vector plot colored by temperature on different y-planes
(a) The entire section model b) Expanded view

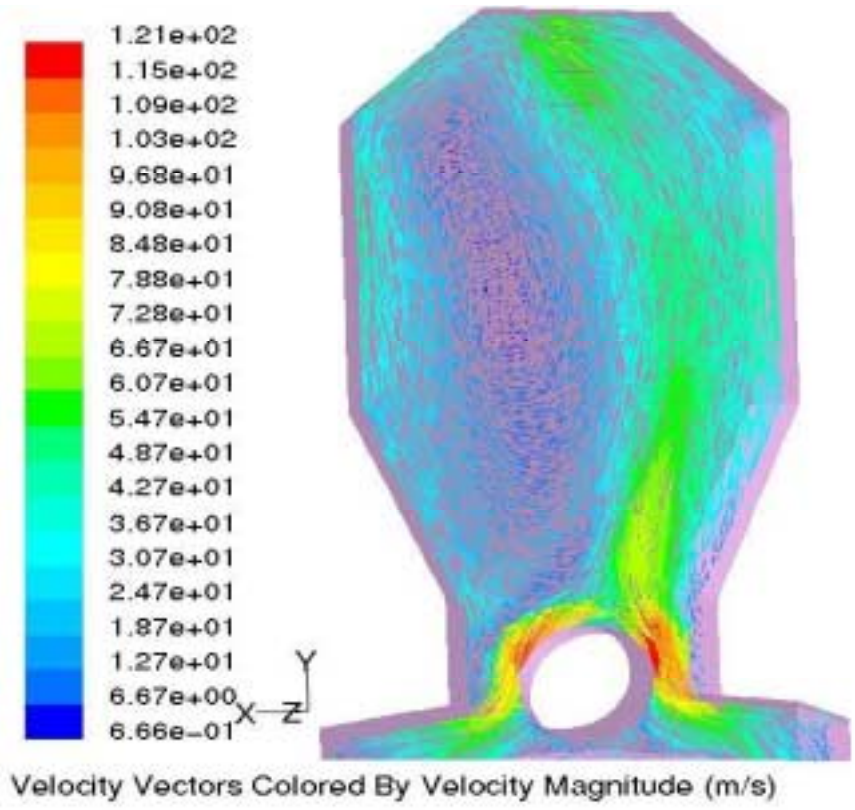

Figure 5.24 Vector plot colored by temperature on z-plane

NOx

A major purpose of many combustion simulations is to predict emissions of pollutants such as NO and CO, which is typically calculated in post-processing fashion once a fully converged flow solution, is obtained. Therefore, accurate predictions of these pollutant quantities are highly dependent on the quality of the flow field solution. With methane combustion, NO results principally from thermal production, and prompt NO production. The NO mass-fraction and NO-ppm at the horizontal plane (x = 0), vertical plane (y = 0) and at the outlet are shown in Figure 5.25 and Figure 5.26. The maximum obtained is about 0.248 ppm, observed at the end furnace. The maximum NO concentration is about 1.65e-07 observed at the center of the combustion chamber as expected, due to the high temperature in this region. The figures show that the NO concentration is low near the inlet of the burner due to low temperature and is maximum at the flame front due to high temperature and then decreases further downstream. The NO concentration at the outlet is about 4.38e-08.

Effect of Air-fuel ratios:

NO emissions are dependent on temperature and therefore on the air-fuel ratios. Low emissions are obtained when using more air than the stoichiometric ratio. Lower excess air levels (fuel rich) starve the reaction for oxygen, and higher excess air levels (lean burn) drive down the flame temperature, slowing the rate of reaction. The NO concentrations for three different air-fuel ratios (stoichiometric, 10% more air, and 35% more air), at selected axial planes are shown in Figure 5.27. The figures show that the NOx emissions are higher when stoichiometric air-fuel condition is used. It also shows that using 35 % more air yields less emissions when compared to 10% more air. The figures also show that the NO concentrations are low near the inlet and

increases further downstream in the combustion chamber. Table 5.3 shows the NO concentrations for three different air-fuel ratios. The peak NO concentrations are observed in stoichiometric air-fuel condition.

Variable	NO-ppm		NO Mass Fraction	
	Peak Value	Exhaust	Peak Value	Exhaust
Stoichiometric	4.23	0.94	2.12e-06	6.63e-07
10% Excess Air	2.54	0.53	1.29e-06	3.81e-07
35% Excess Air	0.24	0.06	1.65e-07	4.38e-08

Table 5.3 NO concentrations and NO-ppm for different air-fuel ratios

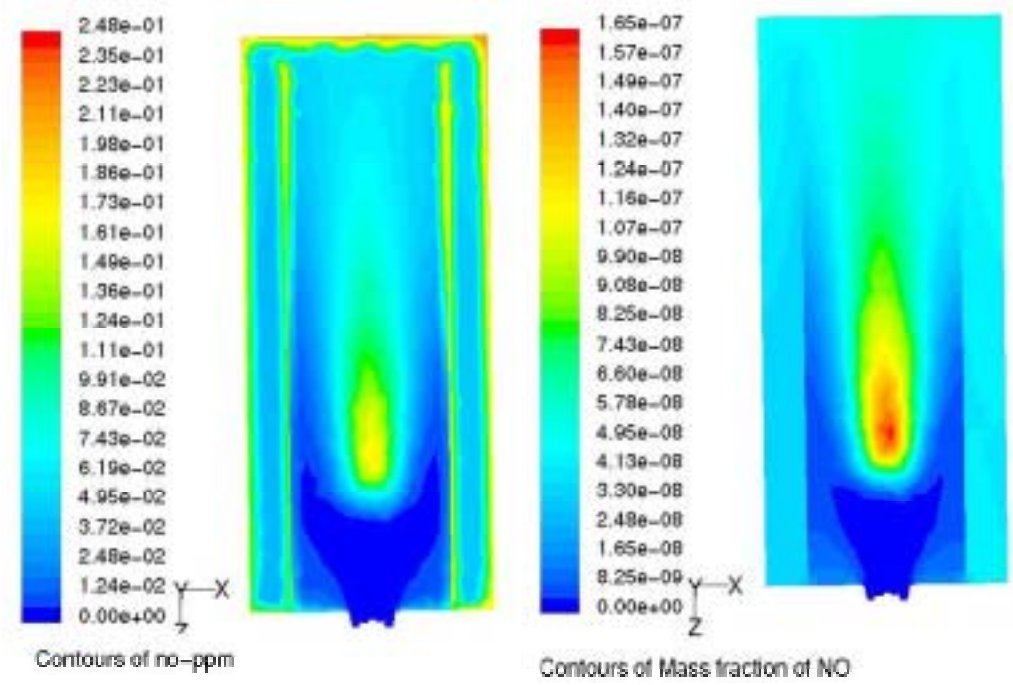

Figure 5.25 Contours of NO-ppm and NO mass fraction at vertical planes y = 0

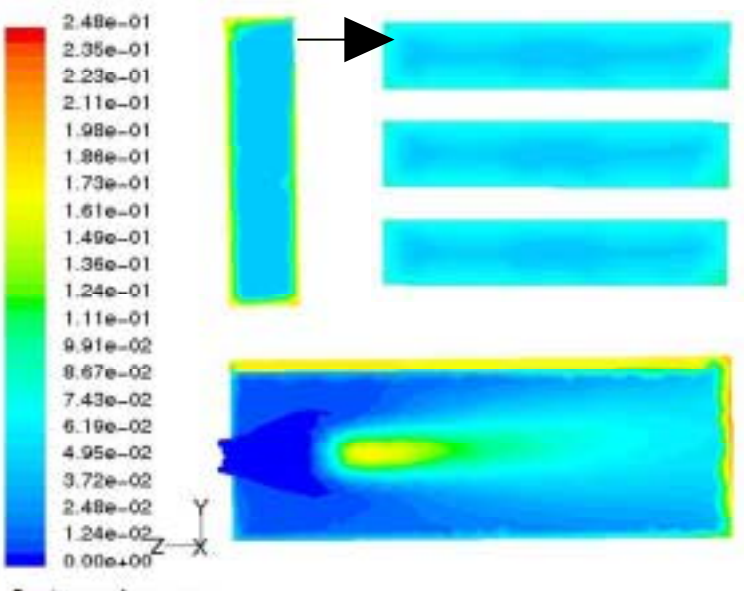

a) NO ppm

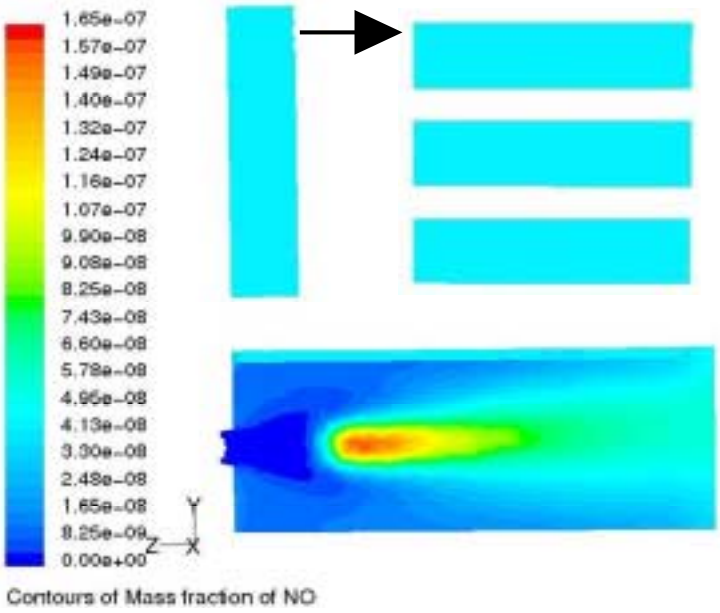

b) NO-ppm

Figure 5.26 Contours of NO-ppm and NO mass fraction on horizontal plane x = 0

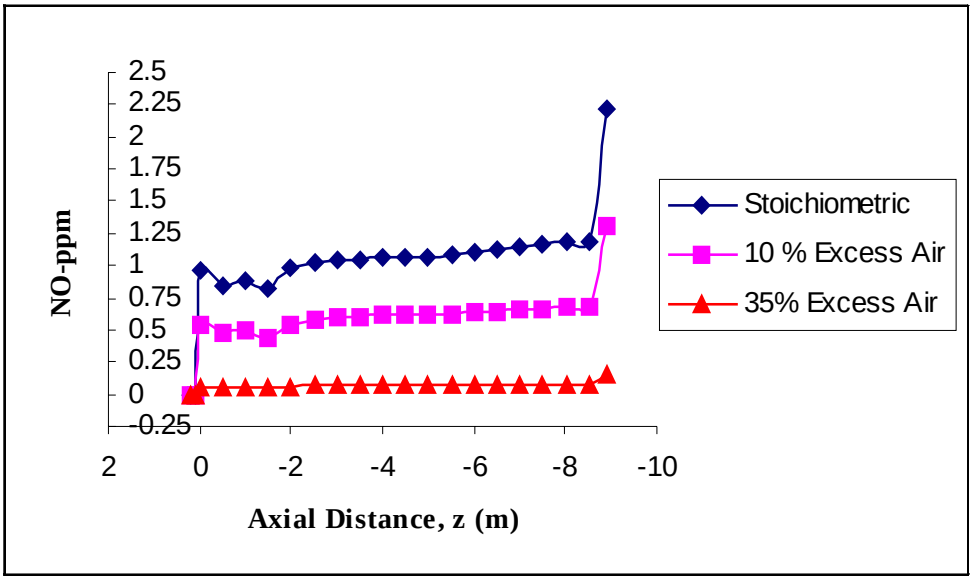

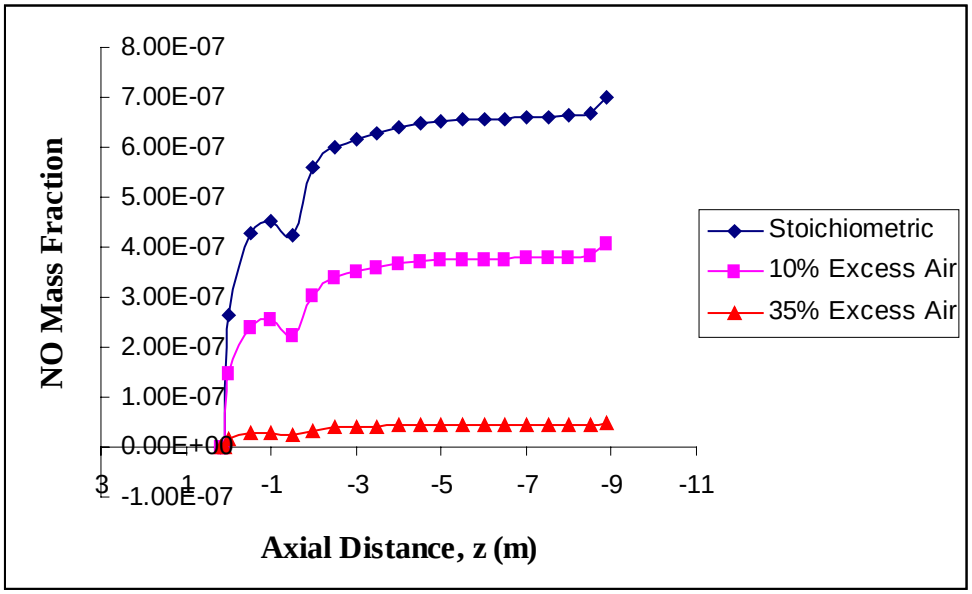

Figure 5.27 NO concentrations for different air-fuel ratios

CHAPTER SIX
CONCLUSIONS

The computational simulation of combustion and thermal-flow behavior inside an industrial boiler was performed in this study using the commercial code FLUENT. The simulations were conducted with and without considering the saturator/superheater tubes. After obtaining a converged flow and combustion solution, the calculation of NOx was performed to obtain NOx concentrations.

The results provide comprehensive information concerning combustion and thermal-flow behavior inside an industrial boiler. The temperature distribution shows combustion starting as a ring at the interface of fuel and primary air and expanding rapidly both inward and outward. The flame propagates as a conical jet slightly bending toward the roof. The hottest region is at the center of the boiler with the peak temperature around 1630 K (2474.33 ^{o}F).

The swirling flow is used to enhance the mixing of air and fuel and to stabilize the flame front. The gas flow distribution shows the flow is characterized by a flame jet spreading over the combustion chamber surface. A recirculation zone in the upper and lower portion of the chamber surface near the burner is observed. The combustion and heat transfer efficiency in this recirculation zone is low. The flame impinges on the combustion chamber sidewalls at 1/3 of the combustion chamber length, with the temperature of the flame about 1500 K (2240.33^{o} F). In the vertical plane, the flame impinges on the floor and roof at about 50% of the combustion chamber length at 1250 K (1790.33 ^{o}F). The hot flames turn around 180 degrees at the end of the

combustion chamber and enter into the superheater section. A large separation bubble forms at the turning location across a dozen rows of tubes. This separation bubble remains relatively cool at 940 K (1232.33 ^{o}F) by entraining downstream cooler gasses. The separation bubble pushes the hot flow towards the mid-section of the passage walls and subjects the superheater tubes to high temperature thermal stress at about 1060 K (1448.33 ^{o}F), which can lead to tube rupture.

An intensive calculation was conducted to compute the flow and heat transfer across the 496 tubes. With the inclusion of the saturated/super-heater tubes, the exit temperature drops from 746 K (without including saturator/super-heater tubes) to almost 465 K (377.33 ^{o}F). The decrease in temperature is due to the heat transfer into the tubes. With the inclusion of tubes, the actual temperature distribution was simulated, and the exit temperature is close to the actual temperature measured by infrared thermograph at about 455 K (360 ^{o}F). The pressure drop, due to the steam tubes, is about 1055 Pascal (0.153 Psi).

The NOx prediction was conducted using both the thermal and prompt NOx. The maximum NO is formed in the core of the combustion. The effect of excess air on NOx production was investigated using three cases – stoichiometric, 10%, and 35% excess air. The results show the NOx production for using stoichiometric air is highest at about 4.23 ppm.

The overall simulation was successful and provides comprehensive information of combustion and thermal-flow in the studied boiler. The prediction of NOx is lower than the actual level. Several ideas were formed from this study to improve boiler efficiency and minimize the thermal stress problem imposed on the super-heater tubes.

APPENDIX A

Application of FLUENT Code

In the present work the generalized finite-rate chemistry model is used to analyze the methane-air combustion system. The combustion is modeled using a global one-step reaction mechanism, assuming complete conversion of fuel to CO_2 and H_2O.

Step 1: Grid

1. Read the grid file

   File → Read → Case...

   After reading the grid file, **FLUENT** will report the number of fluid cells that have been read, along with numbers of boundary faces with different zone identifiers.

2. Check the grid

   Grid → Check

   The grid check lists the minimum and maximum x and y values from the grid, and reports on a number of other grid features that are checked. Any errors in the grid would be reported at this time.

3. Scale the grid

   Since this grid was created in units of inches, the **Scale Grid** panel will be used to scale the grid into meters.

   Grid → Scale...

(a) Under **Units Conversion**, select **in** from the drop-down list to confirm that the **Grid was created in inches**.

(b) Click on **Scale**

4. Display the grid.

Display →Grid...

Step 2: Model

1. Define the domain space as 3D, and choose segregated solver.

Define →Models →Solver...

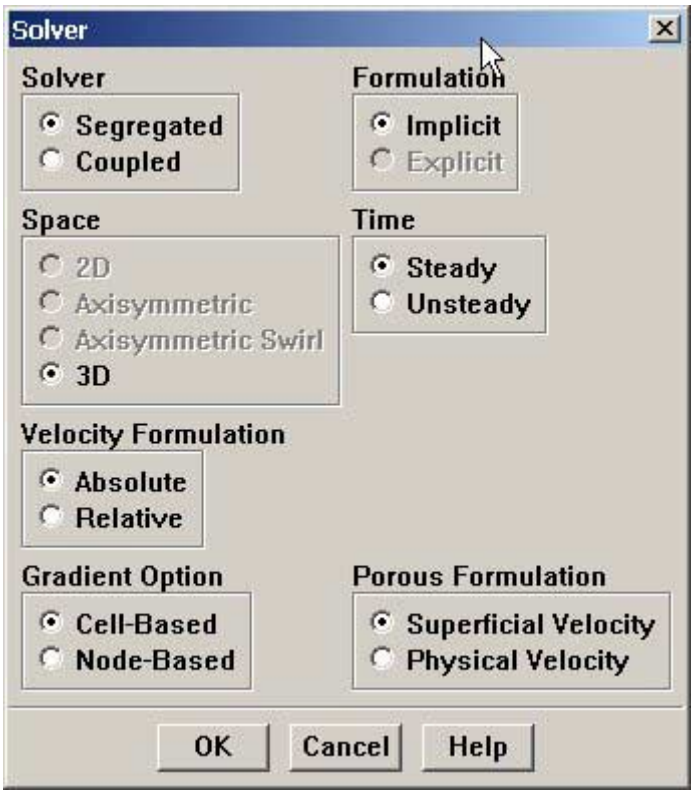

2. Enable the κ-ε turbulence model.

Define →Models →Viscous...

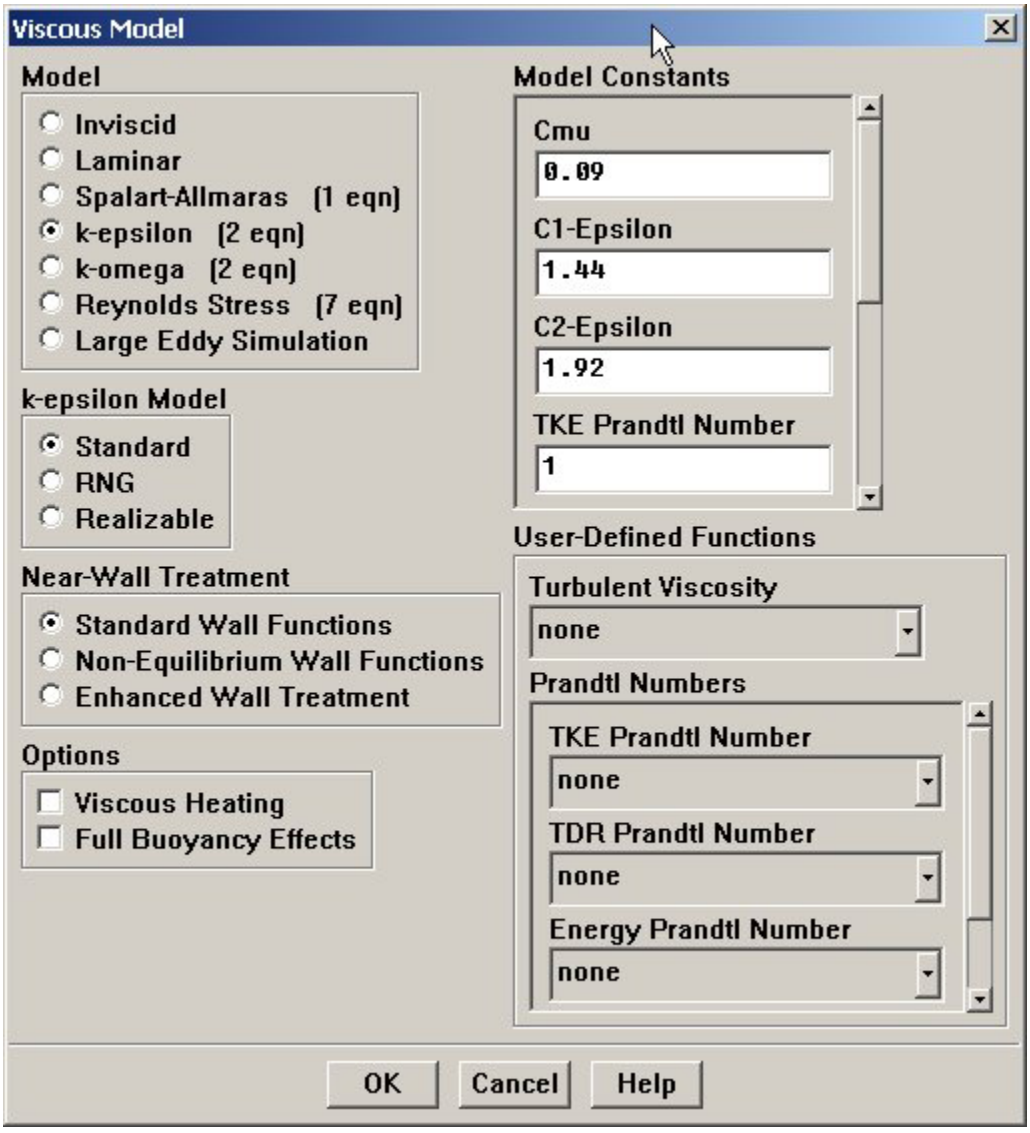

3. Enable heat transfer by activating the energy equation.

   Define → Models → Energy...

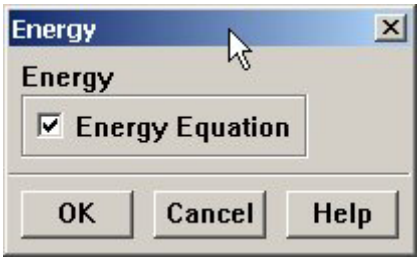

4. Enable Radiation

   Define →Models →Radiation...

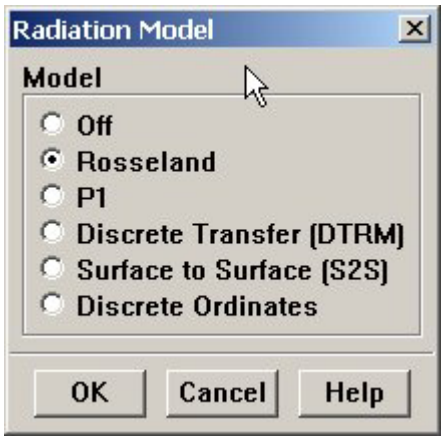

   a) Select Rosseland model as radiation model

5. Enable chemical species transport and reaction.

   Define →Models →Species...

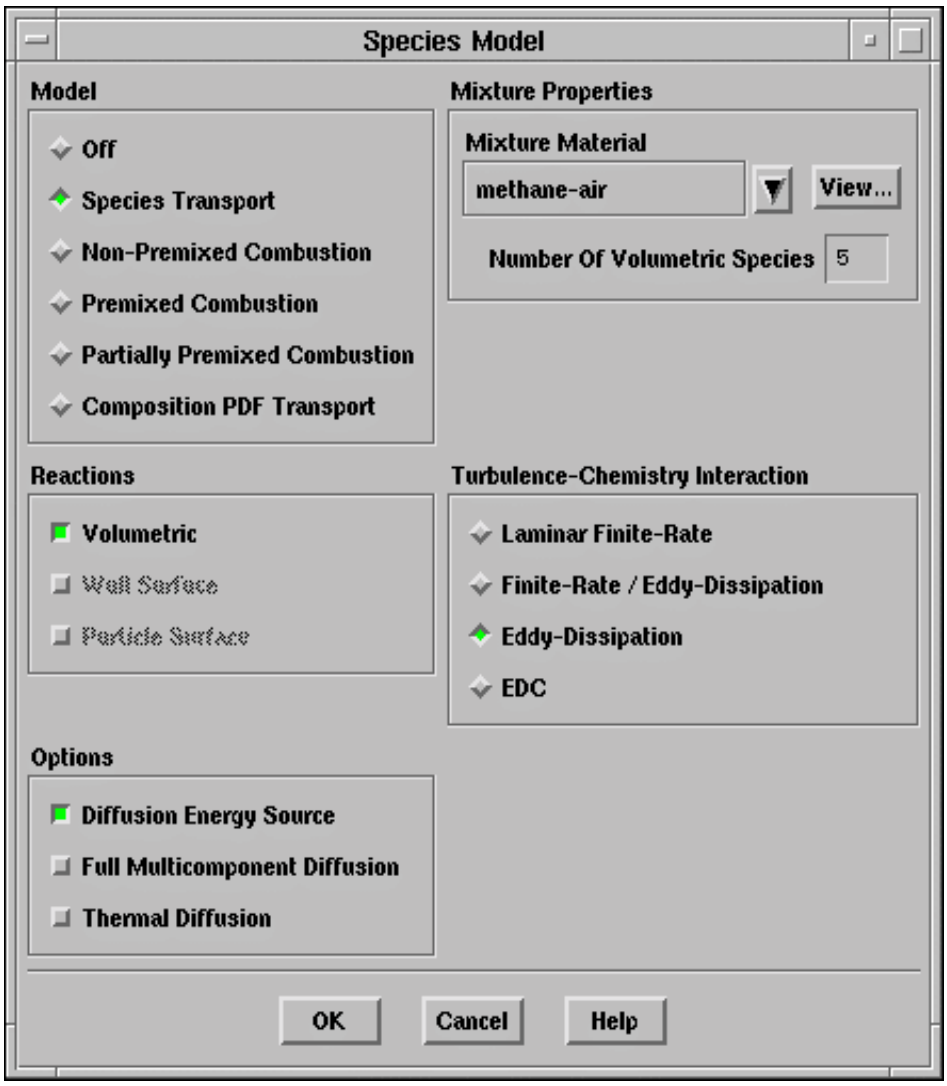

(a) Select **Species Transport** under **Model**.

(b) Select **Volumetric** under **Reactions**.

(c) Choose **methane-air** in the **Mixture Material** drop-down list.

By selecting one of the pre-defined mixtures, the complete description of the reacting system including chemical species and their physical and thermodynamic properties are accessed.

(d) Select **Eddy-Dissipation** under **Turbulence-Chemistry Interaction**.

The eddy-dissipation model computes the rate of reaction under the assumption that chemical kinetics are fast compared to the rate at which reactants are mixed by turbulent fluctuations (eddies).

(e) Click **OK**.

Step 3: Materials

Define → Materials...

The **Materials** panel shows the mixture material, **methane-air**, that was enabled in the **Species Model** panel.

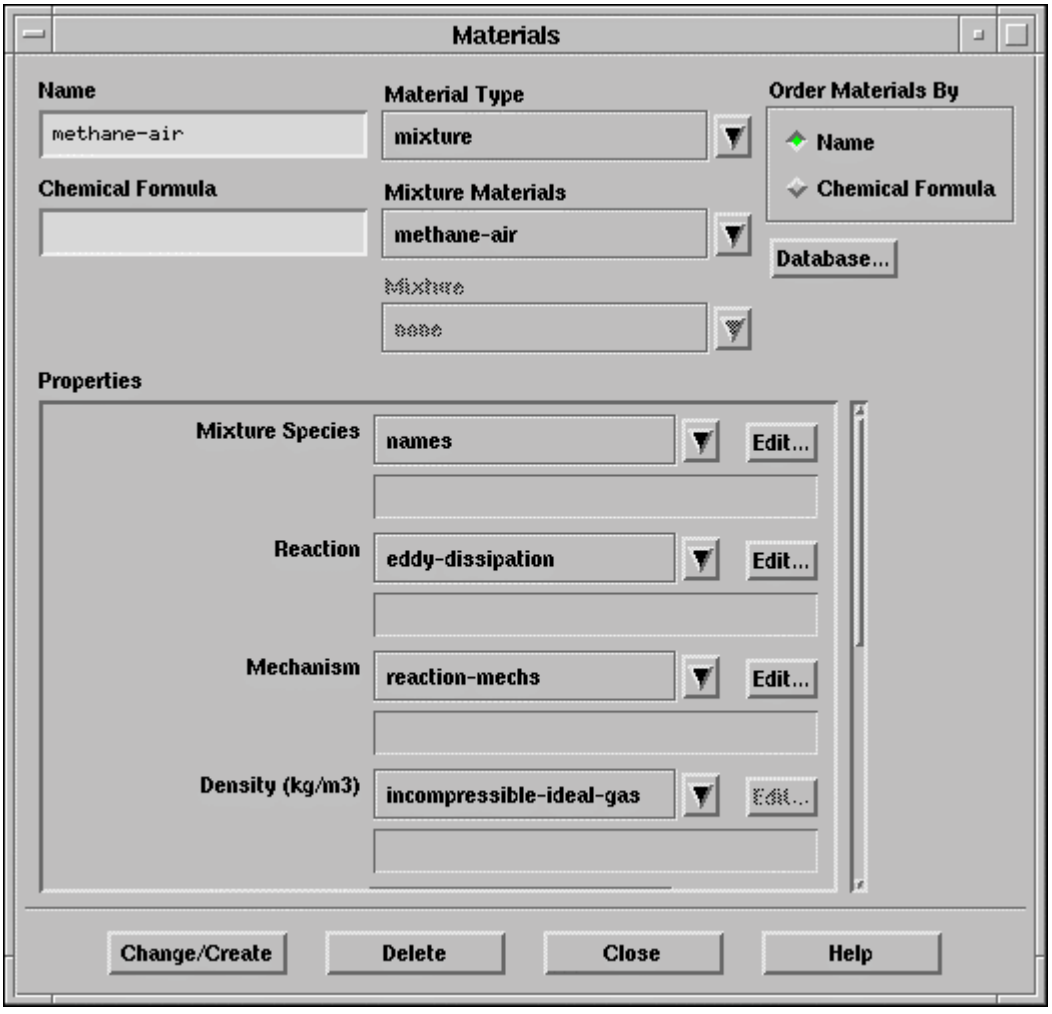

1. Choose **incompressible-ideal-gas** in the **Density** drop-down list.
2. The strong temperature and composition dependence of the specific heat will have a significant impact on the predicted flame temperature.

   Enable composition dependence of the specific heat.

   Define → Materials...

   (a) In the drop-down list next to **Cp**, select **mixing-law** as the specific heat method.

   (b) Click on the **Change/Create** button to render the mixture specific heat based on a local mass-fraction-weighted average of all the species.

3. Enable temperature dependence of the specific heat for each species.

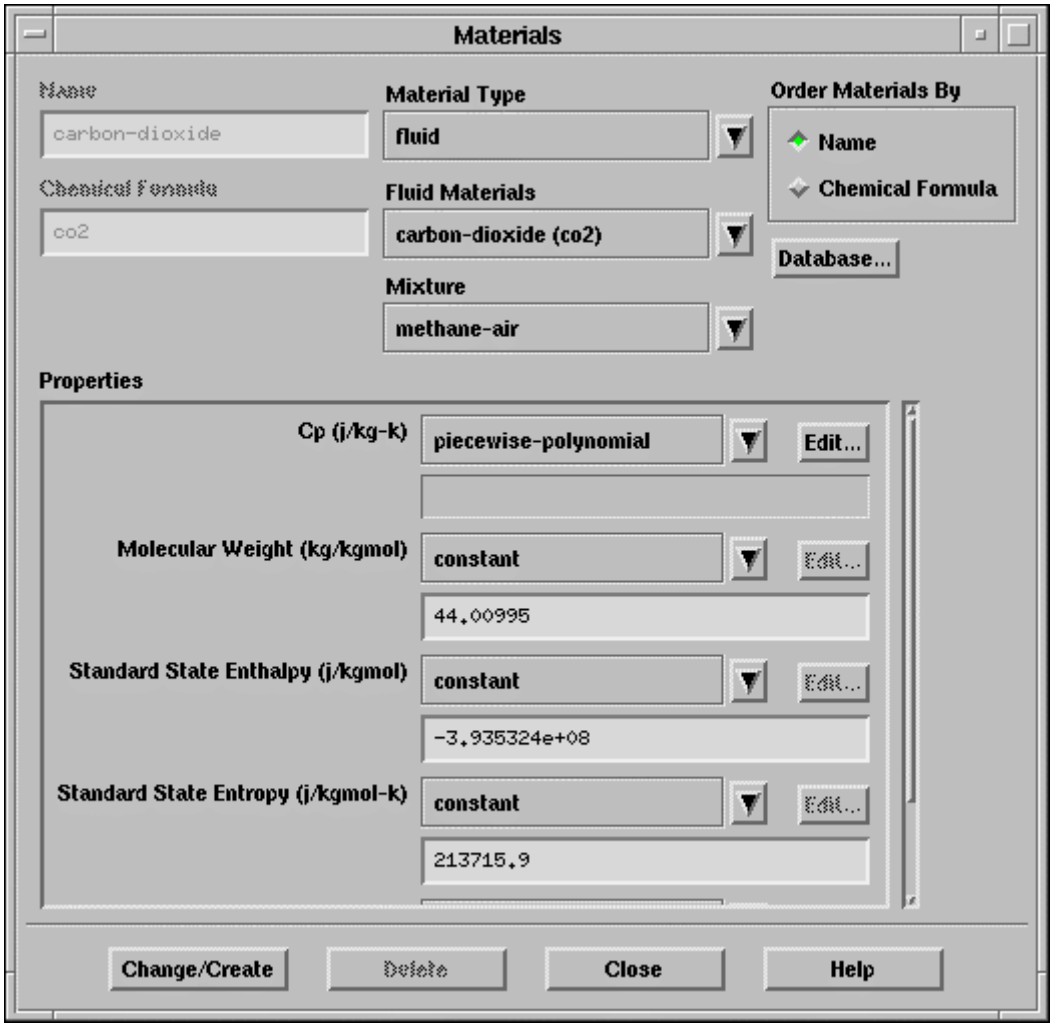

(a) In the **Material Type** drop-down list, select **fluid**.

The **fluid** material type gives you access to each species in the mixture.

(b) Select **carbon-dioxide (CO_2)** under **Fluid Materials**.

(c) In the drop-down list for **Cp**, select **piecewise-polynomial**.

This will open the **Piecewise Polynomial Profile** panel.

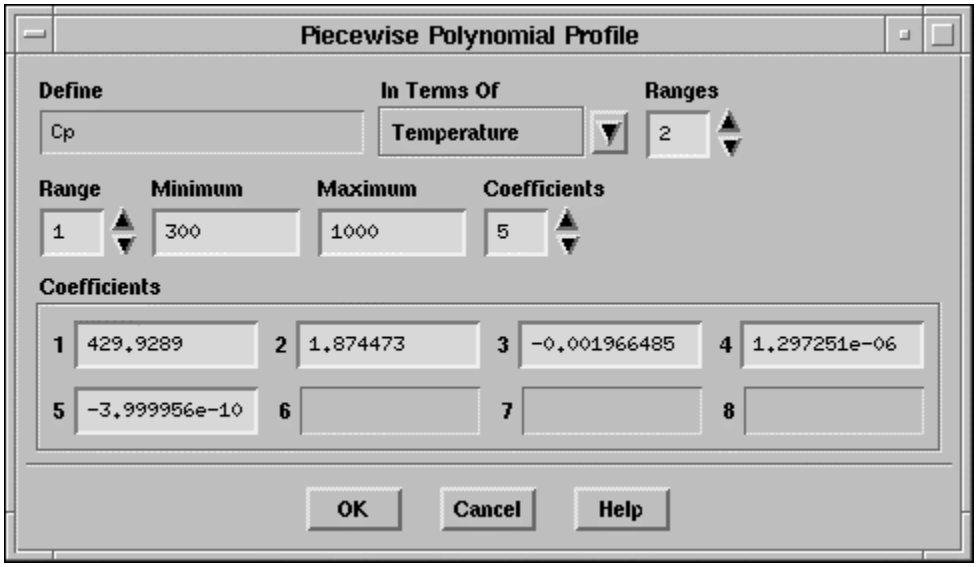

(d)

- Click on OK to accept the coefficients describing the polynomial temperature variation of C_p for carbon dioxide.
- Click on **Change/Create** in the **Materials** panel to accept the change in the properties for carbon dioxide, CO_2.

4. Repeat steps (b), (c) and (d) above for the remaining species (methane, CH_4; nitrogen, N_2; oxygen, O_2; and water, H_2O), and click on **Change/Create** to accept change for each species.

Step 4: Boundary Conditions

Define → Boundary Conditions...

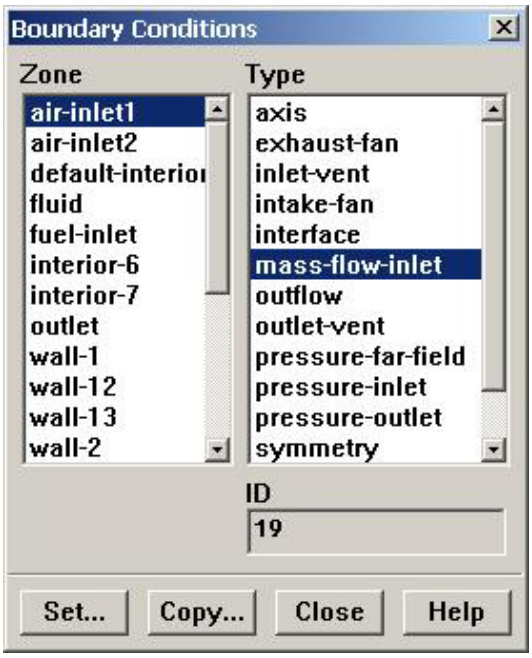

a) Select air-inlet1 (Secondary air) and set the boundary condition, mass-flow-inlet

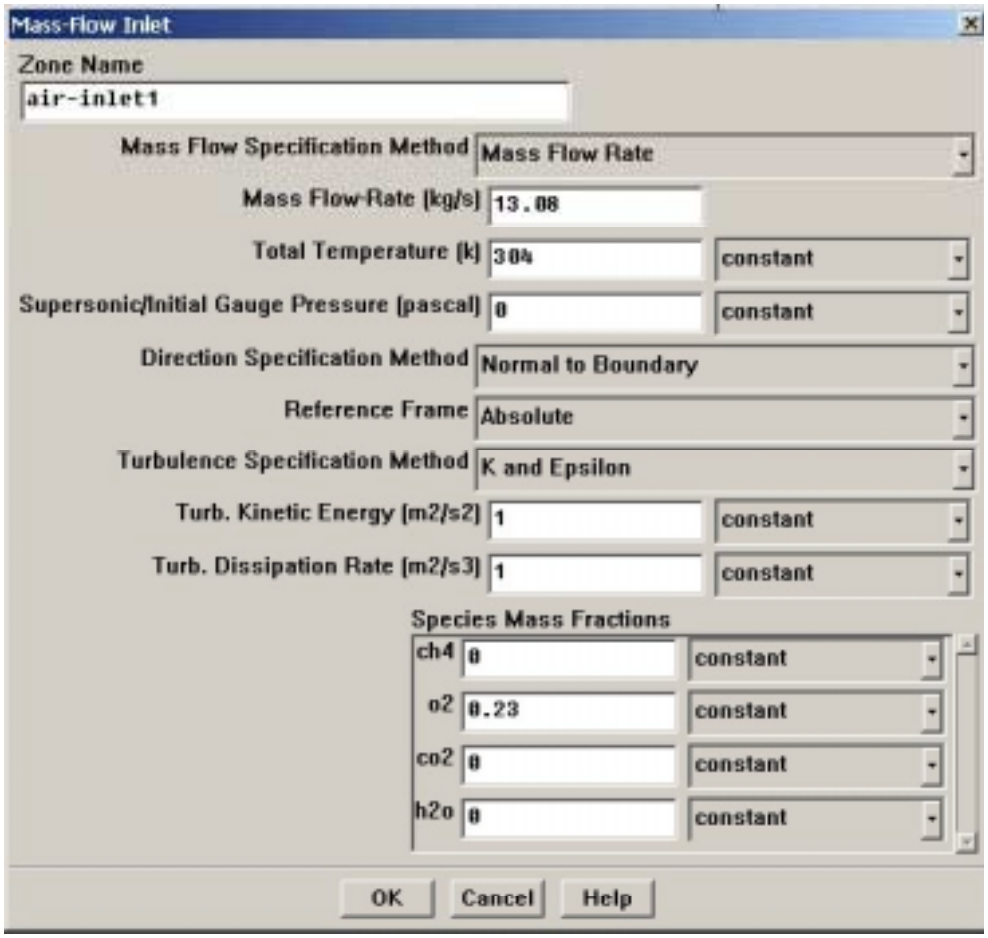

b) Set the boundary condition for air-inlet2 (Primary air with swirl), mass-flow-inlet

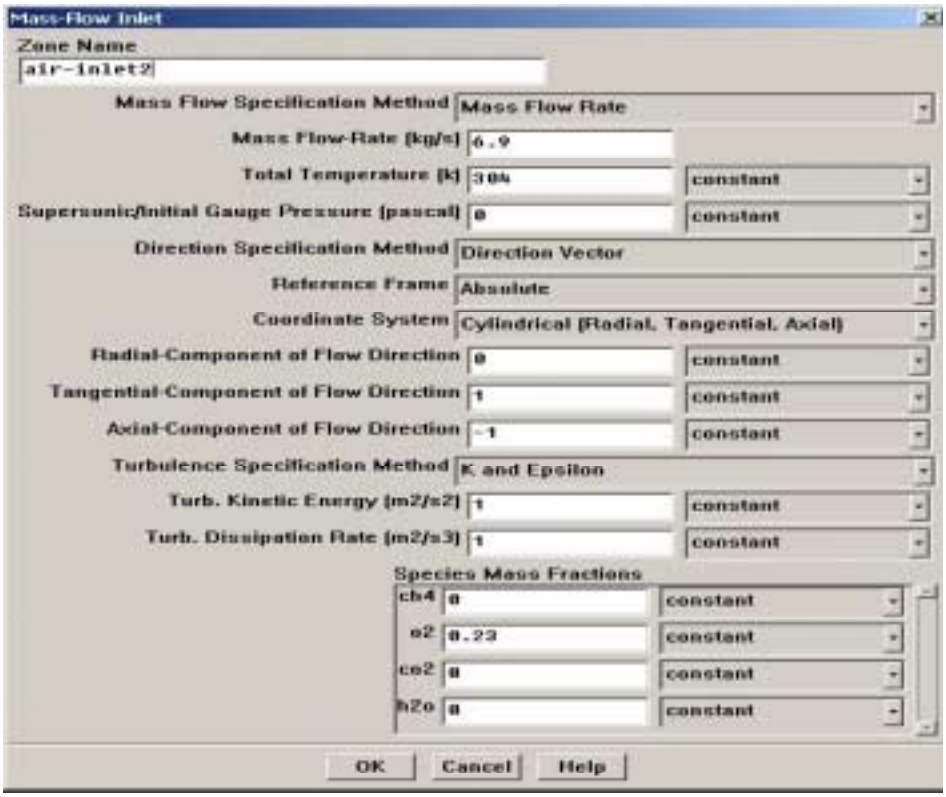

c) Set the boundary condition for fuel-inlet, mass-flow-inlet

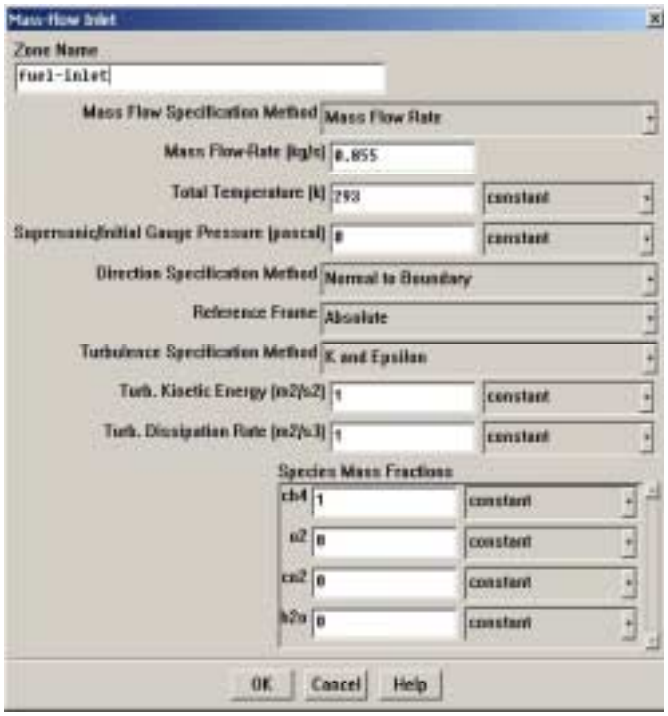

d) Set the outlet boundary condition for outlet, pressure-outlet

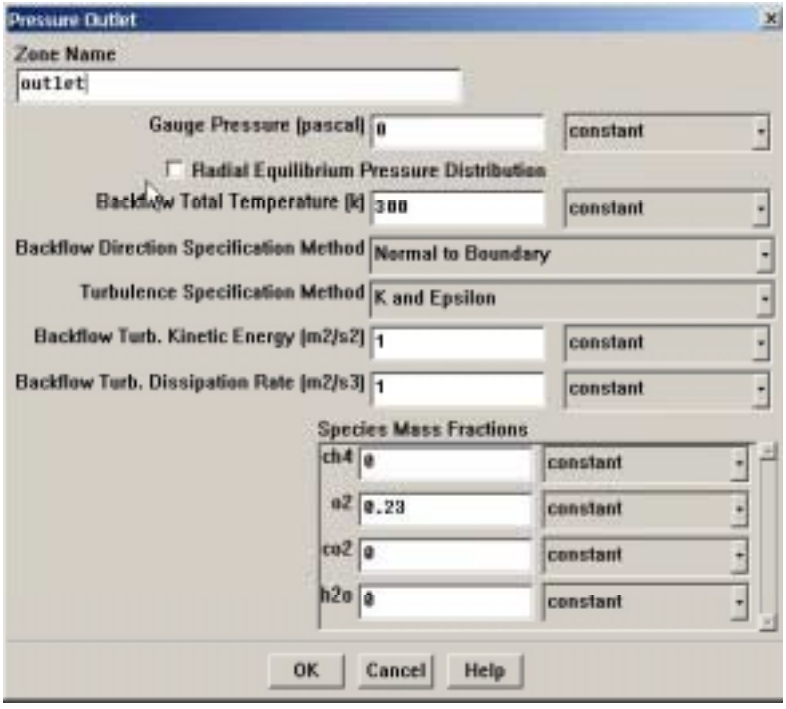

e) Set the boundary conditions for all the walls, one example is for constant wall temperature (saturators or superheaters) and the other example is for adiabatic wall condition.

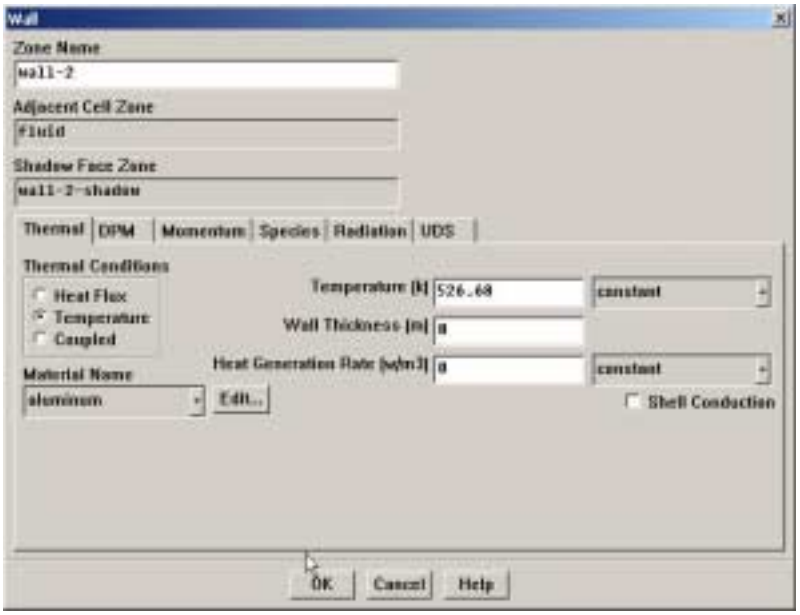

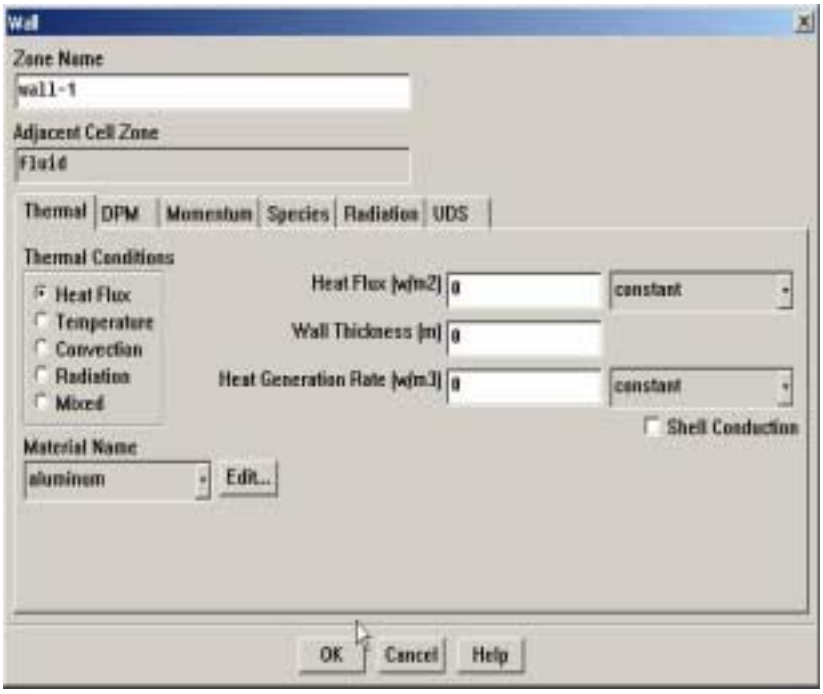

Step 5: Solution Initialization

1. Initialize the field variables.

Solve → Initialize → Initialize...

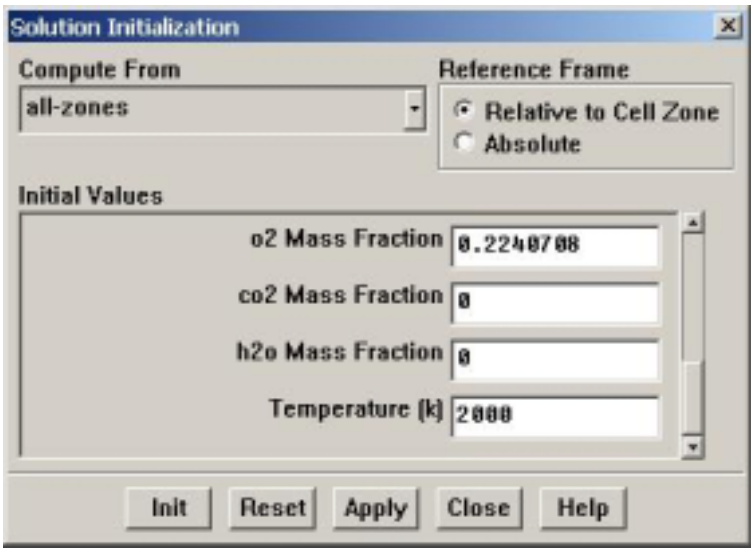

(a) Select **all-zones** in the **Compute From** drop-down list.

(b) Adjust the **Initial Values** for **Temperature** to `2000`

(c) Click **Init** to initialize the variables, and then close the panel.

2. Set the under-relaxation factors.

Solve → Controls → Solution...

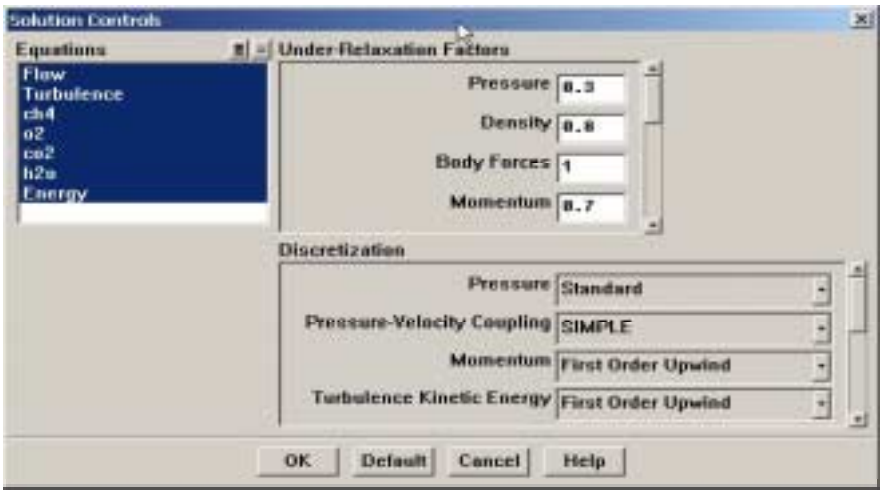

(a)

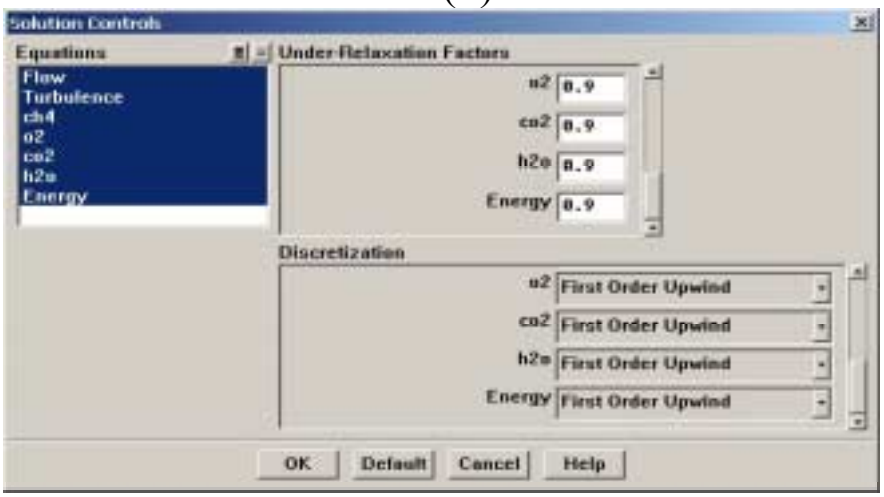

(b)

3. Turn on residual plotting during calculation

Solve → Monitors → Residual...

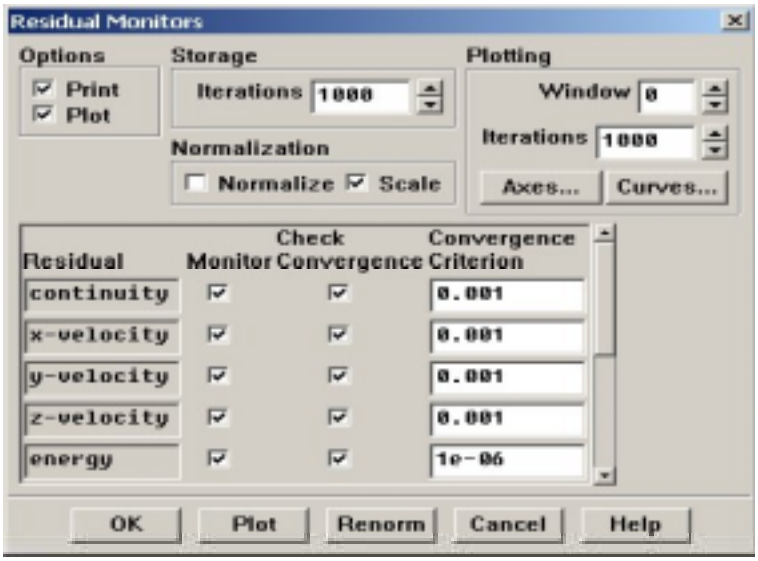

4. Start the calculation by requesting 1000 iterations

Solve → Iterate...

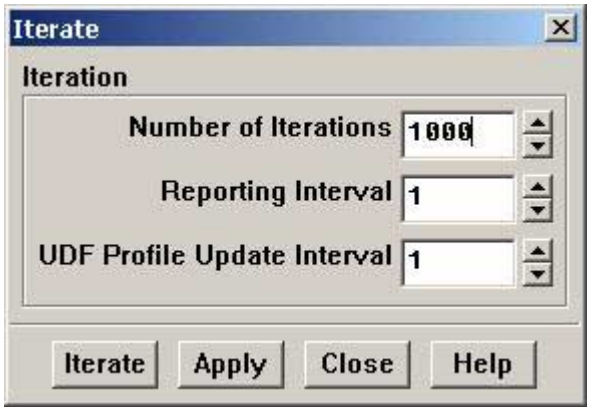

Step 6: Post-processing

Review the solution by examining graphical displays of the results and performing surface integrations and making energy balance

APPENDIX-B

NOx Prediction Using FLUENT NOx Model

During combustion of fuels with air, a small part of the nitrogen present in the air or in the fuel itself reacts with oxygen to form nitric oxide in the flame gases. NOx concentrations generated in combustion systems are generally low. As a result, NOx chemistry has negligible influence on the predicted flow field, temperature, and major combustion product concentrations. Therefore, the prediction of NOx production can be post-processed after the thermal flow and major species concentrations are calculated. But combustion-generated pollution is a threat to the environment.

NOx emissions mainly consist of nitric oxide, less significant nitrogen oxide and nitrous oxide. To predict NOx emission, a transport equation for nitric oxide is solved. NOx calculations are obtained using FLUENT NOx model as a postprocessor to the main combustion calculation. The restrictions for using the FLUENT NOx model are

- Can be used only for segregated solver and not for coupled solver.
- The NOx models cannot be used in conjunction with the premixed combustion model.

In this study both thermal and prompt NOx are calculated. The procedure for NOx prediction is as follows:

Step-1: Combustion Simulation

Calculate the combustion problem using FLUENT.

Step-2: NOx Prediction

1. Enable the desired NOx model

   Define → Models → Pollutants → NOx...

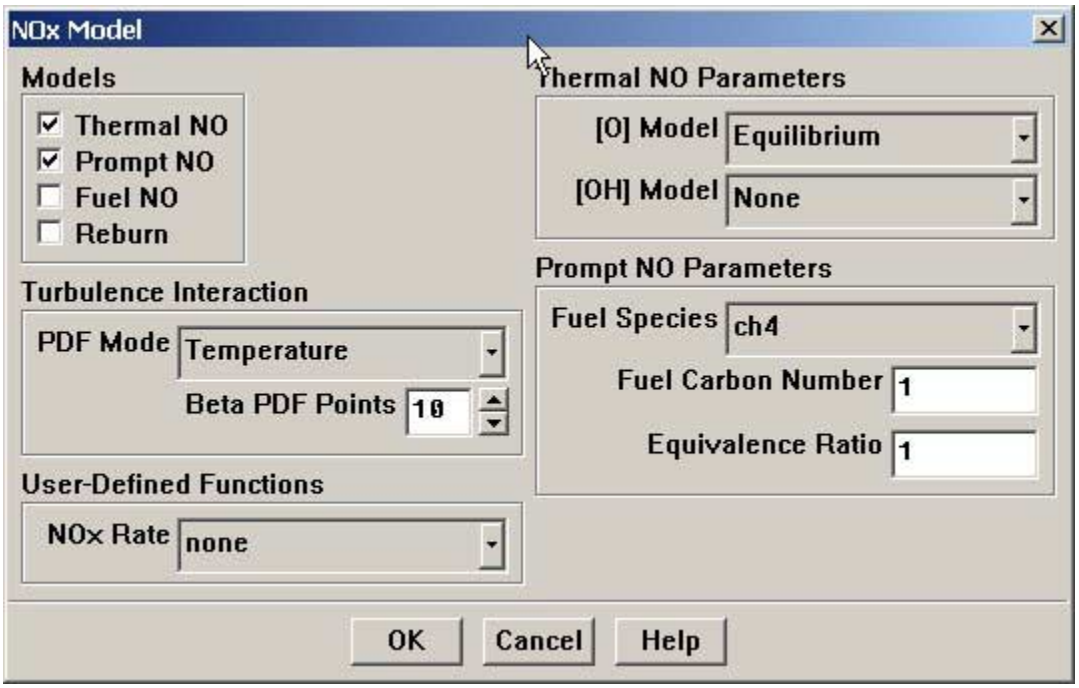

(a) Under **Models**, enable **Thermal NO** and **Prompt NO**.

(b) Select **Temperature** in the **PDF Mode** drop-down list under **Turbulence Interaction** to enable the turbulence-chemistry interaction.

(c) Select **Partial-equilibrium** in the **[O] Model** drop down list under **Thermal NO Parameters**.

The partial-equilibrium model is used to predict the O radical concentration required for thermal NOx prediction.

(d) Set the **Equivalence Ratio** to `1` under **Prompt NO Parameters**, and keep the default **Fuel Species** and **Fuel Carbon Number.**

The equivalence ratio defines the fuel-air ratio (relative to stoichiometric conditions) and is used in the calculation of prompt NOx formation. The **Fuel Carbon Number** is the number of carbon atoms per molecule of fuel and is used in the prompt NOx prediction.

(e) Click **OK** to accept these changes.

2. Enable the calculation of only the NO species, and set the under-relaxation factor for this equation.

Solve → **Controls** → **Solution...**

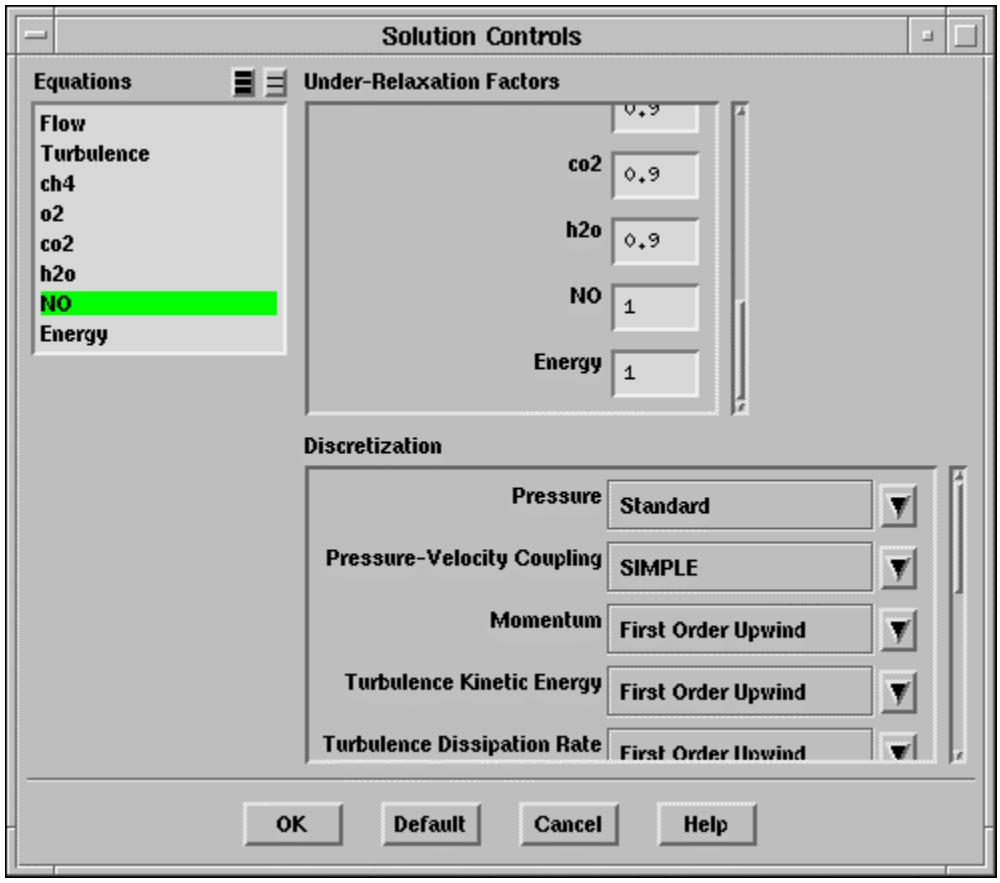

(a) In the **Equations** list, deselect all variables except the **NO** species.

(b) Increase the **NO** under-relaxation factor to `1.0`.

Formation of NOx is predicted in a ``post-processing" mode, with the flow field, temperature, and hydrocarbon combustion species concentrations fixed. Thus, only the NO equation is computed. Prediction of NO in this mode is justified on the grounds that the NO concentrations are very low and have negligible impact on the hydrocarbon combustion results.

3. Reduce the convergence criterion for the NO species equation.

   Solve →**Monitors** →**Residual...**

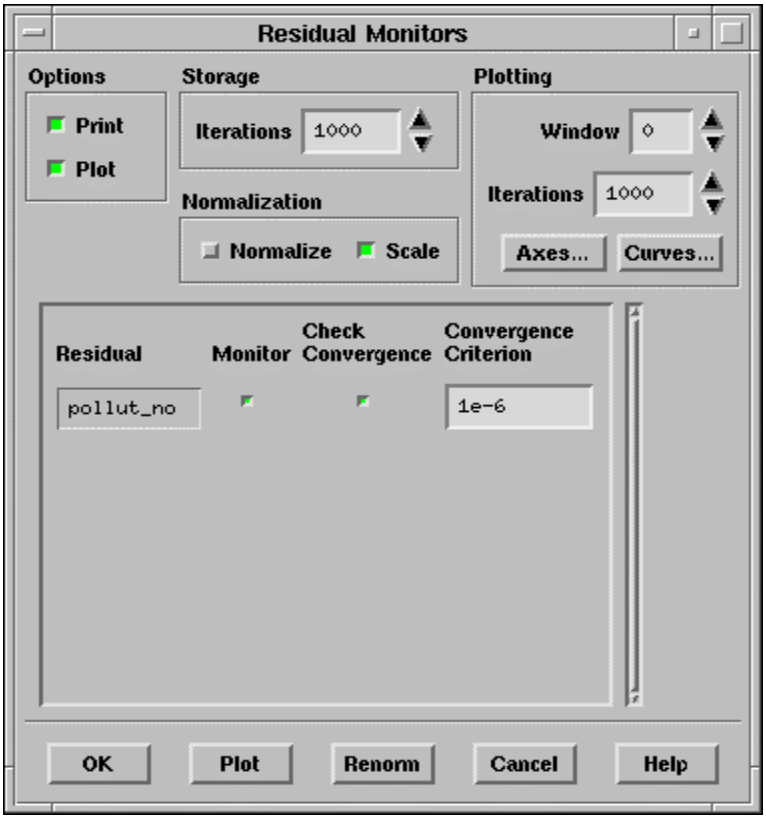

   (a) Set the **Convergence Criterion** to `1e-6` and click **OK.**

4. Start the calculation by requesting 1000 iterations

   Solve → Iterate...

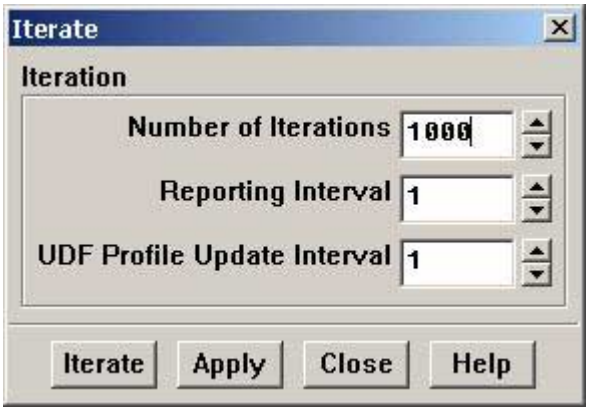

   The solution is converged after certain iterations.

5. Post-processing

   Review the mass fractions of NO by examining graphical displays of the results and performing surface integration.

6. Use a custom field function to compute NO parts per million (ppm).

   Define → Custom Field Functions...

   NO ppm is computed from the following equation:

$$\text{NOppm} = \frac{\text{NO mole fraction x } 10^6}{1 - \text{H}_2\text{O mole fraction}} \tag{A-1}$$

   where

$$\text{NOmolefraction} = \frac{\text{NO mass fraction} \times \text{mixture molecular weight}}{30} \tag{A-2}$$

   and the mixture molecular weight is

$$\text{mixture} \quad MW = \frac{1}{\sum_i \frac{\text{mass} \quad \text{fraction}}{MW}} \tag{A-3}$$

where MW is the molecular weight of each species.

(a) Create a custom field function for the mixture molecular weight.

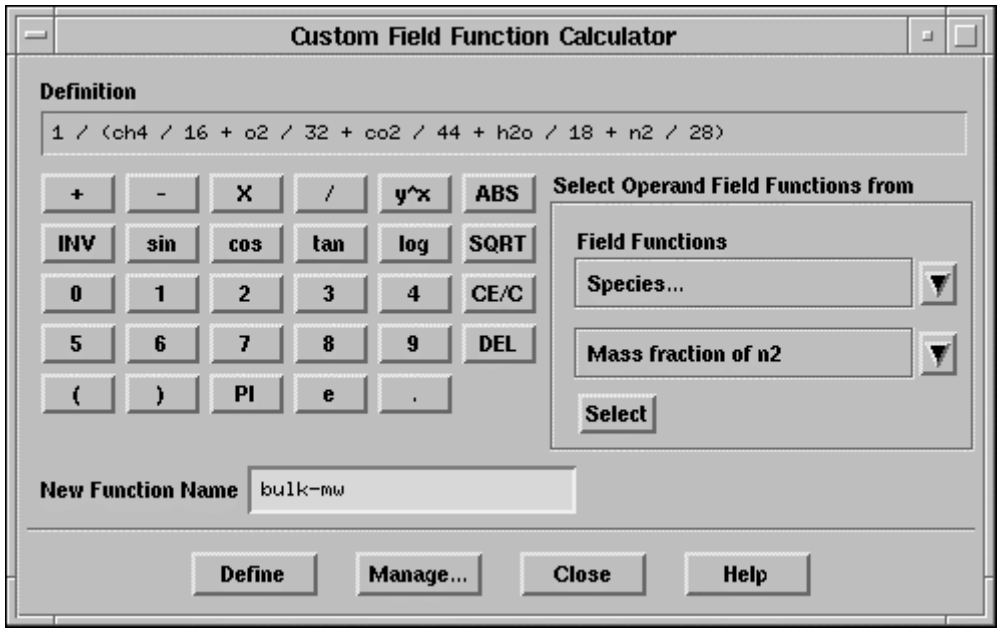

i. Click on the **1** calculator button, then on /, and then on **(**.

ii. Select **Species...** and **Mass fraction of ch4** in the **Field Functions** drop-down list. Click **Select** to add this variable to the field function **Definition**.

iii. Click on **/** and then click on **1** and **6** to enter 16 (the molecular weight of methane).

iv. Continue in this fashion to complete the definition of the mixture molecular weight field function.

v. Enter bulk-mw in the **New Function Name** text entry box.

vi. Click **Define** to add the new field function to the variable list.

(b) Create a field function for NO ppm.

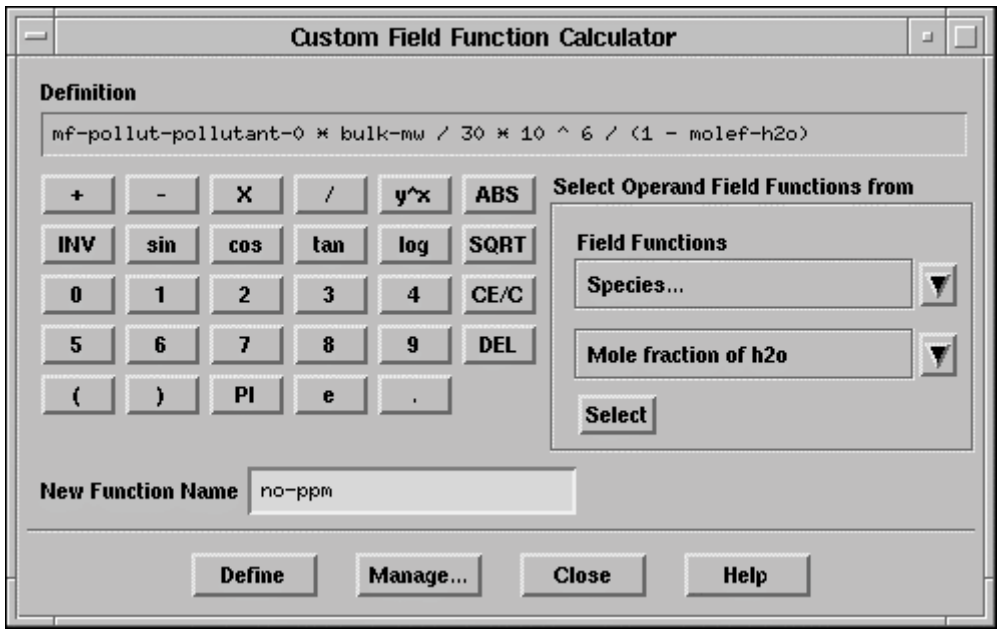

i. Select **NOx...** and **Mass fraction of NO** in the **Field Functions** drop-down list. Click **Select** to add this variable to the field function **Definition**.

ii. Click the **X** button to introduce the multiplication sign.

iii. Select **Custom Field Functions...** and **bulk-mw** in the **Field Functions** drop-down list. Click **Select** to add this variable to the field function **Definition**.

iv. Click on **/** and then click on **3** and **0** to enter 30 (the molecular weight of NO).

v. Click the **X** button and then click on **1** and **0** to enter 10.

vi. Click on **y ^ x** and then on **6**.

vii. Complete the definition of NO ppm as shown in the panel above.

viii. Enter no-ppm in the **New Function Name** text entry box.

ix. Click **Define** to add the new field function to the variable list.

7. Review the results of NO ppm by examining the graphical display.

APPENDIX-C

Energy Balance

The energy conservation is made by enforcing the thermal energy transfer out of the domain equal to that transfer into the domain. Energy balance using the enthalpy of formation approach is given by

$H_{in} = H_{out}$ (Q=0) (C-1)

Step-1: Combustion Simulation

Calculate the combustion problem using FLUENT.

Step-2: Energy Balance

1. Calculate the net inlet enthalpy formation at inlet and outlet

   Define → Materials...

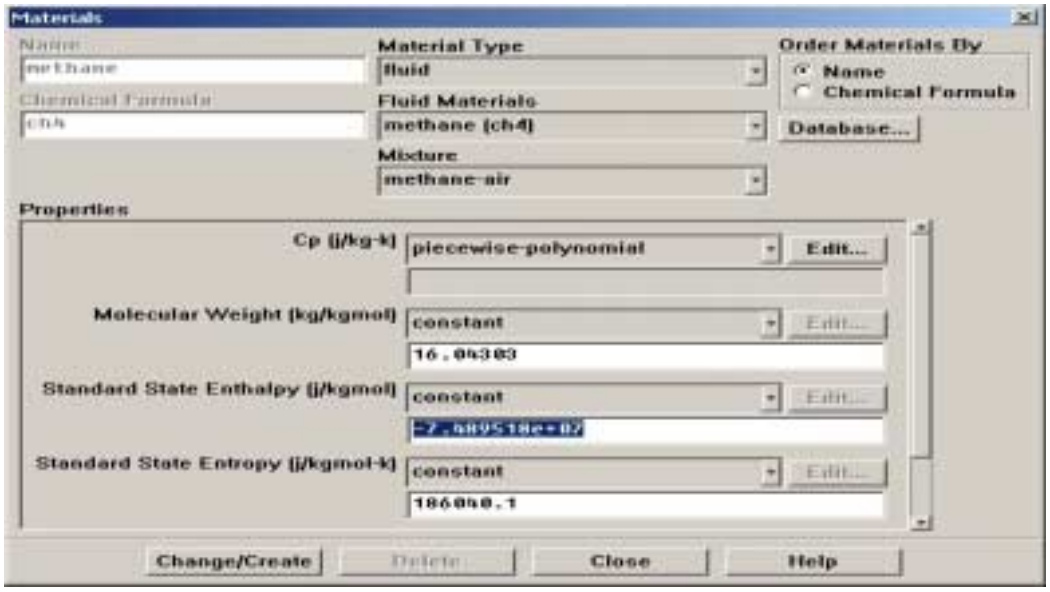

(a) Under **Material Type**, select **fluid**

(b) Under **Fluid Materials**, select **methane (ch4)**

The Standard State Enthalpy (j/kgmol) of methane is obtained

(c) In a similar way, obtain the Standard State Enthalpy of the other Fluid Materials

(d) The net enthalpy formation at inlet is obtained by

$$E_{inlet} = \text{Mass Flow Rate} * \text{Standard State Enthalpy} * \text{Mole Fraction} \quad \text{(C-2)}$$

(e) The net enthalpy formation at the outlet is obtained as

$$E_{out} = (\text{Mass Flow Rate})_{out} * \Sigma(\text{Standard State Enthalpy})_i * (\text{Mole Fraction})_I \quad \text{(C-3)}$$

2. Calculate mass flow rate of fuel

Report → Flux Reports...

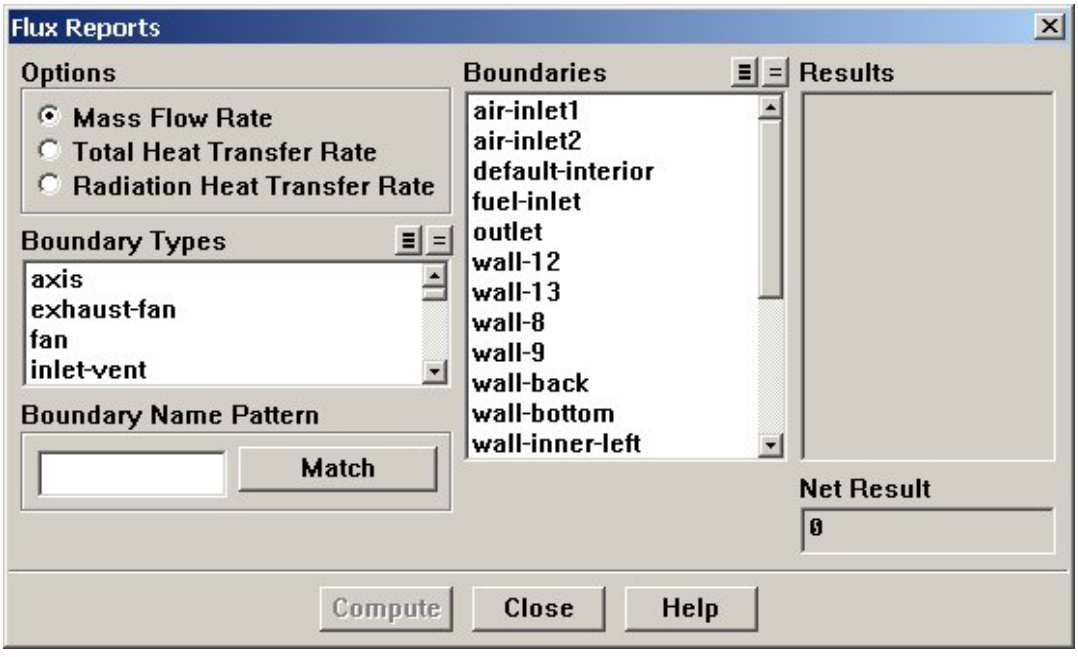

(a) Under **Options**, select **Mass Flow Rate**

(b) Select **fuel-inlet** and **outlet** under **Boundaries**.

The mass flow rate of the fuel and outlet is calculated.

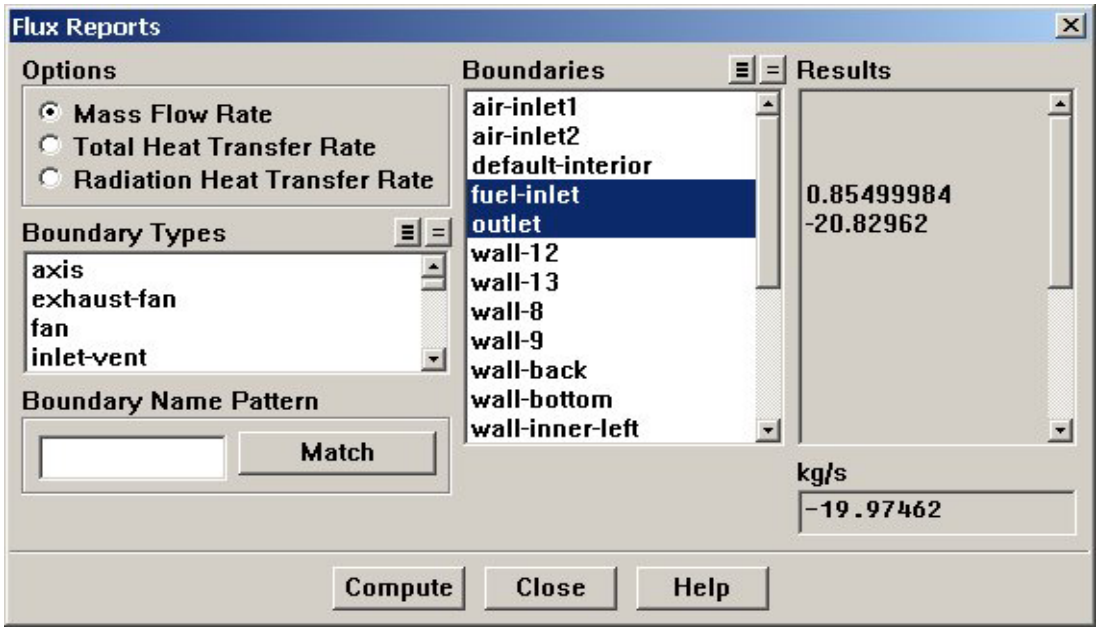

3. Calculate heat transfer rate

Report → Flux Reports...

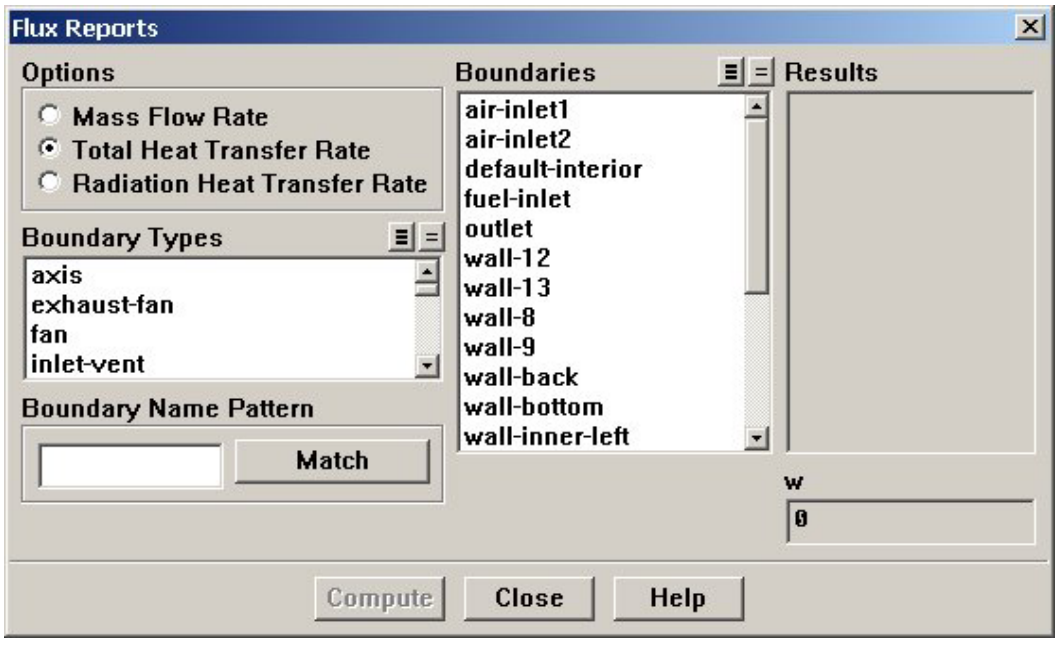

(c) Under **Options**, select **Total Heat Transfer Rate**

(d) Select **all** under **Boundaries**.

The heat transfer rate of all the boundaries is calculated

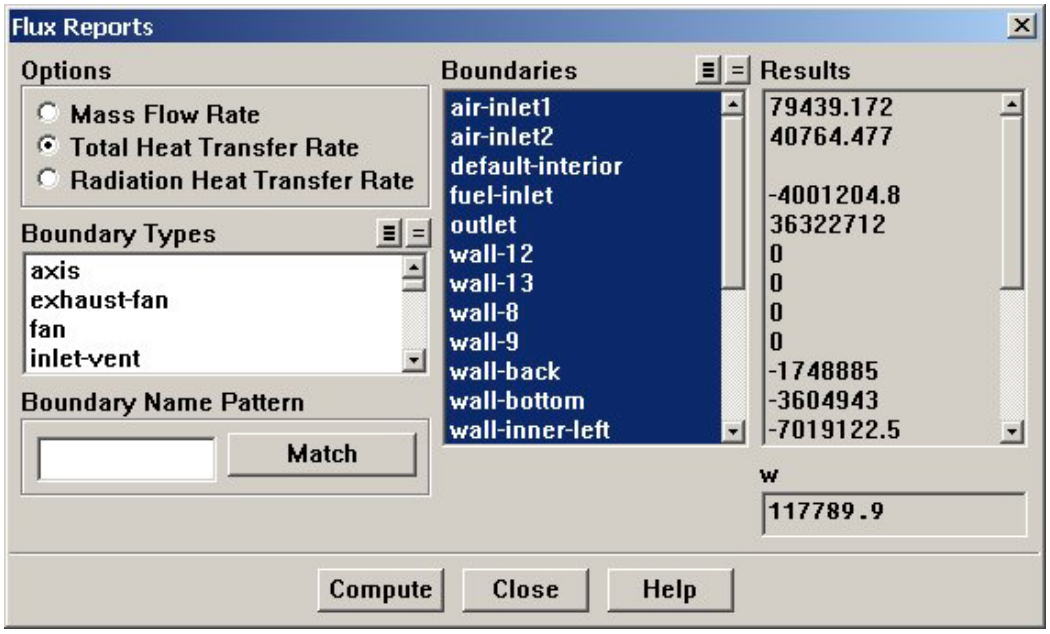

Note: Fluent uses the following sign convection for heat flux at each boundary: Q is positive for the heat transfer into the domain and Q is negative for heat transfer out of the domain. For example, a negative Q_{inlet} at inlet means heat transfer from inside to outside. At outlet, a negative Q_{outlet} also means heat transfer from inside to outside.

4. Calculate the net energy.

   (a) The net energy is calculated as

$$\{E_{inlet} + (\text{Heat Transfer Rate})_{\text{fuel-inlet}}\} - \{ E_{out} + (\text{Heat Transfer Rate})_{\text{all walls and outlet}}\} \quad \text{(C-4)}$$

$$\text{Energy of fuel, } E_{fuel} = LHV_{fuel} * (\text{Mass Flow Rate})_{fuel} \quad \text{(C-5)}$$

5. Energy Balance

   For energy balance equation (C-4) must be equal to equation (C-5)

REFERENCES

[1] Stephen R. Turns, “An Introduction to Combustion”, Second Edition.

[2] Frank P. Incropera, David P. DeWitt, “Introduction to Heat Transfer”, Third Edition.

[3] Munson, Young, Okiishi, “Fundamentals Of Fluid Mechanics”, Third Edition.

[4] Gordon J. Van Wylen, Richard E. Sonntag, “Fundamentals of Classical Thermodynamics”, 3rd Edition.

[5] FLUENT 6.1 User’s Guide, February 2003

[6] Babcock & Wilcox, “Steam its generation and use”, Thirty-ninth edition.

[7] R. Siegel and J. R. Howell, “Thermal Radiation Heat Transfer”, Hemisphere Publishing Corporation, Washington D.C., 1992.

[8] S.V. Patankar, “Numerical Heat Transfer and Fluid Flow”, McGraw Hill, Hemisphere, 1980.

[9] R C Sachdeva, “Fundamentals of Engineering Heat and Mass Transfer”, New Age International Publishers.

[10] Anderson John D. Jr, “ Computational Fluid Dynamics, the basics with application”, McGraw-Hill Inc.

[11] White Frank, “Viscous Flow”, McGraw-Hill Inc.

[12] Louis C. Burmeister, “Convective Heat Transfer”, John Wiley & Sons Inc.

[13] Wlodzimierz Blasiak and Yang Weihong, “Combustion Improvement System In Boilers and Incinerators, Proceedings of IJPGC’03, pp-IJPGC2003-40141.

[14] Lindon C. Thomas, second edition, “Heat Transfer”, Capstone Publishing Corporation.J

[15] Everett B. Woodruff and Herbert B. Lammers, “Steam Plant Operation”, McGraw-Hill Book Company.

[16] John Zink, “The John Zink Combustion Handbook”.

[17] L. Arellano, K. Smith, and A. Fahme, “ Combined Back-Side Cooled Combustor Liner And Variable Geometry Injector Technology”, Proceedings of ASME TURBO EXPO 2001, pp-2001-GT-0086.

[18] Sasan Armand and Mei Chen, “A Combustion Study Of Gas Turbine Using Multi-Species/Reacting Computational Fluid Dynamics”, Proceedings of ASME TURBO EXPO 2002, pp-GT-2002-30105.

[19] A. Williams, M. Pourkashanian, J. M. Jones, and N. Skorupska, “Combustion And Gasification Of Coal”, Taylor & Francis, New York.

VITA

Mr. Raja Saripalli was born in Bobbilli, a small town in South India. He did his bachelors in Mechanical Engineering from Jawaharlal Nehru Technological University, a reputed university in India, in 2001. He joined the MS program in Mechanical Engineering at University of New Orleans in Spring 2002.